



Durham E-Theses

The scheme-dependence of power correction fits to event shape observables

Dinsdale, Michael J.

How to cite:

Dinsdale, Michael J. (2005) *The scheme-dependence of power correction fits to event shape observables*, Durham theses, Durham University. Available at Durham E-Theses Online: <http://etheses.dur.ac.uk/3011/>

Use policy

The full-text may be used and/or reproduced, and given to third parties in any format or medium, without prior permission or charge, for personal research or study, educational, or not-for-profit purposes provided that:

- a full bibliographic reference is made to the original source
- a [link](#) is made to the metadata record in Durham E-Theses
- the full-text is not changed in any way

The full-text must not be sold in any format or medium without the formal permission of the copyright holders.

Please consult the [full Durham E-Theses policy](#) for further details.

The Scheme-Dependence of Power Correction Fits to Event Shape Observables

A thesis presented for the degree of

Doctor of Philosophy

by

Michael J. Dinsdale

Institute of Particle Physics Phenomenology

University of Durham

September 2005

A copyright of this thesis rests with the author. No quotation from it should be published without his prior written consent and information derived from it should be acknowledged.



04 NOV 2005

Abstract

A recent analysis by the DELPHI collaboration showed that if one uses an “optimised” choice of renormalization scale, some e^+e^- event shape means can be described without significant power corrections. Motivated by this, in this thesis optimised scales (and schemes) are applied to similar observables. First, a brief review of QCD and scale/scheme optimisation is given. Then, the distributions of the e^+e^- event shapes 1-thrust and heavy-jet mass are studied within the Method of Effective Charges, including performing a next-to-leading log resummation of the effective charge beta function. There is some reduction in the apparent size of power corrections, but the resummed results behave pathologically in the 2-jet limit. Next, the Principle of Minimal Sensitivity is applied to the choice of renormalization and factorization scales for event shape means defined in the Breit frame of ep DIS. This has little effect on the perturbative predictions and large power corrections are still required. However, if one introduces separate renormalization scales for the $q\gamma^*$ and $g\gamma^*$ sub-processes, a substantial reduction in the size of the power corrections is seen for most observables.

Acknowledgements

I'd like to thank first my supervisor, Chris Maxwell, for all his guidance and encouragement, and for putting things in perspective when everything seemed to be going wrong!

Thanks also to my officemates: Darren, Graeme, George and James for making the IPPP such a fun place to study, and for all their help with physics over the years. Also thanks to my housemates, who have been too numerous to mention – but especially Jon F who actually put up with me for three whole years.

I'd like to thank PPARC for funding me, and the staff and students of the IPPP for providing a great working environment.

Last but not least, thanks to my parents for their continued support and for giving me somewhere to live for the last few months.

Declaration

I declare that no material in this thesis has been previously submitted for a degree at this or any other university.

The research described in Chapter 4 was carried out in collaboration with Dr C. J. Maxwell, and has appeared in

- M. J. Dinsdale and C. J. Maxwell, “Lambda-based QCD perturbation theory: Side-stepping the scheme dependence problem,” arXiv:hep-ph/0408114.
- M. J. Dinsdale and C. J. Maxwell, “Resummation of Large Logarithms Within the Method of Effective Charges,” Nucl. Phys. B **713** (2005) 465.

Chapter 5 is derived from

- M. J. Dinsdale, “Scale Optimisation and Event Shape Means in Deep-Inelastic Scattering,” *in preparation*.

The copyright of this thesis rests with the author. No quotation from it should be published without their prior written consent and information derived from it should be acknowledged.

Contents

Abstract	i
Acknowledgements	ii
Declaration	iii
1 Introduction	1
1.1 Motivation	1
1.2 Thesis Outline	5
2 Quantum Chromodynamics	7
2.1 QCD as a Quantum Field Theory	7
2.1.1 The QCD Lagrangian	7
2.1.2 The Feynman Rules	12
2.2 UV Singularities	18
2.2.1 Regularisation	18
2.2.2 Renormalization	19
2.2.3 The Beta-Function	22
2.2.4 Hadronization	27
2.2.5 Minimal Subtraction Schemes	28
2.3 IR Singularities	29
2.3.1 Cross-Section for $e^+e^- \rightarrow \bar{q}q$	29

2.3.2	Inclusive Hadron Production	31
2.3.3	Exclusive Processes and IR Safety	33
2.4	Initial State Hadrons	37
2.4.1	Initial State IR Singularities	37
2.4.2	Factorisation	37
2.4.3	Removing the Singularities	38
2.4.4	DGLAP Evolution	40
2.5	Power Corrections to Event Shapes	41
2.5.1	Non-Perturbative Effects	41
2.5.2	The Dokshitzer-Webber Model	41
3	Renormalization Prescription Dependence	44
3.1	The Problem	44
3.1.1	Ambiguities in Perturbation Theory	44
3.2	The “Physical Scale”	48
3.2.1	Method	48
3.2.2	Motivation	48
3.3	The Method of Effective Charges	50
3.3.1	Method	50
3.3.2	Motivations	55
3.4	The Principle of Minimal Sensitivity	57
3.4.1	Method	57
3.4.2	Motivations	59
4	NLL ECH and Event Shape Distributions	61
4.1	Background	61
4.2	Resummation of Logarithms in the ECH Beta-Function	62
4.3	ECH for Event Shapes at Next-to-leading Logarithmic Accuracy	66

4.3.1	Outline	66
4.3.2	Analytical Power Corrections in the Approach of Burby and Maxwell	68
4.3.3	Exponentiation	69
4.3.4	Resummation of ρ	75
4.3.5	Fits	77
4.3.6	Resummation without Exponentiation	79
4.4	Discussion and Conclusions	86
5	PMS and DIS Event Shape Means	90
5.1	Introduction	90
5.2	Definition of the Observables	91
5.3	Applying The Principle of Minimal Sensitivity to DIS	95
5.4	Calculational Methods	98
5.5	Case Study: τ_c	100
5.6	Results	107
5.7	Conclusions	111
6	Summary and Outlook	114

List of Figures

2.1	QCD Feynman rules for internal lines.	15
2.2	QCD Feynman rules for vertices.	16
2.3	QCD Feynman rules for external lines.	17
2.4	Some of the QCD Feynman rules for counterterm vertices.	23
2.5	LO diagrams used in calculating $\sigma(e^+e^- \rightarrow \bar{q}q)$	31
2.6	Cut diagrams for $e^+e^- \rightarrow \bar{q}q$ at $O(a)$	32
2.7	Cut diagrams for $e^+e^- \rightarrow \bar{q}qg$ at $O(a)$	34
4.1	Comparison of NLO fits to the distribution of τ	70
4.2	Comparison of NLO fits to the distribution of ρ_h	71
4.3	Prediction of NL $\overline{\text{MSPS}}$ logs for τ	74
4.4	Prediction of NL $\overline{\text{MSPS}}$ logs for ρ_h	75
4.5	Various NLO τ distributions in the 2-jet region	76
4.6	Fits to the τ distribution using exponentiation	81
4.7	Fits to the ρ_h distribution using exponentiation	82
4.8	Examples of our best fit NLL ECH 1-thrust τ distributions	83
5.1	Dependence of $\langle \tau_c \rangle^{(\text{NLO})}$ on μ and M	101
5.2	Comparison of NLO predictions to H1 data [63] for $\langle \tau_c \rangle$	102
5.3	Dependence of $\langle \tau_c \rangle^{(\text{NLO})}$ on μ_q, μ_g and M	105
5.4	Predictions of our three perturbative predictions compared to data	108

5.5	Predictions of our three perturbative predictions compared to data	109
-----	--	-----

List of Tables

4.1	Fit range sensitivity study for τ	80
4.2	Fit range sensitivity study for ρ_h	80
4.3	Summary of the data used in our fits for thrust.	84
4.4	Summary of the data used in our fits for heavy-jet mass.	85
5.1	PMS ₁ scales for $\langle\tau_c\rangle$	100
5.2	PMS ₂ scales for $\langle\tau_c\rangle$	104
5.3	Fits for C_1 and C_2	110
5.4	Fits for $\bar{\alpha}_0$	111

Chapter 1

Introduction

1.1 Motivation

One of the remarkable things about QCD is that in the limit of massless quarks it has only a single free parameter, usually taken to be $\alpha_{\overline{\text{MS}}}(M_Z)$. Therefore, many tests of QCD reduce to attempts to extract values of $\alpha_{\overline{\text{MS}}}(M_Z)$ from different types of experimental observables. In order to do this accurately it is important to choose the right kind of observable. The physical processes described by QCD can be divided into two rough categories according to the characteristic momentum transfers involved: soft (low momentum transfers) and hard (high momentum transfers). Of the two, the soft processes are by far the less well-understood. These involve things like the structure of bound states, the confinement mechanism and the properties of hadronization. The hard processes all relate to scattering among the elementary quanta of the theory, the quarks and gluons. These are easier to understand because the asymptotic freedom of QCD allows one to describe them in terms of perturbation theory. However, it is unfortunately impossible to perform an experiment where *only* a hard process occurs. This is because free quarks and gluons never appear in asymptotic states - one cannot escape the effects of hadronization. It is therefore necessary to find observables that are relatively



insensitive to the soft processes going on in the experiment, whilst maintaining sufficient sensitivity to the hard, perturbatively calculable parts that a meaningful measurement of $\alpha_{\overline{\text{MS}}}(M_Z)$ can be made.

These rough ideas can be made rigorous by appealing to the factorization theorems of QCD. These theorems allow one to express many classes of physical quantities as a convolution of a hard, perturbative cross-section with some universal parton distribution functions, plus terms suppressed by powers of the hard momentum scale (power corrections).

Consider for example the simplest QCD observable, the R -ratio, which measures the ratio of the hadronic to the muonic cross-section in e^+e^- annihilation. This has been calculated perturbatively to $O(\alpha_s^3)$ and the leading power corrections are suppressed by the fourth power of the hard scale. This should make it ideal for measuring α_s at collider energies where $\alpha_s \sim 0.1$ and the power-suppressed terms should be negligible. However, the R -ratio is dominated by the parton model $O(\alpha_s^0)$ term and thus very small errors are needed to see the α_s dependence. Moreover it contains no detailed information on the final state and so allows only a very simple test of the validity of QCD.

These vices and virtues are exactly reversed for the so-called event shape variables [1] which measure properties of the energy-momentum distribution in the final state of some QCD process. They exhibit very strong dependence on α_s and contain a lot of information about the detailed structure of the final state. However, they have so far only been computed to $O(\alpha_s^2)$. Worse, one can deduce from simple models of hadronization [2] or through a renormalon analysis [3], that they should receive power corrections suppressed only by one power of the relevant hard scale. These corrections may therefore be expected to be sizeable even at collider energies $\sim M_Z$. For example, one might expect the numerator in the power correction to be of the order of some confinement scale, say 1GeV; in that

case the power correction at M_Z could be of order $1\% \sim \alpha_s^2$.

Despite these problems event shapes are a very powerful means for measuring α_s and testing the detailed predictions of QCD. Still, they would be even more useful if the power corrections which affect their values so substantially could be understood. The magnitudes of these corrections are not at present calculable in a truly systematic way from the QCD Lagrangian. Therefore to fit the data we require the introduction of either a phenomenological hadronization model or additional non-perturbative parameters. Although this hampers attempts to extract reliable measurements of α_s from the data, it also provides a good opportunity to study the IR behaviour of QCD experimentally.

A particular approach to modelling these corrections, which has become the standard one employed in analysing data, was proposed in Ref.[4]. In this approach, which we shall refer to as the Dokshitzer-Webber approach after the initiating authors, power corrections to many event shape means are parametrized by one additional parameter, $\bar{\alpha}_0$ which has the interpretation of the mean value of the strong coupling over some infra-red energy range.

This model does indeed appear to give a reasonable description of the data, with the $\bar{\alpha}_0$ values derived from several observables agreeing to within about 25% – the mean value being around 0.5 (see e.g. the review Ref. [1] and references therein). However, the interpretation of this is not completely straightforward because of a subtlety that was glossed over in the above. This is the so-called *scheme dependence problem*, which we will refer to here (a bit pedantically) as the renormalization prescription dependence problem. In a renormalizable theory like QCD there is no natural expansion parameter to use in formulating perturbation theory because the bare coupling which appears in the Lagrangian is related to physical quantities by divergent expressions. Renormalization eliminates this problem by defining a new, renormalized, coupling which absorbs the divergent terms, but

there is a considerable ambiguity in how this is achieved. Fixing this ambiguity amounts to defining the coupling by giving a renormalization prescription (RP) [5]. An RP consists of a choice of renormalization scheme (RS) and renormalization scale (μ). An exact calculation of a physical quantity is independent of the RP, so the choice of RP is unphysical, but unfortunately fixed-order perturbative approximations *do* depend on it. In fact, this ambiguity is essentially total - by a suitable choice of RP one can get any answer one wishes from a fixed-order perturbation series. Therefore one needs to make some “reasonable” choice of RP if perturbation theory is to have any chance of working. In QCD phenomenology one usually uses the $\overline{\text{MS}}$ renormalization scheme [7] and sets the corresponding renormalization scale $\mu_{\overline{\text{MS}}}$ equal to some relevant hard physical scale. Varying $\mu_{\overline{\text{MS}}}$ by a factor of 2 (or sometimes $\sqrt{2}$ or 4) is taken to indicate the likely size of higher-order corrections. Although this approach basically works as is shown by the overall success and consistency of perturbative QCD phenomenology [6] there is very little theoretical motivation for it (setting μ equal to a hard scale Q is often explained on the grounds that terms like $\ln^n(\mu/Q)$ otherwise appear at the n th order of perturbation theory, but strictly speaking $\mu = xQ$ would suffice to eliminate these for arbitrary x).

Most of the fits using the model of Ref. [4] have used this standard approach to fixing the RP. An exception is work within the Dressed Gluon Exponentiation (DGE) framework (see Refs.[8, 9, 10] for the application to average thrust, and the thrust and heavy-jet mass distributions). For the event shape means, another possible approach is to use a so-called “optimisation” procedure to choose the RP. Several such proposals have appeared in the literature (some of them will be described in Chapter 3 of this thesis). One of these, the Method of Effective Charges (ECH) [11] was applied to the mean of the e^+e^- event shape 1-thrust in Ref.[12], and somewhat reduced power corrections were found compared to the

physical scale approach. This suggests the possibility that the power suppressed effects are partly compensating for missing higher-order perturbative terms associated with the running of the coupling. Indeed, similar conclusions were reached in the DGE approach, although there the subset of terms resummed differs significantly from that resummed by the change of scale implicit in NLO ECH: the former is factorially divergent, the latter actually converges. Recently an analysis similar to that of Ref.[12], though more extensive, was performed by the DELPHI collaboration [13], taking into account effects arising from the finite bottom quark mass via Monte Carlo simulations. Remarkably, with the ECH choice of RP the perturbative predictions were in good agreement with the data; for several observables there was no need to add additional power corrections. Even the *deviations* from universality of the apparent $\bar{\alpha}_0$ values seen when working in the $\overline{\text{MS}}$ scheme could be predicted by NLO ECH perturbation theory.

These results motivate looking at other observables where the DW model has been applied and studying the effect of using “optimized” RPs. In this thesis, two sets of observables are investigated: event shape distributions (specifically those of 1-thrust and heavy-jet mass) in e^+e^- annihilation, and event shape means in the Breit frame of ep DIS.

1.2 Thesis Outline

Chapter 2 contains a brief summary of the main ideas from QCD needed for the rest of the thesis. A review of the RP-dependence problem and various proposed solutions to it is presented in Chapter 3. In Chapter 4 we apply the ECH to distributions of the e^+e^- annihilation event shapes thrust and heavy jet mass, incorporating a resummation of infrared logarithms to next-to-leading log accuracy. Then in Chapter 5 we turn to event shape means in the Breit frame of ep DIS. In this case, a new unphysical parameter appears: the factorization scale. We exam-

ine the effects of optimizing both renormalization and factorization scales using the Principle of Minimal Sensitivity (PMS). Chapter 6 summarises our conclusions.

Chapter 2

Quantum Chromodynamics

The aim of this chapter is to review the basic physics background needed for understanding the later chapters. For reasons of space only a brief sketch of each idea can be included, but references are given to other, more comprehensive, reviews.

2.1 QCD as a Quantum Field Theory

2.1.1 The QCD Lagrangian

Quantum Chromodynamics (QCD) forms one half of the Standard Model of particle physics [14, 15], providing a simple explanation for the profusion of hadronic and strong-interaction phenomenology in terms of an underlying quantum field theory (QFT). As with any QFT, we can specify the theory by giving its *Lagrangian density*, \mathcal{L} . In the case of QCD (as with the other parts of the standard model) this is far from arbitrary; indeed it is almost uniquely determined by simply asking for a “renormalizable theory of Dirac fermions in the fundamental representation of an $SU(3)$ gauge symmetry”. The fermions are called *quarks*, and the gauge bosons *gluons*. The familiar strongly-interacting particles, such as nucleons and pions, are composite objects constructed out of the fundamental quarks and

gluons.

To construct \mathcal{L}_{QCD} we can start with the Lagrangian density (often simply called the Lagrangian) for a single species of Dirac fermion with mass m :

$$\mathcal{L} = \bar{\psi}(i\gamma^\mu\partial_\mu - m)\psi. \quad (2.1)$$

In QCD, the quark fields transform in the fundamental representation (**3**) of the gauge group,¹ so they must be three-component objects, ψ^i , $i = 1, 2, 3$. The conjugate fields must transform in the conjugate fundamental representation ($\bar{\mathbf{3}}$), and this can be emphasised by writing them with a lower index as $\bar{\psi}_i$. This suggests the Lagrangian (using the summation convention)

$$\mathcal{L} = \bar{\psi}_i(i\gamma^\mu\partial_\mu - m)\psi^i \quad (2.2)$$

which is invariant under a global SU(3) transformation $\psi^i \rightarrow U_j^i\psi^j$, $\bar{\psi}_i \rightarrow \bar{\psi}_j(U^\dagger)^j_i$. Here, the U are unitary, so they satisfy $UU^\dagger = \mathbb{I}$ where \mathbb{I} is the 3×3 identity matrix. To promote this global symmetry to a gauge (i.e. local) symmetry requires some more work. Consider the effect on \mathcal{L} of a local transformation

$$\begin{aligned} \mathcal{L} &\rightarrow \bar{\psi}_j(U(x)^\dagger)^j_i(i\gamma^\mu\partial_\mu - m)U(x)^i_k\psi^k \\ &= \bar{\psi}_j(U(x)^\dagger U(x))^j_k(i\gamma^\mu\partial_\mu - m)\psi^k + \bar{\psi}_j(U(x)^\dagger)^j_i(i\gamma^\mu(\partial_\mu U(x)^i_k))\psi^k \\ &= \bar{\psi}_k(i\gamma^\mu\partial_\mu - m)\psi^k + \bar{\psi}_j(i\gamma^\mu((U(x)^\dagger)^j_i\partial_\mu U(x)^i_k))\psi^k. \end{aligned} \quad (2.3)$$

So, \mathcal{L} returns to itself plus an extra term involving $U^\dagger\partial_\mu U$. If we define a new *covariant* derivative

$$D_\mu = \partial_\mu + i\Delta_\mu \quad (2.4)$$

and require that Δ_μ satisfy the (matrix) transformation law

$$\Delta_\mu \rightarrow U\Delta_\mu U^\dagger + i(\partial_\mu U)U^\dagger \quad (2.5)$$

¹For group theory background, see Ref. [18].

then the Lagrangian rewritten using D_μ

$$\mathcal{L} = \bar{\psi}_i (i\gamma^\mu D_\mu - m)\psi^i \quad (2.6)$$

will be invariant under the action of a local $U(x)$.

At the moment, Δ_μ is playing the role of an additional background field. To get to QCD we need to promote it to a full dynamical field, which requires looking more closely at what values it can take. Note that it is a 3×3 matrix, and must be hermitian to give a real contribution to the Lagrangian. Any such matrix has a unique expansion of the form

$$\Delta_\mu = \Delta_\mu^0 \mathbb{I} + \sum_{a=1}^8 \Delta_\mu^a t^a \quad (2.7)$$

where the t^a are matrices called the *generators* of $SU(3)$. These are closed under taking commutators

$$[t^a, t^b] = if^{abc}t^c \quad (2.8)$$

(the real constants f^{abc} are called *structure constants* [18]).

The uniqueness of the expansion in Eq. (2.7) follows from the fact that these matrices form a basis for the space of 3×3 matrices, considered as a 9-dimensional vector space.

We will now show that the transformation Eq. (2.5) doesn't affect the value of Δ_μ^0 , so this can be set to zero without violating the $SU(3)$ gauge invariance (choosing a non-zero value would correspond to coupling the quarks to an additional background $U(1)$ field). Note that of the basis matrices in Eq. (2.7) only \mathbb{I} has non-zero trace (the t^a can be seen to be traceless by taking the trace of Eq. (2.8)). Substituting Eq. (2.7) into Eq. (2.5) and taking the trace, we see immediately that the value of Δ_μ^0 will be unchanged if and only if the second term, $(\partial_\mu U)U^\dagger$, is traceless. To see that this is so we can start from the fact that any U in $SU(3)$ can be written $U = \exp(i\alpha^a t^a)$ (using the summation convention). Using

the relation $\exp(O) = \lim_{N \rightarrow \infty} (1 + \frac{O}{N})^N$ we can express the second term as

$$(\partial_\mu U)U^\dagger = \lim_{N \rightarrow \infty} \left(\partial_\mu \left(1 + \frac{i\alpha^a t^a}{N} \right)^N \right) \left(1 + \frac{i\alpha^a t^a}{N} \right)^{-N}. \quad (2.9)$$

Introducing the notation $C = (1 + \frac{i\alpha^a t^a}{N})$, $C' = \partial_\mu C$, we have

$$(\partial_\mu U)U^\dagger = \lim_{N \rightarrow \infty} ([C'C \dots C] + [CC' \dots C] + \dots + [CC \dots C'])C^{-N}. \quad (2.10)$$

Here each $[\dots]$ contains $N - 1$ factors of C and a single C' . This is difficult to simplify further because in general C and C' do not commute. However, in computing the trace we can use cyclicity to cancel all the C terms from each of the N orderings to arrive at

$$\begin{aligned} \text{tr}[(\partial_\mu U)U^\dagger] &= \lim_{N \rightarrow \infty} \text{tr}[NC'C^{-1}] \\ &= \lim_{N \rightarrow \infty} \text{tr} \left[i(\partial_\mu \alpha^a) t^a + \mathcal{O}\left(\frac{1}{N}\right) \right] \\ &= 0 \end{aligned} \quad (2.11)$$

as advertised.

After setting $\Delta_\mu^0 = 0$ we are left with 8 background fields Δ_μ^a ; these are the *gluon* fields. Extracting a factor of the strong coupling g for convenience we write $\Delta_\mu^a = gA_\mu^a$ so the covariant derivative becomes

$$D_\mu = \partial_\mu - igA_\mu^a t^a. \quad (2.12)$$

To complete the construction of the QCD Lagrangian it remains to promote the A_μ^a to true dynamical fields. This requires adding a kinetic term which is fully determined by the requirement of SU(3)-gauge invariance. First we construct a field strength tensor (analogous to $F_{\mu\nu}$ in electrodynamics) by noting that the commutator of covariant derivatives acting on the fermion field behaves like a matrix multiplication

$$[D_\mu, D_\nu]\psi = -igF_{\mu\nu}^a t^a \psi \quad (2.13)$$

with

$$F_{\mu\nu}^a = \partial_\mu A_\nu^a - \partial_\nu A_\mu^a + gf^{abc}A_\mu^b A_\nu^c. \quad (2.14)$$

Now, the covariant derivative of ψ transforms under a gauge transformation in the same way as ψ itself

$$\psi \rightarrow U\psi, \quad D_\mu\psi \rightarrow UD_\mu\psi \quad (2.15)$$

and this must also hold for the commutator in Eq. (2.13), implying that $F_{\mu\nu}^a t^a$ transforms according to

$$F_{\mu\nu}^a t^a \rightarrow U(F_{\mu\nu}^a t^a)U^\dagger. \quad (2.16)$$

Therefore, a gauge invariant kinetic term can be written in terms of F

$$\begin{aligned} -\frac{1}{2}\text{tr}[F_{\mu\nu}^a t^a F_b^{\mu\nu} t^b] &= -\frac{1}{2}F_{\mu\nu}^a F_b^{\mu\nu} \text{tr}[t^a t^b] \\ &= -\frac{1}{4}F_{\mu\nu}^a F_a^{\mu\nu} \end{aligned} \quad (2.17)$$

(the normalisation is conventional).

Putting all this together, the QCD Lagrangian (generalised for N_f flavours of quark) is

$$\mathcal{L}_{\text{QCD}} = \sum_{f=1}^{N_f} \bar{\psi}_{i,f} (i\gamma^\mu D_\mu - m_f) \psi_f^i - \frac{1}{4} F_{\mu\nu}^a F_a^{\mu\nu}. \quad (2.18)$$

If we require renormalizability, which just as in QED prevents operators of dimension greater than 4 appearing in the Lagrangian, and SU(3) invariance which prevents for example a gluon mass term $\propto A^2$, there is only one other term we could possibly add to the Lagrangian. This is the so-called *theta term*

$$\frac{\theta g^2}{64\pi^2} \epsilon_{\mu\nu\rho\sigma} F^{a,\mu\nu} F_a^{\rho\sigma} \quad (2.19)$$

which is a total derivative and produces no effects at the perturbative level. However, if $\theta \neq 0$ non-perturbative effects would induce a CP-violating electric dipole moment for the neutron, and experimental constraints on this provide a bound $|\theta| < 3 \cdot 10^{-10}$ [19].

Although the $SU(3)$ gauge symmetry of QCD has been stressed as being of paramount importance, if we want to actually calculate predictions from the QCD Lagrangian it will be necessary to explicitly break this symmetry by fixing the gauge. This is evident already at the classical level; because the gauge transformation can have an arbitrary time-dependence, it cannot be possible to write equations of motion to describe the solutions of the theory. Classically it is sufficient to add to the Lagrangian a gauge-fixing term

$$\mathcal{L}_{\text{gauge-fixing}} = \frac{1}{2\xi} (\partial^\mu A_\mu^a)^2 \quad (2.20)$$

where ξ is an adjustable parameter selecting one from an infinite family of covariant gauges (other more general gauge choices exist, such as axial gauges which break manifest Lorentz invariance). At the quantum level (for non-Abelian gauge theories) additional complications arise, which require so-called *ghosts* to be added into the theory. These are unphysical anti-commuting scalar degrees of freedom, whose effect is to cancel unphysical longitudinal gluons. Writing η for the gluon fields, we must add to the Lagrangian

$$\mathcal{L}_{\text{ghost}} = \bar{\eta}^a (-\partial^2 \delta^{ac} - g \partial^\mu f^{abc} A_\mu^b) \eta^c. \quad (2.21)$$

(see Ref. [14], p 514). It should be stressed that the manner in which the gauge is fixed has no effect on the predictions of the theory for observable quantities, precisely because the theory before gauge fixing is gauge invariant. However, unobservable objects like Green's functions can depend on the choice of gauge (e.g. the value of ξ).

2.1.2 The Feynman Rules

As with all QFTs of physical relevance, QCD is much too complex to solve exactly, but useful predictions can be obtained using *perturbation theory* (there are also other approaches, e.g. lattice gauge theory, but they aren't relevant to this thesis).

Perturbation theory involves expanding some quantity of physical interest (perhaps a scattering amplitude or a cross-section) as a power series in the coupling constant g . The coefficients at each order in the expansion can be calculated by the method of Feynman diagrams [14, 16]. Let us sketch how this works for the case of scattering amplitudes.

Suppose $\mathcal{M}(I \rightarrow F)$ is the amplitude for a scattering process where a set of particles I with definite momenta comes in from infinity and scatters, and then a set of particles F (again with definite momenta) emerges. To construct a perturbative expansion for this quantity, start by drawing external lines as shown in Fig. 2.3 for each particle in I and F . Consider all the ways of joining these external lines using the internal lines shown on Fig. 2.1 and the vertices shown on Fig. 2.2 (which give fully connected diagrams). Remove from these any diagrams containing loops attached to outgoing lines (that is, any diagrams which have pieces that can be detached by cutting a single line). This leaves only the so-called “amputated” diagrams. Each of the diagrams in this set will contribute to the amplitude $\mathcal{M}(I \rightarrow F)$.

To calculate the contribution from each diagram we first need to assign a momentum vector to each line. This can be done as follows: assign to external lines momenta equal to the observed momenta of the initial state/final state particles. Use momentum conservation at each vertex (i.e. ensure the incoming momentum balances the outgoing momentum) to fix the other momenta; for diagrams containing loops this will not be sufficient to fix all momenta, so some will be left undetermined. Now for each line or vertex in the diagram write down the corresponding factor given by the *Feynman rules* shown in Figs. 2.1-2.3. Whenever a line meets a vertex, corresponding spin/colour/lorentz indices should be identified. Integrate over each undetermined momentum, and sum over all internal spin/colour/lorentz indices (this latter is implicit in the form of the expression

if we use the summation convention). For each closed fermion or ghost loop, an additional factor of -1 is required. For some diagrams, it is also necessary to divide by a *symmetry factor* (the number of ways of switching vertices and lines in the diagram that leave it unchanged).

The sum of the contributions from all diagrams, calculated in this way, should equal $i\mathcal{M}(I \rightarrow F)$. It is then straightforward to square this amplitude and multiply by some kinematic factors (specific to the number of final state particles) to obtain a (fully differential) cross-section. If the momenta and other quantum numbers of the particles are not observed, they can then be summed over, subject to constraints imposed by conservation laws. However, there are clearly an infinite number of diagrams, growing to arbitrary complexity as more vertices are added. Still, looking at Fig. 2.2 one notes that every vertex carries at least one factor of g . So if one is interested in computing \mathcal{M} to a fixed order in g , only a finite number of vertices (and hence a finite number of diagrams) are required.

But how useful is working at a fixed order in g in QCD? The problem is that the interaction between quarks and gluons is strong, in fact so strong that they are confined inside hadrons. This makes it seem doubtful that g would be small enough for a fixed-order approximation to be useful. An even bigger problem arises when we actually try to use the rules given above to compute diagrams with loops. It very often happens that the integration over undetermined momenta diverges, giving nonsensical answers for scattering amplitudes. Remarkably both these problems can be addressed together, as we will see in the next sections.

$$\begin{aligned}
 i \text{ --- } \xrightarrow[p]{\blacktriangleright} \text{ --- } j &= \frac{i(\not{p} + m)}{p^2 - m^2 + i\epsilon} \delta^{ij} \\
 a, \mu \text{ --- } \underbrace{\text{~~~~~}}_p \text{ --- } b, \nu &= \frac{i}{p^2 + i\epsilon} \left(-g^{\mu\nu} + (1 - \xi) \frac{p^\mu p^\nu}{p^2 + i\epsilon} \right) \delta^{ab} \\
 a, \mu \text{ \cdots\cdots\cdots } \xrightarrow[p]{\blacktriangleright} \text{ \cdots\cdots\cdots } b, \nu &= \frac{i\delta^{ab}}{p^2}
 \end{aligned}$$

Figure 2.1: QCD Feynman rules for internal lines.

The figure displays four Feynman diagrams for QCD vertices, each with its corresponding mathematical expression:

- Diagram 1:** A vertex where two fermion lines (solid arrows) meet. One line enters from the bottom left, labeled with index i . The other line enters from the top left, labeled with index j . A gluon line (curly) exits to the right, labeled with index a, μ . The expression is $= -ig\gamma^\mu t_{ij}^a$.
- Diagram 2:** A vertex where a fermion line (solid arrow) enters from the bottom left, labeled with index c, σ . Two gluon lines (curly) enter from the top left, labeled with indices p_2 and p_3 . A gluon line (curly) exits to the right, labeled with index a, μ . The expression is $= -gf^{abc}[(p_1 - p_2)^\sigma g^{\mu\nu} + (p_2 - p_3)^\mu g^{\nu\sigma} + (p_3 - p_1)^\nu g^{\sigma\mu}]$.
- Diagram 3:** A vertex where a fermion line (solid arrow) enters from the bottom left, labeled with index d, ρ . Two gluon lines (curly) enter from the top left, labeled with indices p_2 and p_3 . Two gluon lines (curly) exit to the right, labeled with indices p_1 and p_4 . The expression is $= -ig^2[f^{ace}f^{bde}(g^{\mu\nu}g^{\sigma\rho} - g^{\mu\rho}g^{\nu\sigma}) + f^{ade}f^{bce}(g^{\mu\nu}g^{\sigma\rho} - g^{\mu\sigma}g^{\nu\rho}) + f^{abe}f^{cde}(g^{\mu\sigma}g^{\nu\rho} - g^{\mu\rho}g^{\nu\sigma})]$.
- Diagram 4:** A vertex where two fermion lines (dotted arrows) meet. One line enters from the bottom left, labeled with index b . The other line enters from the top left, labeled with index c . A gluon line (curly) exits to the right, labeled with index a, μ . The expression is $= gf^{abc}p^\mu$.

Figure 2.2: QCD Feynman rules for vertices.

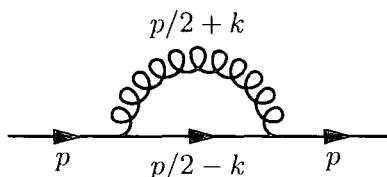
$$\begin{array}{l}
 \begin{array}{c} \longrightarrow \\ p \end{array} \bullet = u(p) \\
 \begin{array}{c} \longleftarrow \\ p \end{array} \bullet = \bar{v}(p) \\
 \begin{array}{c} \text{~~~~~} \\ p \end{array} \bullet = \epsilon^\mu(p) \\
 \bullet \begin{array}{c} \longrightarrow \\ p \end{array} = \bar{u}(p) \\
 \bullet \begin{array}{c} \longleftarrow \\ p \end{array} = v(p) \\
 \bullet \begin{array}{c} \text{~~~~~} \\ p \end{array} = \epsilon^{\mu*}(p)
 \end{array}$$

Figure 2.3: QCD Feynman rules for external lines. The solid point marks the connection to the rest of the diagram; this stands to the right for incoming lines and to the left for outgoing lines. Momentum flow is always left-to-right (i.e. inwards for incoming particles, outwards for outgoing ones). Arrows indicate the direction of fermion number flow.

2.2 UV Singularities

2.2.1 Regularisation

Consider the diagram



$$(2.22)$$

which appears as a sub-diagram in various scattering processes, as well as a contribution to the 2-point function for the quark field. Note that it contains a loop, so there is an undetermined momentum, k . When evaluating this diagram we need to perform an integral over k . For simplicity let us discard the propagator factors coming from the outer fermion propagators, and work with massless quarks. Then, evaluating the diagram using the Feynman rules of Figs. 2.1-2.3 with $\xi = 1$ (Feynman gauge) we obtain

$$\int \frac{d^4 k}{(2\pi)^4} (-igt^a \gamma^\mu) \frac{i(\not{p}/2 - \not{k})}{(p/2 - k)^2 + i\epsilon} (-igt^b \gamma^\nu) \frac{-ig_{\mu\nu} \delta_{ab}}{(p/2 + k)^2 + i\epsilon}. \quad (2.23)$$

The \not{k} can be dropped from the numerator because it gives a contribution which is odd in k . Simplifying the expression using $t^a t^b \delta^{ab} = C_F \mathbb{1}$ ($C_F = 4/3$ for SU(3) QCD) gives

$$-\gamma^\mu \not{p} \gamma_\mu C_F g^2 \int \frac{d^4 k}{(2\pi)^4} \frac{1}{((p/2 - k)^2 + i\epsilon)((p/2 + k)^2 + i\epsilon)}. \quad (2.24)$$

This integral can be evaluated by Wick rotation to Euclidean momenta $k \rightarrow k_E$. For large $|k_E|$, the integrand goes like

$$\frac{d^4 k_E}{(2\pi)^4} \frac{1}{k_E^4} = \frac{d\Omega_3}{(2\pi)^4} \frac{d|k_E|}{|k_E|} \quad (2.25)$$

which fails to converge. If the integral were cut off at $|k_E| \sim \Lambda$, the results would behave like $\ln(\Lambda)$ as $\Lambda \rightarrow \infty$, so this is referred to as a *logarithmic ultraviolet (UV) divergence*.

How can this be interpreted physically? The first step towards doing so is to gain control over the divergence by *regularising* it. We introduce a parameter (such as the above-mentioned Λ), called a regulator, which removes the divergence; the divergence only reappears in the limit when the regulator is removed (e.g. $\Lambda \rightarrow \infty$). Here we will use so-called *dimensional regularisation* [20], where the number of space-time dimensions d is analytically continued away from $d = 4$ to $d = 4 - 2\epsilon$. This renders the integrals finite for $\epsilon > 0$, the divergences showing up as poles in ϵ at $\epsilon = 0$. Changing the dimension of space-time in this way alters the mass dimension of the fields and coupling constants, because the d -dimensional integral of \mathcal{L} is the (dimensionless) action and therefore every term in the \mathcal{L} must have mass dimension d . Looking at the kinetic terms allows us to deduce that $[A] = (d - 2)/2$ and $[\psi] = (d - 1)/2$. The interaction term then gives $[g\bar{\psi}A\psi] = [g] + (d - 1) + (d - 2)/2 = d$, implying that $[g] = (4 - d)/2 = \epsilon$. To achieve this we introduce a scale μ and replace $g \rightarrow \mu^\epsilon g$ (so g is still dimensionless). This breaks the scale invariance that the (massless) theory has at the classical level.

Dimensionally regularising the integral in Eq. (2.24) gives

$$-C_F g^2 \frac{i\not{p}}{(4\pi)^2} \left[\frac{1}{\epsilon} + \ln 4\pi - \gamma_E - \ln \frac{p^2}{\mu^2} + 1 + \mathcal{O}(\epsilon) \right] \quad (2.26)$$

where the 4-dimensional divergence is clearly visible as the simple pole at $\epsilon = 0$.

This diagram is far from unique in containing a divergence. In fact in QCD there are an infinite number of divergent diagrams. How we deal with this physically is the subject of the next subsection.

2.2.2 Renormalization

The key observation that lets us make sense of the divergences is that they all arise when we follow the standard practice in physics of relating our predictions back to the parameters of our theory (in this case, g). However, these parameters are not observable, so this is not necessarily a disaster. It is still possible that the theory

predicts sensible, finite relations between observable quantities. This is indeed the case, and the process that extracts these predictions is called *renormalization*.

To renormalize the theory, we introduce for each field and parameter appearing in the Lagrangian a renormalization factor, Z . This relates it to a “renormalized” counterpart of that field/parameter in terms of which physical predictions will come out finite. In massless QCD this means we have

$$\begin{aligned}\psi_B &= Z_2^{1/2} \psi, \quad A_B^\mu = Z_3^{1/2} A^\mu, \quad \eta_B = (Z_2^\eta)^{1/2} \eta \\ g_B &= Z_g g, \quad \xi_B = Z_\xi \xi\end{aligned}$$

where the subscript B indicates “bare” quantities – i.e. those appearing in the Lagrangian. Using these relations, we can rewrite the Lagrangian

$$\begin{aligned}\mathcal{L}_{\text{QCD}} &= \sum_{f=1}^{N_f} \bar{\psi}_{i,f} (i\not{D}_\mu) \psi_f^i - \frac{1}{4} F_{\mu\nu}^a F_a^{\mu\nu} + \frac{1}{2\xi} (\partial^\mu A_\mu^a)^2 + \bar{\eta}^a (-\partial^2 \delta^{ac} - g \partial^\mu f^{abc} A_\mu^b) \eta^c \\ &\quad - \frac{1}{4} \delta_3 (\partial_\mu A_\nu^a - \partial_\nu A_\mu^a)^2 + \delta_2 \bar{\psi} (i\not{\partial}) \psi - \delta_2^\eta \bar{\eta}^a \partial^2 \eta^a \\ &\quad + g \delta_1 \bar{\psi} \gamma^\mu A_\mu^a t^a \psi - g \delta_1^{3g} f^{abc} (\partial_\mu A_\nu^a) A_\mu^b A_\nu^c \\ &\quad - g^2 \delta_1^{4g} (f^{cab} A_\mu^a A_\nu^b) (f^{ecd} A_\mu^c A_\nu^d) - g \delta_1^\eta \bar{\eta}^a f^{abc} \partial^\mu A_\mu^b \eta^c.\end{aligned}$$

This breaks the Lagrangian into a piece looking just like the bare Lagrangian but written in terms of renormalized quantities, and a set of *counterterms*. The coefficients of the counterterms $\delta_1, \delta_2, \dots$ are functions of the renormalization factors (for details, see Ref. [14], Ch. 10 and 16).

Deriving Feynman rules from this new Lagrangian gives us a set identical to those shown on Figs. 2.1-2.3 but written in terms of the renormalized parameters and fields, plus a set of new counterterm vertices. Some of these are shown on Fig. 2.4. When we now draw the diagrams for a scattering amplitude or correlation function, these vertices need to be included. For example, whenever evaluating a diagram containing the sub-diagram illustrated in Eq. (2.22), one has to consider also the diagram where the external quark lines connect not to the quark-gluon

loop, but to the first counterterm vertex of Fig. 2.4. The total contribution from both possibilities is

$$-C_F g^2 \frac{i\not{p}}{(4\pi)^2} \left[\frac{1}{\epsilon} + \ln 4\pi - \gamma_E - \ln \frac{p^2}{\mu^2} + 1 + O(\epsilon) \right] + i\not{p}\delta_2. \quad (2.27)$$

By choosing a suitable ϵ -dependent value for δ_2 , the $1/\epsilon$ pole can be subtracted. This part of the diagram will then be finite in the limit $\epsilon \rightarrow 0$ (i.e. in 4 dimensions). It is possible to show to all orders in perturbation theory that a single choice for the counterterm coefficients $\delta_1, \delta_2, \dots$ is capable of removing all the UV divergences from every physical prediction (in other words, QCD is *renormalizable* [21]). The divergences only appear in the relations between these renormalized parameters and their bare counterparts, which are unobservable. Therefore one can take the limit $\epsilon \rightarrow 0$ with the *renormalized* parameters fixed. This produces physical predictions which are finite functions of the renormalized parameters.

However, this procedure is not uniquely defined because although the singular parts of the counterterm coefficients are fixed by requiring a finite result, their finite parts are arbitrary. The precise choice of counterterms is called a *renormalization scheme* (RS). Coupling this with a choice of the *renormalization scale* μ we arrive at a full *renormalization prescription* (RP). This describes precisely how the renormalized parameters are related to the bare parameters. Fortunately, this freedom in choosing an RP does not lead to an ambiguity in the physical content of the theory. The reason is that a choice of RP can be thought of as a change in the *definition* of the theory's parameters: the parameters in two different RP's are said to differ by a *finite renormalization*. If we compensate for this fact by suitably altering the value of each parameter when the RP is changed, the choice of RP becomes purely conventional.

Unfortunately, this invariance of predictions under a change of RP does not hold for the perturbative approximations discussed in Subsection 2.1.2. In particular, problems arise from the dependence of the renormalized coupling on the

RP, because the compensation between the effects of changing the counterterms and changing the value of the coupling requires cancellations between different orders of perturbation theory. To see this, note that in perturbation theory the renormalized coupling equals the bare coupling at leading order (because there are no loops, and hence no renormalization, at leading order). Therefore it can be expanded in terms of the bare coupling as follows

$$g = g_B + v_1 g_B^2 + \dots \quad (2.28)$$

where the coefficients v_n depend on the RP. Suppose we compute an observable quantity S whose bare perturbation series is

$$S = g_B + S_1 g_B^2 + \dots \quad (2.29)$$

The renormalized perturbation series for S will be

$$S = g + (S_1 - v_1)g^2 + \dots \quad (2.30)$$

Although S is itself independent of the RP, its truncation to order g^2 is not. For example, varying v_1 leads to a change of order g^3 .

This makes it vital to choose the “correct” RP when using perturbation theory if reasonable answers are to be obtained. The first step in doing this is to find how the coupling depends on the RP.

2.2.3 The Beta-Function

An important aspect of the choice of RP is the choice of the scale μ which breaks the classical scale invariance of the theory (here μ appeared through the shift $g \rightarrow \mu^\epsilon g$ made when using dimensional regularisation, but a similar scale will appear however we regularise the theory). The dependence of the coupling on μ is governed by the so-called beta-function:

$$\frac{\partial g}{\partial \ln \mu} = \beta(g). \quad (2.31)$$

combination $\mu^\epsilon g_B$, we arrive at the Callan-Symanzik equation

$$\left(\frac{\partial}{\partial \ln \mu} + \beta(g) \frac{\partial}{\partial g} - n\gamma_A(g) - m\gamma_\psi(g) + \delta(g) \frac{\partial}{\partial \xi} \right) G^{(n,m)}(\{x_i, y_j\}; \xi, \mu, g(\mu)) = 0. \quad (2.35)$$

The functions γ_A and γ_ψ are anomalous dimensions for the gluon and quark fields respectively. They satisfy

$$\gamma_A(g) = -\frac{1}{2} \frac{\partial \ln Z_3}{\partial \ln \mu}, \quad \gamma_\psi(g) = -\frac{1}{2} \frac{\partial \ln Z_2}{\partial \ln \mu}. \quad (2.36)$$

$\delta(g)$ describes the evolution of the gauge parameter with the renormalization scale

$$\delta(g) \equiv \frac{\partial \xi}{\partial \ln \mu}. \quad (2.37)$$

Calculating a sufficient set of Green's functions then allows one to solve Eq. (2.35) for β , γ_A , γ_ψ and δ . In particular, one can obtain a perturbative expansion for the beta-function governing the evolution of the coupling. At leading order (one-loop) in SU(3) QCD this is

$$\frac{\partial g}{\partial \ln \mu} = \beta(g) = -\frac{g^3}{(4\pi)^2} \left(11 - \frac{2N_f}{3} \right) + O(g^5). \quad (2.38)$$

It is often more convenient to work instead with the expansion parameter $a \equiv g^2/4\pi^2$ (the ‘‘couplant’’) which puts the beta-function coefficients in a very simple form. At leading order, for SU(3) QCD:

$$\frac{\partial a}{\partial \ln \mu} = \beta(a) = -(11 - \frac{2N_f}{3})a^2 + O(a^3). \quad (2.39)$$

For $N_f \leq 16$, the sign of the beta-function is negative, which means that the couplant a decreases as the renormalization scale μ is increased (so long as there is some μ such that $a(\mu)$ is small enough for the leading order term to dominate the beta-function). This can be seen explicitly if we solve the one-loop beta function equation Eq. (2.39) to obtain

$$a(\mu) = \frac{1}{b \ln \frac{\mu}{\Lambda}}, \quad b = 11 - \frac{2N_f}{3} \quad (2.40)$$

where Λ is the undetermined parameter one expects to find when solving a first order ODE.

Going beyond leading order the beta-function takes the form

$$\frac{\partial a}{\partial \ln \mu} = \beta(a) = -ba^2(1 + ca + c_2a^2 + c_3a^3 + \dots). \quad (2.41)$$

It turns out that this equation is also relevant for understanding the rest of the RP-dependence of a , the RS dependence (i.e. the dependence on the choice of counterterm coefficients) [22]. The first two coefficients, b and c , are independent of the RS as can easily be checked by making a general transformation $a \rightarrow a' = a + O(a^2)$, which is the effect a change of RS has on a (because $a = a_B + O(a_B^2)$, c.f. Eq. (2.28)). In contrast, the higher order coefficients $\{c_2, c_3, \dots\}$ depend on the RS. In fact, if we restrict our attention to physical quantities (rather than Green's functions) so the gauge parameter can be ignored, the RS can be labelled by the values of these coefficients, along with the scale Λ which appears when we solve Eq. (2.41), as it did when we solved Eq. (2.39).²

In fact the couplant does not depend separately on μ and Λ , because by simple dimensional analysis the solution to Eq. (2.41) must be a function of μ/Λ . Therefore to describe the RP through a set of independent parameters one can use $\{\tau, c_2, c_3, \dots\}$ with $\tau \equiv b \ln(\mu/\Lambda)$.

Something slightly odd has happened here, because this set of parameters fixes not just the definition of a in terms of its bare counterpart a_B , but its actual *value*. What happened to the free dimensionless parameter in the QCD Lagrangian? It turns out that it has been eliminated by the process of renormalization, and converted into a freedom in the overall energy scale of the theory – an effect called dimensional transmutation. To see this, imagine we compute some dimensionless observable R which depends on a and an overall energy scale Q . The perturbative

²This is evident from the fact that these parameters, along with μ , are sufficient to fix a . Therefore, since this is the only parameter of the (massless) theory, they totally fix the RS.

coefficients are dimensionless and can only depend on μ and Q , so we must find

$$R = R(a(\mu), \mu/Q). \quad (2.42)$$

If we set $\mu = Q$ (which we can do as μ has no effect on the physics) this reduces to

$$R = R(a(Q), 1), \quad (2.43)$$

which inherits all its dependence on Q through a – therefore the scale for its energy evolution is set by Λ . This is the true parameter we must fit from experimental measurements of R . But isn't Λ supposed to be a parameter describing the RP, which should not affect the physics? It turns out that although different values of Λ differentiate between different schemes, the actual value of Λ in a given scheme cannot be uniquely determined from the recipe we use to renormalize the theory. There is a freedom in rescaling the Λ values in every scheme simultaneously which functions as a free, dimensionful parameter. This will be further discussed in Chapter 3.

Another important consequence of Eq. (2.43) is that it gives the evolution of a some physical significance. It implies that as $Q \rightarrow \infty$, the QCD contributions to R (involving powers of a) will decrease. This is called *asymptotic freedom* [23, 24, 25] and was one of the most important clues in picking out QCD as the correct theory of the strong force. It also answers the question raised at the end of Subsection 2.1.2 about the validity of perturbation theory in QCD where the interaction is very strong. It is true that for low energies Q (in practice of order a few GeV or so) perturbation theory fails because $a(Q)$ is large (in some appropriate scheme; this will be discussed further in Chapter 3). However, as we increase Q , a exhibits the fall-off approximately illustrated in Eq. (2.40), allowing perturbation theory to come into its own.

Note that in the original equation, Eq. (2.42), the argument of a is the unphysical scale μ . As R is independent of μ , it is perfectly legitimate to send $\mu \rightarrow \infty$, in

which case a goes to zero without requiring Q to be large. However, this does not allow one to improve perturbation theory, because R also depends on μ through μ/Q . In fact

$$\frac{d}{d \ln \mu} R(a(\mu), \mu/Q) = \left(\frac{\partial}{\partial \ln \mu} + \beta(a) \frac{\partial}{\partial a} \right) R(a(\mu), \mu/Q) = 0. \quad (2.44)$$

Expanding this in a allows one to deduce how the perturbative coefficients of r depends on μ : the coefficient of a^n is a degree $n-1$ polynomial in $\ln(\mu/Q)$. Therefore if one takes μ very different from Q the higher order perturbative coefficients will become large, spoiling the convergence of the perturbation series. It seems best to set $\mu = Q$ (the so-called renormalization group (RG) improvement of perturbation theory), but things are actually not so straightforward (see Section 3.2).

2.2.4 Hadronization

So far we have discussed how to obtain perturbative predictions for scattering amplitudes between states containing quarks and gluons. However, real quarks and gluons (collectively partons) are actually confined inside hadrons. What relevance, then, do these partonic scattering amplitudes have? Because of asymptotic freedom, the strength of the QCD coupling is effectively smaller for processes occurring at higher energies. Therefore, at these energies quarks and gluons behave essentially like free particles. If we consider a process such as the annihilation of an electron and a positron to produce hadrons at low centre-of-mass energy (e.g. $Q \sim 1\text{GeV}$), the small momentum transfers involved will ensure that the effective QCD coupling $a(Q)$ is strong, and an analysis in terms of quarks and gluons will be impractical. However, as the centre-of-mass energy Q is increased, $a(Q)$ will decrease until the basic e^+e^- annihilation process can be described in terms of weakly coupled quarks and gluons. These partons, however, will never be observed coming out from the scattering event. Once the initial hard scattering has occurred, soft, long-distance interactions will take over, transforming the emerging

partons into jets of hadrons. This process is called *hadronization*. Various phenomenological models have been constructed to describe hadronization [2], but it is not well understood from a fundamental point of view.

Processes with incoming hadrons can also be described in terms of quarks and gluons. This is briefly discussed in Section 2.4.

2.2.5 Minimal Subtraction Schemes

The simplest renormalization scheme to use in practice is the Minimal Subtraction (MS) scheme [7]. This involves fixing the counterterms to subtract only the divergent $1/\epsilon$ terms. For example, Eq. (2.27) would allow us to fix δ_2 at order a to be

$$\delta_2^{\text{MS}} = \frac{C_F a}{4} \frac{1}{\epsilon}. \quad (2.45)$$

More popular in practice is the Modified Minimal Subtraction scheme ($\overline{\text{MS}}$), where one also subtracts the $\ln 4\pi - \gamma_E$ which invariably appears from dimensionally regulating divergent integrals. In this scheme

$$\delta_2^{\overline{\text{MS}}} = \frac{C_F a}{4} \left(\frac{1}{\epsilon} + \ln 4\pi - \gamma_E \right). \quad (2.46)$$

2.3 IR Singularities

2.3.1 Cross-Section for $e^+e^- \rightarrow \bar{q}q$

In the last section it was explained how the UV divergences could be removed from the predictions of QCD by absorbing them into singularities in the unobserved parameters of the theory. However, these are not the only divergences that can appear in Feynman diagram calculations. To show this we will take as an example the cross-section for the process $e^+e^- \rightarrow \bar{q}q$ (at leading order in the QED coupling).

A cross-section is obtained as a phase space integral over the absolute square of the corresponding amplitude $|\mathcal{M}|^2$, and if the beams are unpolarized and no polarization information is measured in the final state (as we assume here) one must average over initial spins and sum over final spins. This can be elegantly done using the method of cut diagrams. In this, the product of one diagram and the complex conjugate of another is drawn as a single diagram making use of “cut propagators” arising from the spin sums $\sum_s u^s(p)\bar{u}^s(p) = \not{p} + m$ and $\sum_s v^s(p)\bar{v}^s(p) = \not{p} - m$. Note that there is no integration over the momenta carried by cut propagators. The cut diagram for the leading order (LO) $\mathcal{O}(a^0)$ contribution to $\sigma(e^+e^- \rightarrow \bar{q}q)$ is shown in Fig. 2.5. Taking all masses to be negligible, the cut diagram can be easily evaluated using the Feynman rules of QCD and QED (which resemble those of QCD but with no colour factors or gauge boson self-interactions, and with $g^2/4\pi \rightarrow \alpha \simeq 1/137$ – the “fine structure constant”).

Finally performing the phase-space integral yields

$$\sigma_{\text{LO}}(e^+e^- \rightarrow \bar{q}q) = \frac{4\pi\alpha^2}{s} \sum_f Q_f^2 \equiv \sigma_0 \quad (2.47)$$

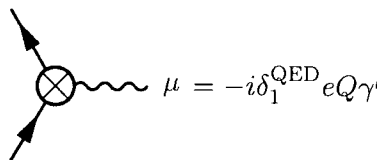
where $s = (q_1 + q_2)^2$ is the square of the centre of mass energy. Q_f is the charge of the quark of flavour f in units of e (e.g. $Q_u = +2/3$).

Next, consider the next-to-leading order (NLO) $\mathcal{O}(a)$ corrections to this cross-

section. These arise from the cut diagram shown in Fig. 2.6 (plus its complex conjugate). Unlike the LO diagram, this contains a loop, so we must integrate over the momentum k . The evaluation of the diagram therefore contains a factor

$$\int \frac{d^4 k}{(2\pi)^4} \frac{(\not{p}_1 + \not{k})}{(p_1 + k)^2 + i\epsilon} \gamma^\mu \frac{(\not{p}_2 - \not{k})}{(p_2 - k)^2 + i\epsilon} \frac{1}{k^2 + i\epsilon}. \quad (2.48)$$

For large Euclidean momenta, we again find a logarithmic UV divergence ($d^4 k_E \cdot k_E^2/k_E^6 \sim d|k_E|/|k_E|$). This can be cancelled by adjusting the $O(a)$ part of the QED counterterm vertex for a quark of charge Q



$$\mu = -i\delta_1^{\text{QED}} eQ\gamma^\mu \quad (2.49)$$

so as to fix the $\gamma q\bar{q}$ vertex at zero momentum to be $-ieQ\gamma^\mu$ (this amounts to defining the renormalized QED coupling in terms of the charge measured on long distance scales e.g. in the Coulomb potential). However, there is also a divergence for *small* k . To see this, note that we are assuming massless quarks, so $(p_1 + k)^2 = 2p_1 \cdot k + k^2$, which is $O(k)$ in the $k \rightarrow 0$ limit (and similarly for $(p_2 - k)^2$). So as $k \rightarrow 0$, the denominator falls like k^4 . If we insert an infra-red cutoff at $k_E = m$, the loop integral diverges like $\ln(m)$ – a logarithmic infrared (IR) divergence. This is clearly going to cause problems. For the moment, let us regulate it by adding a small gluon mass m_g . Evaluating the full renormalized diagram then gives

$$\sigma_{\text{NLO}}(e^+e^- \rightarrow \bar{q}q) = \sigma_0 \left(1 + \frac{3C_F a}{2} \left[L^2 + 3L - \frac{\pi^2}{3} + \frac{7}{2} + O\left(\frac{m_g^2}{s}\right) \right] \right) \quad (2.50)$$

where $L = \log(m_g^2/s) = \log(m_g^2/(q_1 + q_2)^2)$ diverges as the IR regulator m_g is sent to zero.

The fact that this cross-section diverges in the physical $m_g = 0$ case seems disastrous, but in fact it is just a sign that the quantity $\sigma(e^+e^- \rightarrow \bar{q}q)$ is not truly observable. In reality, no experiment could distinguish a simple $q\bar{q}$ final state from one accompanied by any number of other particles which are either

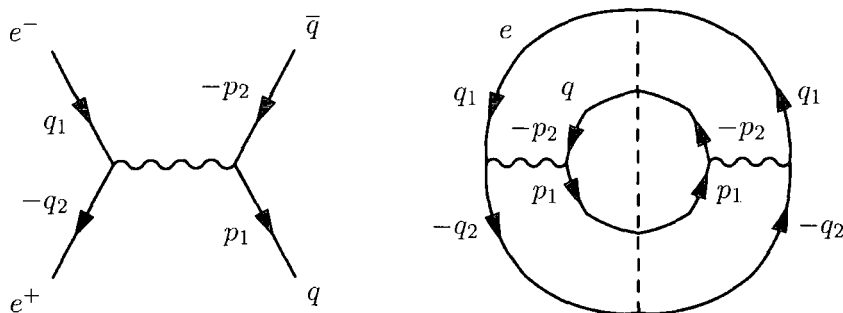


Figure 2.5: LO diagrams used in calculating $\sigma(e^+e^- \rightarrow \bar{q}q)$. On the left is the contribution to the amplitude \mathcal{M} , on the right the contribution to $|\mathcal{M}|^2$ obtained by joining this diagram to its mirror image with a cut. The cut quark propagators are given in the text. The momenta are taken to point in the direction of fermion number flow.

soft or collinear with the quark/anti-quark (of course, as noted in Subsection 2.2.4, the observed final states actually contain hadrons, but this doesn't affect the argument: the hadrons corresponding to a $q\bar{q}$ state would be indistinguishable from those corresponding to a $q\bar{q}$ +soft/collinear final state). Therefore, if we want to compute a physical cross-section we need to include contributions from emission of additional soft or collinear particles. The simplest quantity that illustrates this is the total cross-section for $e^+e^- \rightarrow \text{hadrons}$.

2.3.2 Inclusive Hadron Production

Consider the cross-section $\sigma(e^+e^- \rightarrow \text{hadrons})$. This is referred to as an “inclusive” observable, because all possible hadronic states are included. At $O(\alpha)$, it receives the leading order and virtual next-to-leading order corrections described in Subsection 2.3.1, but it also receives contributions from the emission of a single real gluon. These can be computed from the cut diagrams shown in Fig. 2.7. If we ignore the overall orientation of the final state, it can be described by the

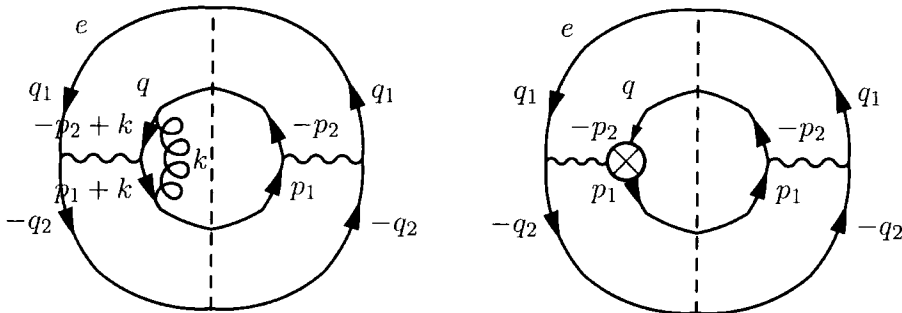


Figure 2.6: On the left is the cut diagram for the $O(a)$ contribution to $|\mathcal{M}|^2$ for the process $e^+e^- \rightarrow \bar{q}q$. There is also a contribution given by the complex conjugate (left-right reflection) of this diagram. The right hand diagram shows how the $\gamma q\bar{q}$ counterterm vertex cancels the UV singularities from the loop integration on the left.

dimensionless quantities

$$x_i = \left. \frac{p_i^0}{q_1^0} \right|_{\text{CMS}} \quad (i = 1, 2, 3) \quad (2.51)$$

which satisfy $x_1 + x_2 + x_3 = 2$, $x_i < 1$. Evaluating these diagrams then allows one to calculate the differential cross-section

$$\frac{d\sigma}{dx_1 dx_2}(e^+e^- \rightarrow q\bar{q}g) = \sigma_0 \frac{C_F a}{2} \frac{x_1^2 + x_2^2}{(1-x_1)(1-x_2)}. \quad (2.52)$$

This becomes singular as $x_1 \rightarrow 1, x_2 < 1$ (gluon becomes collinear with anti-quark) and $x_2 \rightarrow 1, x_1 < 1$ (gluon becomes collinear with quark), and also as $x_1 \rightarrow 1, x_2 \rightarrow 1$ (gluon becomes soft).

The singularities in Eq. (2.52) cause its integral, the cross-section $\sigma(e^+e^- \rightarrow q\bar{q}g)$, to diverge. Just as with $\sigma(e^+e^- \rightarrow q\bar{q})$, this is a sign that this is an unphysical cross-section. Instead, we wish to calculate the physical cross-section $\sigma(e^+e^- \rightarrow \text{hadrons}) = \sigma(e^+e^- \rightarrow q\bar{q}) + \sigma(e^+e^- \rightarrow q\bar{q}g) + \dots$. This is finite, so singularities must cancel between the virtual and real gluon contributions. To see this cancellation explicitly, we need to add a gluon mass regulator to our calculation

of Eq. (2.52), obtaining

$$\begin{aligned} \frac{d\sigma}{dx_1 dx_2}(e^+e^- \rightarrow \text{hadrons}) &= \sigma_0 \frac{C_F a}{2} \left(\frac{(x_1 + \frac{m_g^2}{s})^2 + (x_2 + \frac{m_g^2}{s})^2}{(1-x_1)(1-x_2)} \right. \\ &\quad \left. - \frac{m_g^2}{s} \left[\frac{1}{(1-x_1)^2} + \frac{1}{(1-x_2)^2} \right] \right). \end{aligned} \quad (2.53)$$

Integrating this over the allowed phase space (which is now slightly reduced because of the gluon mass so as to avoid the divergent regions) we arrive at a cross-section

$$\sigma_{\text{LO}}(e^+e^- \rightarrow \bar{q}qg) = \sigma_0 \frac{3C_F a}{2} \left[-L^2 - 3L + \frac{\pi^2}{3} - 3 + \mathcal{O}\left(\frac{m_g^2}{s}\right) \right]. \quad (2.54)$$

Combining this with Eq. (2.50), the logarithmic terms cancel and the gluon mass can safely be set to zero. We are left with the simple result

$$\begin{aligned} \sigma_{\text{NLO}}(e^+e^- \rightarrow \text{hadrons}) &= \sigma_0 \left(1 + \frac{3C_F a}{4} \right) \\ &= \sigma_0 (1 + a). \end{aligned} \quad (2.55)$$

Dividing this by the cross-section $\sigma(e^+e^- \rightarrow \mu^+\mu^-)$, which receives no QCD corrections (at $\mathcal{O}(\alpha_{\text{QED}}^2)$), we obtain the R -ratio described in Chapter 1:

$$R_{\text{NLO}}(\sqrt{s}) = \frac{\sigma_{\text{NLO}}(e^+e^- \rightarrow \text{hadrons})}{\sigma(e^+e^- \rightarrow \mu^+\mu^-)} = 3 \left(\sum_f Q_f^2 \right) (1 + a). \quad (2.56)$$

2.3.3 Exclusive Processes and IR Safety

In the last subsection the cancellation of IR singularities between virtual and real corrections was demonstrated for the total cross-section $\sigma(e^+e^- \rightarrow \text{hadrons})$ at $\mathcal{O}(a)$. However, the phenomenon is much more general, and we can ask what exactly characterises the quantities where the cancellation occurs. Recall that the real emission cross-section Eq. (2.52) exhibits singularities only when the gluon becomes soft or collinear with one of the other particles. It is the contributions

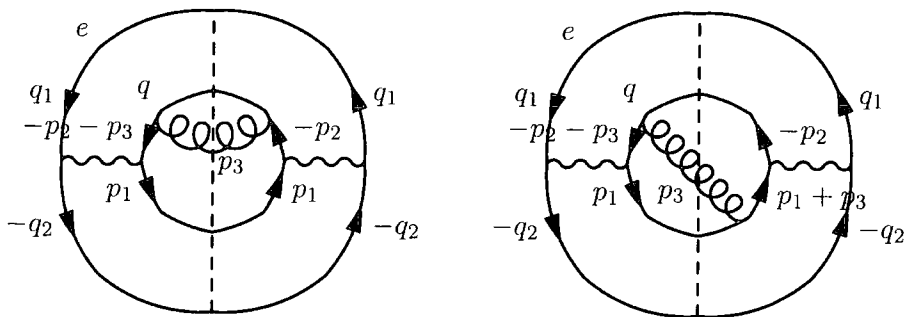


Figure 2.7: Cut diagrams for the process $e^+e^- \rightarrow q\bar{q}g$ at order a . There are also an additional two diagrams where the gluon is attached differently to the inner loop (these look like reflections of the diagrams shown). The cut gluon propagator is $-g^{\mu\nu}$.

from these regions of phase space that cancel the divergences in the virtual corrections. In fact this can be shown to extend to all orders of perturbation theory, and to all processes (although there are subtleties when there are hadrons in the initial state, see Section 2.4). Therefore, any quantity which always sums contributions from the soft and collinear real emissions with the virtual corrections to the process without real emissions will be free of IR singularities.

Consider a variable O which depends on the final state momenta $\{p_i\}$ (but not on their arbitrary ordering). Given the definition of O we can define the differential cross-section $\frac{d\sigma}{dO}$. How can we guarantee that this will be free of IR singularities? The answer is to require O to be insensitive to the addition of soft particles to the final state, and to the collinear splitting of final state particles. That is

$$\begin{aligned} \lim_{p_s \rightarrow 0} O(p_1, p_2, \dots, p_n, p_s) &= O(p_1, p_2, \dots, p_n) \\ \lim_{p_c \rightarrow x p_n} O(p_1, p_2, \dots, p_n, p_c) &= O(p_1, p_2, \dots, p_n + p_c). \end{aligned} \quad (2.57)$$

Such a variable is said to be *infrared safe*. The reason this works is that $\frac{d\sigma}{dO}(o)$ is

computed by summing the fully differential cross-section over all final states with $O = o$, so for an IR safe O the contributions from soft/collinear real emissions are always added to the contributions without such emissions.

A very important class of infrared safe variables are the so-called event shapes which are the subject of this thesis. The prototypical example of an event shape is Thrust, defined in the centre-of-mass frame in e^+e^- annihilation:

$$T = \max_{\vec{n}} \frac{\sum_i |\vec{p}_i \cdot \vec{n}|}{\sum_i |\vec{p}_i|}. \quad (2.58)$$

For a $q\bar{q}$ final state, $T = 1$. Considering final states with more and more evenly spread emissions, T decreases, reaching a minimum value of $1/2$ for an isotropic event. Because T is IR safe, the differential cross-section $\frac{d\sigma}{dT}$, and the corresponding distribution $\frac{1}{\sigma} \frac{d\sigma}{dT}$, are finite. However, the IR singularities leave a nasty legacy in the perturbative coefficients for $\frac{d\sigma}{dT}$. This is easiest to understand at $O(a)$. We can convert Eq. (2.52) into $\frac{d\sigma}{dT}$ by noting that for a $q\bar{q}g$ state

$$T = \max(x_1, x_2, x_3). \quad (2.59)$$

The distribution of T as $T \rightarrow 1$ therefore comes from integrating Eq. (2.52) along a path in the (x_1, x_2) plane that approaches the singular region $x_1, x_2 \sim 1$. This causes the $O(a)$ contribution to $\frac{d\sigma}{dT}$ to blow up like $\log(1-T)/(1-T)$ as $T \rightarrow 1$. This divergence is not unexpected, because when T equals 1 exactly, the $q\bar{q}$ final state will make an $O(a)$ IR-divergent contribution to the T -distribution. The integral over the whole distribution is finite, so the contribution from the real-emission $q\bar{q}g$ final state must be IR-divergent when integrated over all T . More specifically, the finiteness of the observables

$$R_T(T_0) = \frac{1}{\sigma_{\text{tot}}} \int_{T_0}^1 dT \frac{d\sigma}{dT}, \quad \frac{1}{2} < T_0 < 1 \quad (2.60)$$

($R_T(T_0)$ is the fraction of events with $T > T_0$) implies that the real-emission contribution must diverge as $T \rightarrow 1$.

Although $R_T(T_0)$ is observable and hence IR-finite for all $T_0 < 1$, it too has diverging perturbative coefficients as $T_0 \rightarrow 1$. These arise because imposing the condition $T > T_0$ limits the cancellation of real and virtual IR singularities. When $T_0 = 1/2$, the integral in Eq. (2.60) runs over all the possible final states; in this case, the real and virtual corrections cancel almost exactly, leaving over the small contribution shown to $O(a)$ in Eq. (2.55). However, as T_0 is increased, the integral in Eq. (2.60) misses more and more of the phase space for emission of a real gluon. The cancellation between real and virtual singularities is impaired, and the perturbative coefficients grow as a result.

This divergence in the distribution is clearly unphysical (for one thing, $R_T(T_0)$ is a fraction, so it must lie in the interval $[0, 1]$). Indeed, the actual behaviour of the thrust distribution is very different from what this leading order calculation might suggest. Rather than growing as $T \rightarrow 1$, it first rises to a peak and then falls off to zero. This conclusion can be obtained from perturbation theory if one takes into account the fact that the growth in perturbative coefficients is not unique to LO. At higher orders, emission of soft/collinear gluons is also enhanced in a manner similar to Eq. (2.52), so emission of n gluons gives factors like $a^n \log^{2n-1}(1-T)/(1-T)$ in the distribution, and $a^n \log^{2n}(1-T_0)$ in $R_T(T_0)$. The effective expansion parameter for the perturbative series becomes $a \log^2(1-T)$, damaging its convergence for $T \sim 1$. To fix this one requires some form of resummation. For example, one can show that including the leading logs at each order of perturbation theory gives

$$R_T(T_0) = \exp(-C_F \log^2(1-T_0)a). \quad (2.61)$$

As $T_0 \rightarrow 1$ this gives $R_T \rightarrow 0$ even though all fixed order approximations to R_T diverge. Resummations like this will be further discussed in Chapter 4.

It is worth noting that although resummed perturbation theory gives the correct qualitative behaviour for the thrust distribution near $T = 1$, its detailed shape is expected to be subject to large non-perturbative corrections. This is because

gluon emissions at low transverse momentum dominate the distribution for $T \sim 1$, and these are not expected to be under perturbative control due to the low scales involved.

2.4 Initial State Hadrons

2.4.1 Initial State IR Singularities

In the last subsection we saw how IR singularities arising in soft or collinear final-state emissions cancel with those from virtual corrections. However, there is another kind of IR singularity, which appears when an *initial state particle* emits collinear radiation. Just like all IR singularities, it appears because an internal propagator goes on-shell and leads to a singular cross-section.

In the case of collinear radiation from a final state particle, we argued that no experiment could distinguish the state with radiation from the state without, so the cross-sections needed to be combined, allowing the divergence to cancel. However, this is not the case for initial state collinear radiation – it is not collinear to anything in the final state, so there is no problem of principle in detecting it. Thus, there seems to be no possibility of removing the divergence from physically observable cross-sections.

2.4.2 Factorisation

The solution to this problem comes from recognising that it is impossible to carry out a scattering experiment with incoming quarks or gluons because they are confined inside hadrons. The closest we can come is to consider a scattering experiment with hadrons in the initial state e.g. electron-proton (ep) scattering. Because the proton is a composite object made of partons, ep scattering can be analyzed in terms of all the possible partonic subprocesses, weighted by factors giving the probability of a particular parton being found in the proton with a

given momentum.

For a high energy process we can treat the proton as massless. This means it will have an almost lightlike momentum P , and all its constituents will have momenta collinear with this (one would expect the constituents to have a typical transverse momentum of order the inverse width of the proton, which is similar to its mass and so negligible here). Therefore to characterise a constituent one need give only its species (gluon, up quark, down quark...) and its momentum fraction ξ (which is a number between 0 and 1 such that its momentum is $p = \xi P$). We denote the probability of finding a parton of species a with momentum fraction ξ by

$$f_a(\xi). \quad (2.62)$$

These are the *parton distribution functions* (PDFs).

Because of asymptotic freedom, for large momentum transfers we would expect the quarks and gluons to behave like weakly interacting particles. This should allow us to calculate the cross-section $\sigma(ep \rightarrow X)$ for a process $ep \rightarrow X$ in terms of the partonic cross-sections $\hat{\sigma}(ea \rightarrow X)$ (where a represents a generic parton) and the PDFs

$$\sigma(ep \rightarrow X) = \sum_a \int_0^1 d\xi f_a(\xi) \hat{\sigma}(ea \rightarrow X). \quad (2.63)$$

This is called *factorisation*. $\hat{\sigma}$ should be calculable in terms of QCD Feynman diagrams – but these diagrams will have initial state quarks and gluons, and therefore initial state collinear singularities. So, even requiring the initial state to contain only physical particles like hadrons does not remove these singularities from the predictions of the theory.

2.4.3 Removing the Singularities

The way in which initial state collinear singularities can finally be removed from the predictions of the theory closely parallels the method of renormalization sketched

in Subsection 2.2.2. The key idea is to recognise that the only observable quantity in Eq. (2.63) is $\sigma(ep \rightarrow X)$. The diagrams that go into calculating the unobservable quantity $\hat{\sigma}(ea \rightarrow X)$ have singularities in them, but all this means is that there are singularities in the relation between $\sigma(ep \rightarrow X)$ and the PDFs $f_a(\xi)$, which are themselves unobservable. To avoid singularities in the physical predictions, the PDFs can be made singular in such a way that the observable cross-section $\sigma(ep \rightarrow X)$ comes out finite. Accordingly, we rewrite Eq. (2.63)

$$\sigma(ep \rightarrow X) = \sum_a \int_0^1 d\xi f_a^B(\xi) \hat{\sigma}^B(ea \rightarrow X) \quad (2.64)$$

where B indicates that these are “bare” quantities that may be singular. The singularities can be regulated by adding a small gluon mass m_g , leading to singularities of the form $\log(m_g^2/s)$, or by using dimensional regularisation which leads to poles in ϵ . In any case, these singularities can be cancelled by choosing a suitably singular value for $f_a^B(\xi)$ (which is playing a role similar to the bare coupling in renormalization) in terms of the finite $f_a(\xi)$ (which is playing a role similar to the renormalized coupling). The way in which we do this defines a factorisation prescription (FP). This consists of a scale, called the factorization scale M , and a factorization scheme (FS). M appears either through the shift $g \rightarrow M^\epsilon g$ in dimensional regularisation, or in the process of splitting the divergent term $\log(m_g^2/s) = \log(m_g^2/M^2) + \log(M^2/s)$ to remove the divergence from $\hat{\sigma}^B$. The FS specifies the details of how much of the finite parts of $\hat{\sigma}^B$ are absorbed into the definition of $f_a(\xi)$ at each order in perturbation theory.

After the divergences have been removed, we are left with a finite expression

$$\sigma(ep \rightarrow X) = \sum_a \int_0^1 d\xi f_a(\xi, M, \text{FS}) \hat{\sigma}(ea \rightarrow X, M, \text{FS}). \quad (2.65)$$

Note that $\sigma(ep \rightarrow X)$ is independent of the FP; just like the RP the FP is arbitrary and does not affect the physical content of the theory. However, the cancellation of the FP-dependence between the various f_a and $\hat{\sigma}$'s on the RHS of Eq. (2.65)

requires all orders of perturbation theory to be present. Just as with the RP, finite order approximations will exhibit an unphysical dependence on the FP.

2.4.4 DGLAP Evolution

We saw in Subsection 2.2.3 that the renormalized coupling evolves with the renormalization scale according to the beta-function. The “renormalized” PDFs $f_a(\xi, M, FS)$ similarly evolve with the *factorization* scale according to a system of integro-differential equations called the Dokshitzer-Gribov-Lipatov-Altarelli-Parisi (DGLAP) equations

$$\frac{df_a(\xi, M, FS)}{d \ln M} = a(M) \int_{\xi}^1 \frac{dz}{z} \sum_b P_{a \leftarrow b}^{FS}(z) f_b\left(\frac{\xi}{z}, M, FS\right). \quad (2.66)$$

The functions $P_{a \leftarrow b}^{FS}(z)$ are called *splitting functions*. They have a perturbative expansion

$$P_{a \leftarrow b}^{FS}(z) = P_{a \leftarrow b}^{(0)}(z) + a(M) P_{a \leftarrow b}^{(1), FS}(z) + \dots \quad (2.67)$$

where the LO term is independent of the FS, and the higher order terms depend on (and in fact label) the FS (note the similarity to the beta-function).

As remarked above, after rendering $\hat{\sigma}$ finite, it will contain terms like $\log(M^2/s)$ in its perturbation series (indeed an additional power of this log at every order). These can be removed by setting the unphysical scale $M \propto \sqrt{s}$ – this resembles RG-improvement (see Subsection 2.2.3), and should improve the convergence of the perturbation series.

Because of the factor $a(M)$ in Eq. (2.66), the behaviour of the PDFs cannot be computed in QCD perturbation theory for small M . Instead, one treats the PDFs at some low scale (e.g. 1GeV) as an additional set of phenomenological parameters to be fitted to data, by writing the PDFs in terms of some simple, physically motivated functions of a handful of parameters. Because the PDFs are process-independent (all the process-dependence being carried by $\hat{\sigma}$), they can be extracted from one set of experiments and used to predict the results of others.

2.5 Power Corrections to Event Shapes

2.5.1 Non-Perturbative Effects

So far in this chapter we have mostly discussed perturbative QCD, but have also mentioned that there are important effects (such as confinement) which cannot be understood at a perturbative level. Indeed, it is possible for an observable to receive contributions which fail to show up in its perturbation series at all. For example, consider an expression like

$$P(a) = P_0 \exp\left(\frac{-bk}{a}\right). \quad (2.68)$$

Taking n derivatives of P gives a polynomial in a^{-1} times $P(a)$, and in the limit $a \rightarrow 0$ from above the exponential always wins (for positive k). Therefore every term in the perturbation series of P vanishes. One can add a term like $P(a)$ to any observable without changing its perturbation series.

Applying renormalization group improvement to turn the dependence on a into a dependence on the energy scale Q using $a \sim 1/(b \ln(Q/\Lambda))$ we find

$$P(a) = P_0 \left(\frac{\Lambda}{Q}\right)^k. \quad (2.69)$$

This is called a power correction, because it falls off like a power of the energy scale Q . In contrast, the RG-improved perturbative terms go roughly like powers of $1/\ln Q$. All power corrections therefore fall off faster as $Q \rightarrow \infty$ than any perturbative term, but at finite energies they can still have important phenomenological effects.

2.5.2 The Dokshitzer-Webber Model

In Subsection 2.3.3 we introduced the class of observables known as event shapes. It turns out that to describe them correctly one requires rather large $1/Q$ power corrections to be added to the NLO perturbative result (in the $\overline{\text{MS}}$ scheme with μ

set to the centre-of-mass energy Q). For example, to fit the evolution of the mean value of thrust $\langle T \rangle$, one requires a power correction $\simeq 1\text{GeV}/Q$, which provides of order 10% of the total value at $Q = M_Z$.

In Ref. [4] Dokshitzer and Webber proposed a way to predict the power corrections to various event shapes by relating them to a single non-perturbative parameter. The basic assumption is that the power corrections can be described by assuming that soft gluon emission is governed by a universal couplant which freezes to a finite value in the infrared (in contrast with the solutions to the perturbative beta-function at one or two loops which become singular).

To make use of this, one takes the LO result for an event shape mean and expresses it as an integral over the transverse momentum of the gluon k_T

$$\langle y \rangle_{\text{LO}} = a(\mu) \int_0^Q dk_T \frac{d\sigma}{dk_T} y. \quad (2.70)$$

The next step is to choose to evaluate the differential cross-section with $\mu = k_T$; this is supposed to approximately include the effects of higher order diagrams (a form of RG-improvement). This gives

$$\langle y \rangle_{\text{resummed}} = \int_0^Q dk_T \frac{d\sigma}{dk_T} a(k_T) y \quad (2.71)$$

which is ill-defined for a solving the one/two loop beta-function equation because of the singularity in a in the infrared (c.f. Eq. (2.40)).

Instead one assumes that a follows the perturbative beta-function equation only down to an infrared matching scale μ_I . Below this it is to be parametrized by some phenomenological parameters. Suppose $\frac{d\sigma}{dk_T} y \sim a_y \pi k_T^p / Q^{p+1}$ for $k_T \ll Q$ with a_y a constant. Then we can divide the integral over k_T at the matching scale to obtain

$$\langle y \rangle \sim a_y \frac{1}{Q^{p+1}} \int_0^{\mu_I} dk_T \pi k_T^p a(k_T) + \int_{\mu_I}^Q dk_T \frac{d\sigma}{dk_T} a(k_T) y. \quad (2.72)$$

The first integral is proportional to a moment of the coupling in the infrared

$$\int_0^{\mu_I} dk_T \pi k_T^p a(k_T) = \frac{\mu_I^{p+1}}{p+1} \bar{\alpha}_p(\mu_I). \quad (2.73)$$

This implies that the first integral in fact gives a power correction proportional to $\bar{\alpha}_p(\mu_I)$ – this will be our non-perturbative parameter. a_y is observable dependent, but calculable, so we can relate power corrections for different observables.

One final subtlety is that in adding this power correction to a perturbative result we need to avoid double counting, because the perturbative result already includes part of this correction (as can be seen by expanding it in perturbation theory). Further taking the coupling which freezes to be in the CMW scheme [26] one obtains the final formula

$$\begin{aligned} \langle y \rangle_{\text{PC}} = & a_y \frac{\mathcal{M}}{p} \left(\frac{\mu_I}{Q} \right)^p \left[\bar{\alpha}_{p-1}(\mu_I) - \alpha_{\overline{\text{MS}}}(\mu) \right. \\ & \left. - \frac{\beta_0}{2\pi} (\log(\mu/\mu_I) + K/\beta_0 + 1/p) \alpha_{\overline{\text{MS}}}^2(\mu) \right]. \end{aligned} \quad (2.74)$$

$\mathcal{M} \simeq 1.49$ is the so-called Milan factor [27], which arises from taking into account certain 2-loop effects. K appears because of using the CMW scheme for the IR-freezing coupling:

$$K = \frac{67}{6} - \frac{\pi^2}{2} - \frac{5}{9} N_f. \quad (2.75)$$

In Ref.[28] it was shown how this approach could be extended to apply to event shape distributions. Since then many experimental studies have appeared, fitting event shape means and distributions simultaneously for $\alpha_{\overline{\text{MS}}}(M_Z)$ and $\bar{\alpha}_0(\mu_I)$. Generally an approximate (up to corrections $\simeq 25\%$) universality of the $\bar{\alpha}_0$ values is observed, supporting the hypothesis that power corrections can be related to a universal coupling in this way.

Chapter 3

Renormalization Prescription Dependence

This chapter reviews the problem of renormalization prescription dependence, along with several proposed solutions. These include the standard $\overline{\text{MS}}$ -scheme, physical scale approach, along with the Method of Effective Charges and the Principle of Minimal Sensitivity which will be used in Chapters 4 and 5 respectively.

3.1 The Problem

3.1.1 Ambiguities in Perturbation Theory

As discussed in the previous chapter, QCD and the other QFTs that make up the Standard Model of particle physics cannot be solved exactly; some approximation method must be used to produce physical predictions. By far the most popular such method is the perturbative approach sketched in Subsection 2.1.2. This chapter is a discussion of some issues that arise in applying this to QCD (with massless quarks only).

Given some physical quantity¹ S depending on the renormalized couplant a , one can use the method described in Subsection 2.1.2 and Subsection 2.2.2 to compute the coefficients in the asymptotic expansion

$$S(a) = S_{\text{QPM}} + S_1 a + S_2 a^2 + \dots \quad (3.1)$$

(here S_{QPM} is the value of S in the Quark Parton Model, i.e. with no QCD radiation). In practice, computing the S_n is so difficult, and the difficulty increases so sharply with n , that for most quantities only S_1 and S_2 are known.

To maintain generality, imagine that the S_n have been computed up to S_N . To obtain a perturbative approximation for S , one truncates the series after the last calculated term and takes the resulting polynomial in a as an approximation to $S(a)$

$$S^{(N)}(a) = S_{\text{QPM}} + S_1 a + \dots + S_N a^N. \quad (3.2)$$

Provided that the series in Eq. (3.1) really is asymptotic to $S(a)$, this means that $S^{(N)}(a) = S(a) + O(a^{N+1})$, i.e. for sufficiently small a

$$|S(a) - S^{(N)}(a)| < K_N |a^{N+1}| \quad (3.3)$$

(K_N is some arbitrary positive constant). This is the sense in which $S^{(N)}$ is an approximation to S . However, in producing physical predictions, the behaviour of $S(a)$ as $a \rightarrow 0$ is not what counts. We really want to know how well $S^{(N)}$ approximates S for a particular finite a ; that is to say, we want to be able to put a bound on the remainder function $R^{(N)}(a) = S(a) - S^{(N)}(a)$. This depends on

1. The size of the unknown higher order coefficients S_n , $n > N$.
2. The size of non-perturbative effects (see Subsection 2.5.1) which leave no trace in the perturbative expansion of Eq. (3.1). Note that in general this

¹Here physical quantity is taken to mean a single number that one could in principle measure in an experiment (for example the mean value of thrust in e^+e^- annihilation at $Q = M_Z$).

series will not converge, and a finite *perturbative* sum will need to be constructed before the *non-perturbative* effects can be unambiguously quantified.

Unfortunately the size of these effects cannot be predicted; in other words, the size of the remainder function $R^{(N)}(a)$ is simply unknown. This is not an uncommon situation in physics, and normally one would simply press ahead using the approximation (perhaps taking the apparent convergence of the series as a crude guide to its likely accuracy).

There is, however, a problem with this solution: our final approximation will be far from unique. Truncating the series at order a^N corresponds to approximating the higher order S_n by 0. However, given that these higher order S_n are unknown, there is nothing to prevent one from defining a “truncation” where they take any arbitrary values (note in particular that this would still differ from the true S by a remainder of order a^{N+1}). Why would anyone do this? It seems that 0 is the most reasonable choice - one could even argue that since the coefficient is unknown, it is as likely to be negative as positive, and so we should take its expectation value to be 0! This cannot always be correct, however, because any such alternative “truncation” is equivalent to a *real* truncation of S expanded in terms of a *different* parameter a' of the form

$$a' = v(a) = a + v_1 a^2 + v_2 a^3 + \dots . \quad (3.4)$$

Using such changes of expansion parameter, arbitrary results can be obtained at any fixed order of perturbation theory. The choice of expansion parameter is therefore absolutely crucial.

This discussion applies quite generally, but outside of renormalizable quantum field theory a variation of expansion parameter would not usually be considered. Rather, a perturbative expansion would only be constructed in terms of some

“natural” parameter (e.g. some quantity from the equations of motion, or Lagrangian). Of course, this is often very successful, even it is not necessarily clear *why*.

In renormalizable QFTs like QCD this “naturalness” criterion is not sufficient to fix the expansion parameter. This is because the “natural” expansion parameter that appears in the Lagrangian is in fact the bare coupling, and using this would cause all the S_n (and, more to the point, the remainder function) to diverge. To get a finite perturbation series we must renormalize the theory, defining a renormalized coupling according to some renormalization prescription. As described in Subsection 2.2.3, there are an infinite number of ways to do this, resulting in couplings related to each other exactly as in Eq. (3.4), and none is obviously more “natural” than any other. This is the *renormalization prescription dependence* problem. Note that the set of renormalized couplings one would consider at a given order in perturbation theory is a *subset* of all those couplings of the form Eq. (3.4), because of the way the beta-function is normally truncated at the same order as the perturbative series. So even in the QCD case not all possible expansion parameters are considered equally natural, but the set of those that are is large and diverse enough to cause significant ambiguity in perturbative predictions.

To summarise the situation, we have one basic underlying problem: lacking any information about higher order corrections, any guess for them gives an equally reasonable approximation (or equivalently, any choice of expansion parameter gives an equally reasonable truncated series). In most situations, non-standard guesses for the higher order corrections (or non-standard expansion parameters) would be ignored as “unnatural”. However, in renormalizable QFTs we have a large number of “natural” expansion parameters. Therefore, we need some more refined criterion for selecting an expansion parameter.

However, this problem can be turned to our advantage, because it makes it possible to tune the expansion parameter (or equivalently the RP) to a particular observable, in the hope of getting a more accurate approximation. This lies behind the idea of renormalization group improvement introduced in Subsection 2.2.3, as well as the so-called “optimized” approaches to fixing the RP that are the subject of this thesis. The remaining sections of this chapter review some of the most popular of these possibilities.

3.2 The “Physical Scale”

3.2.1 Method

By far the most popular choice of RP in practice is to take μ to equal a characteristic “physical scale” of the process, which is generically denoted by Q (for example, the centre of mass energy in e^+e^- annihilation), and to work within the $\overline{\text{MS}}$ -scheme at all times. A variation of μ within the range $Q/2 < \mu < 2Q$ is often taken to indicate a theoretical error on the prediction.

For brevity, this approach will be referred to in this thesis as $\overline{\text{MSPS}}$ (for $\overline{\text{MS}}$ -scheme with the physical scale).

3.2.2 Motivation

The standard argument used to motivate the use of $\overline{\text{MSPS}}$ was briefly given in Subsection 2.2.3. It starts by considering the $\overline{\text{MS}}$ -scheme perturbative series for some single-parameter observable $S(Q)$, which acquires its Q -dependence through $\log s L = \log(\mu/Q)$:

$$S(Q) = S_{\text{QPM}} + s_0 a(\mu) + (s_0 b L + s_1) a^2(\mu) + (s_0 b^2 L^2 + 2s_1 b L + s_2) a^3(\mu) + \dots \quad (3.5)$$

where for simplicity c has been set to zero (see Subsection 2.2.3 for details of the notation). One then notes that the coefficients of $a^n(\mu)$ consist of degree

$n - 1$ polynomials in bL . All but the constant terms in these polynomials can be predicted on the basis of lower order calculations (e.g. the leading terms $\propto b^{n-1}L^{n-1}$ are known once r_0 has been calculated). Since these terms are known, they can be *resummed* by choosing $\mu = Q$. This change in the expansion parameter causes L to vanish, so in effect the terms involving L have been absorbed into the couplant $a(Q)$. This should improve the convergence of the perturbation series, and make maximal use of the information we have at a given order (because all the known logs have been resummed).

On the surface, this argument seems compelling, but this is deceptive. Note that we have been working in the $\overline{\text{MS}}$ -scheme, but nothing in the argument relies on this. Applying the same reasoning in, say, the MS -scheme would lead to us once again choosing $\mu = Q$. The only difference between these two schemes is that the $\overline{\text{MS}}$ scheme subtracts an extra $\ln 4\pi - \gamma_E$ along with the $1/\epsilon$ pole (see for example Eqs. (2.45) and (2.46)). We can simulate setting $\mu = Q$ in the MS scheme by working in the $\overline{\text{MS}}$ scheme with $\mu = Q\sqrt{4\pi}\exp(-\gamma_E/2) \simeq 2.66Q$ (this restores the subtracted $\ln 4\pi - \gamma_E$ term, see for example Eq. (2.26)). This is an instance of the fact, noted in Subsection 2.2.3, that the RP depends not on μ and the RS separately, but rather on the combination μ/Λ and the coefficients c_2, c_3, \dots . The MS and $\overline{\text{MS}}$ schemes must differ only by the value of Λ , because they can be made equivalent by a rescaling of μ .

In short, $\overline{\text{MSPS}}$ gives the $\overline{\text{MS}}$ -scheme a privileged status. It is hard to find even an intuitive justification for why this should work, but nonetheless it is very successful. This can be seen in the overall consistency of QCD phenomenology where $\overline{\text{MSPS}}$ is almost invariably used (see for example Ref. [6]). This provides a pragmatic justification for using $\overline{\text{MSPS}}$, but also leaves open the possibility that more theoretically motivated choices of RP could lead to improved perturbative predictions.

3.3 The Method of Effective Charges

3.3.1 Method

This section briefly summarises the Method of Effective Charges (ECH) originally proposed in Ref. [11]. Consider a function of Q normalised so that its perturbation series takes the form

$$a(\mu, \text{RS}) + r_1(\mu/Q, \text{RS})a^2(\mu, \text{RS}) + r_2(\mu/Q, \text{RS})a^3(\mu, \text{RS}) + \dots, \quad (3.6)$$

Such a quantity could either be the coupling defined in some RS with Q as the renormalization scale or a suitably normalized observable $\mathcal{R}(Q)$ depending on a single energy scale Q . Indeed, these possibilities are not mutually exclusive. Given some observable of the form Eq. (3.6), one can define an RP such that all the r_n vanish; in this RP, $\mathcal{R} = a$, so the observable is equal to the coupling. Such an observable/coupling is called an *effective charge* [11]. A typical example is the R-ratio in e^+e^- annihilation with which one can associate an effective charge $\mathcal{R}(Q)$ via

$$R(Q) = 3 \left(\sum_f Q_f^2 \right) (1 + \mathcal{R}(Q)). \quad (3.7)$$

Comparing this to Eq. (2.56), we see that indeed $\mathcal{R} = a + O(a^2)$.

Whatever the nature of the function represented in Eq. (3.6), it will be independent of the RP in which the expansion is performed. Moreover, when the expansion is truncated at some order, the variation in this partial sum due to a change of RP is always one order higher in a . This implies specific relations between the r_n and the RP [22].

Recall that the dependence of the coupling a defined in some RS on μ is described by the beta-function

$$\frac{da(\mu, \text{RS})}{d \ln(\mu)} = \beta(a) = -ba^2(1 + ca + c_2a^2 + c_3a^3 + \dots), \quad (3.8)$$

where b and c are independent of the RS, and the c_i , $i \geq 2$ can be taken to label the RS, along with the scale parameter Λ . Restricting a to the subset of couplings which are also effective charges, the same equation is conventionally written as

$$\frac{d\mathcal{R}(Q)}{d\ln(Q)} = \rho(\mathcal{R}) = -b\mathcal{R}^2(1 + c\mathcal{R} + \rho_2\mathcal{R}^2 + \rho_3\mathcal{R}^3 + \dots), \quad (3.9)$$

where b and c are now independent of the choice of effective charge, whereas the ρ_n depend on this choice.

When using ECH, one treats ρ as the object which is to be approximated perturbatively. Because it describes a functional relation between two physical quantities, namely \mathcal{R} and its energy derivative, it is automatically independent of any choice of RP we make in calculating it. Clearly, the ρ_n must also be similarly RP-independent. This means that truncating ρ at some fixed order in perturbation theory, and calculating an approximation for \mathcal{R} by integrating the corresponding approximate effective charge beta-function will give RP-independent results. Another way of looking at this is to say that the method of effective charges involves a specific choice of RP (i.e. the RP where $\mathcal{R} = a$), so that the energy evolution of the observable is identical to the beta-function evolution of the coupling. To apply ECH, we must obtain a perturbative approximation to ρ . To this end, consider setting $\mu = Q$ in Eq. (3.6) (which is allowable as the full sum is independent of μ), and then differentiating with respect to $\ln Q$. This gives

$$\rho(\mathcal{R}) \equiv \frac{d\mathcal{R}}{d\ln Q} = \left. \frac{\partial\mathcal{R}}{\partial a} \frac{da(Q)}{d\ln Q} \right|_{a=a(\mathcal{R})} = \left. \frac{\partial\mathcal{R}}{\partial a} \beta(a) \right|_{a=a(\mathcal{R})}. \quad (3.10)$$

Expanding this order-by-order in \mathcal{R} and comparing to Eq. (3.9) gives expressions for the ρ_n as multinomials in the r_n and the c_n ; for example, the first two are

$$\begin{aligned} \rho_2 &= c_2 + r_2 - r_1 c - r_1^2 \\ \rho_3 &= c_3 + 2r_3 - 4r_1 r_2 - 2r_1 \rho_2 - r_1^2 c + 2r_1^3. \end{aligned} \quad (3.11)$$

Suppose we have performed a NLO calculation of \mathcal{R} (in some arbitrary RP). This provides us with r_1 , but not r_2 or any higher-order coefficients. So as

this stage, our best approximation to $\rho(\mathcal{R})$ is simply the universal form $\rho(\mathcal{R}) = -b\mathcal{R}^2(1 + c\mathcal{R})$. This can therefore be termed the “NLO” approximation to ρ . Given the r_i and c_i for $i = 1 \dots n$, we can calculate the ρ_i to the same order, obtaining a NⁿLO approximation.

Having constructed an approximation for ρ it just remains to relate this to the effective charge itself and hence to the corresponding observable. This can be accomplished by integrating the separable differential equation Eq. (3.9). This gives

$$\ln Q = \int_0^{\mathcal{R}(Q)} \frac{dx}{\rho(x)} + C. \quad (3.12)$$

For $\mathcal{R}(Q) > 0$ we need the RHS to be finite; therefore the constant of integration C must be infinitely large to cancel the singularity arising from the pole in the integrand at $x = 0$. In general, C may differ from one effective charge to another, but the differences must be finite, because the singularity in the integral only depends on the universal beta-function coefficients b and c . To see this, expand the integrand for small x as

$$\frac{1}{\rho(x)} = \frac{1}{-bx^2(1 + cx + \rho_2x^2 + \dots)} = \frac{1 - cx + O(x^2)}{-bx^2} \quad (3.13)$$

giving a singular term depending on b and c and a finite part containing dependence on ρ_2, ρ_3, \dots . Therefore C can be split into a universal singular contribution C_∞ and an observable dependent finite part $C_{\mathcal{R}}$. Conventionally we take

$$C_\infty = \int_0^\infty \frac{dx}{-bx^2(1 + cx)} \quad (3.14)$$

which clearly has the same divergence as the integral in Eq. (3.12). For our final equation to be dimensionally correct, we must be able to write $C_{\mathcal{R}}$ as the logarithm of a dimensionful quantity, which we call $\Lambda_{\mathcal{R}}$. Thus we have

$$b \ln \frac{Q}{\Lambda_{\mathcal{R}}} = \int_{\mathcal{R}(Q)}^\infty \frac{dx}{x^2(1 + cx)} + \int_0^{\mathcal{R}(Q)} dx \left[\frac{-1}{x^2(1 + cx + \rho_2x^2 + \dots)} + \frac{1}{x^2(1 + cx)} \right]. \quad (3.15)$$

The first integral is independent of the particular effective charge under consideration (it is just C_∞), whereas the second is not. Exponentiating gives

$$\frac{\Lambda_{\mathcal{R}}}{Q} = \mathcal{F}(\mathcal{R}(Q))\mathcal{G}(\mathcal{R}(Q)) \quad (3.16)$$

where \mathcal{F} is universal and comes from the first integral in Eq. (3.15)

$$\mathcal{F}(\mathcal{R}) = e^{-1/b\mathcal{R}} \left(1 + \frac{1}{c\mathcal{R}}\right)^{c/b}, \quad (3.17)$$

and \mathcal{G} comes from the second integral and depends on the effective charge,

$$\mathcal{G}(\mathcal{R}) = \exp \left[- \int_0^{\mathcal{R}(Q)} dx \frac{1}{\rho(x)} + \frac{1}{bx^2(1+cx)} \right]. \quad (3.18)$$

Approximating ρ by its NLO form gives $\mathcal{G}_{\text{NLO}} = 1$.

The freedom in choosing the constant of integration $\Lambda_{\mathcal{R}}$ means that Eq. (3.9) only fixes \mathcal{R} up to an arbitrary rescaling of Q . This is necessary, as the NLO ρ is the same for *all* effective charges, and they certainly should not all have the same NLO predictions. $\Lambda_{\mathcal{R}}$ is acting here like the one free parameter of QCD – in fact, as the notation suggests, it represents one possible definition of the dimensional transmutation parameter Λ alluded to in Subsection 2.2.3.

For each effective charge, and each unphysical coupling such as $a_{\overline{\text{MS}}}$, there will be a corresponding Λ parameter. By convention, for an unphysical coupling the scheme is used as the subscript, and one writes $\tilde{\Lambda}_{\overline{\text{MS}}}$ rather than $\Lambda_{a_{\overline{\text{MS}}}}$. The tilde is added to avoid confusion with another (more widely used) definition of $\Lambda_{\overline{\text{MS}}}$ [29], the relation between the two being

$$\tilde{\Lambda}_{\overline{\text{MS}}} = \left(\frac{2c}{b}\right)^{-c/b} \Lambda_{\overline{\text{MS}}}. \quad (3.19)$$

Obviously all these different Λ parameters cannot be modified independently as there should only be one free parameter in QCD; therefore, they must all be related. To show how this comes about, suppose we have two effective charges, \mathcal{R}

and \mathcal{R}' , such that $\mathcal{R}'(Q) = \mathcal{R}(Q) + r\mathcal{R}^2(Q) + \mathcal{O}(\mathcal{R}^3(Q))$. Specialising Eq. (3.16) to \mathcal{R}' and \mathcal{R} and taking the ratio between the results one arrives at

$$\frac{\Lambda_{\mathcal{R}'}}{\Lambda_{\mathcal{R}}} = \frac{\mathcal{F}(\mathcal{R}')\mathcal{G}'(\mathcal{R}')}{\mathcal{F}(\mathcal{R})\mathcal{G}(\mathcal{R})} \quad (3.20)$$

(the prime on \mathcal{G} indicates that the ρ function for \mathcal{R}' is being used). This holds as an identity at all energies. If we insert for \mathcal{R}' the perturbative expansion in terms of \mathcal{R} all the energy dependence is carried by \mathcal{R} , so the equation now holds for all \mathcal{R} . Since the LHS is independent of \mathcal{R} we might as well evaluate the RHS for $\mathcal{R} \rightarrow 0$. It is easy to check in this limit that $\mathcal{G}'(\mathcal{R}') = \mathcal{G}(\mathcal{R}) + \mathcal{O}(\mathcal{R})$ and $\mathcal{F}(\mathcal{R}') = \exp(r/b)(\mathcal{F}(\mathcal{R}) + \mathcal{O}(\mathcal{R}))$. Therefore taking $\mathcal{R} \rightarrow 0$ gives

$$\frac{\Lambda_{\mathcal{R}'}}{\Lambda_{\mathcal{R}}} = \exp(r/b). \quad (3.21)$$

This is called the Celmaster-Gonzalves relation [30]. Note that it is exact, but only requires NLO information (the coefficient r).

This relation allows NLO information to be incorporated into ECH, by determining the scale $\Lambda_{\mathcal{R}}$ in terms of some reference scale. Usually $\tilde{\Lambda}_{\overline{\text{MS}}}$ is used, though it is easy to translate to any other scheme using Eq. (3.21). Specifically, we have

$$\Lambda_{\mathcal{R}} = \exp(r_1(1, \overline{\text{MS}})/b)\tilde{\Lambda}_{\overline{\text{MS}}}. \quad (3.22)$$

Putting together Eqs. (3.16),(3.19) and (3.22) gives

$$\Lambda_{\overline{\text{MS}}} = Q\mathcal{F}(\mathcal{R}(Q))\mathcal{G}(\mathcal{R}(Q))e^{-r_1(1, \overline{\text{MS}})/b} \left(\frac{2c}{b}\right)^{c/b}. \quad (3.23)$$

This equation allows us to extract values of $\Lambda_{\overline{\text{MS}}}$ directly from the observed values of \mathcal{R} , or to make predictions for \mathcal{R} (by solving the implicit equation e.g. iteratively).

One way to compare this with the more standard approach of truncating the series for \mathcal{R} in some fixed RP is to write an “effective” effective charge beta-function describing the energy evolution of \mathcal{R} implied by this standard approach.

Let us call this function $\bar{\rho}$. It can be computed from Eq. (3.10) using the truncated relation between \mathcal{R} and a . It always agrees with the true ρ up to the order (NLO, NNLO,...) to which \mathcal{R} has been calculated, but it also includes terms of all higher orders in \mathcal{R} which depend on the RP we chose to perform our truncation in. If the RP is such that r_1 is large, these higher order terms are also large, so the ECH predictions will differ radically from the standard prediction *in that RP*.

3.3.2 Motivations

Many motivations have been given for the Method of Effective Charges.

Uniqueness [11]

Unlike an expansion in some fixed RS, ECH requires no arbitrary choices to be made (except for the choice of observable itself [31]). In this respect, it gives a more “normal” perturbative framework, without the ambiguities that plague PT in renormalizable QFTs.

Complete Renormalization Group Improvement [32]

The perturbative coefficients r_n for an effective charge can be written in terms of the scheme invariants ρ_n and the scheme parameters r_1, c_2, c_3, \dots

$$\mathcal{R} = a + r_1 a^2 + (r_1^2 + c r_1 - c_2 + \rho_2) a^3 + \frac{1}{2} (2r_1^3 + 5c r_1^2 - 4c_2 r_1 + 6r_1 \rho_2 - c_3 + \rho_3) a^4 + \dots \quad (3.24)$$

Note that the coefficient r_n is a degree n polynomial in r_1 . All the dependence on $\mu, \Lambda_{\overline{\text{MS}}}, \Lambda_{\mathcal{R}}$ and especially Q is hidden inside r_1 . In fact

$$r_1 = b \ln \frac{\mu}{\Lambda_{\overline{\text{MS}}}} - b \ln \frac{Q}{\Lambda_{\mathcal{R}}}. \quad (3.25)$$

The standard renormalization group improvement described in Section 3.2 involves setting $\mu = Q$ so $r_1 = b \ln \frac{\Lambda_{\mathcal{R}}}{\Lambda_{\overline{\text{MS}}}}$. The idea behind CORGI is that this resummation

is incomplete because it does not totally eliminate the r_1 terms from the higher-order r_n . To do this, one ought to choose the RP so $r_1 = 0$, which is equivalent to using ECH at NLO (because then at NLO we are in a scheme where $\mathcal{R} = a$). This is similar to the motivation behind the “Physical Scales” approach.

r_1 Is Not Intrinsic to an Effective Charge [11]

Grunberg suggests that r_1 only tells us about the relation between \mathcal{R} and a , rather than providing information intrinsic to \mathcal{R} . In other words, the associated ρ function (the “intrinsic” information, as it could be determined simply by measuring \mathcal{R}) is not predictable on the basis of r_1 . If true, this would imply that one ought to make use of ECH, at least at NLO (going beyond NLO is equivalent to the further assumption that the ρ_n can’t be predicted based on the ρ_m , $m < n$). A good reason to imagine this might be true comes from considering the fact that an observable defined simply by rescaling the energy variable (e.g. $\mathcal{R}'(Q) = \mathcal{R}(2Q)$) is identical except for the value of r_1 .

Renormalization-Scheme-Invariant Perturbation Theory [33]

The Lagrangian of QCD (Eq. (2.18)) contains no dimensional parameters, so by dimensional analysis it cannot make unambiguous predictions for dimensionless observables with any non-trivial energy dependence. However, it *can* unambiguously predict the logarithmic energy derivative of an observable as a function of the observable itself

$$\frac{d\mathcal{R}(Q)}{d \ln Q} = \rho(\mathcal{R}). \quad (3.26)$$

The fact that $\rho(\mathcal{R})$ is an *unambiguous* prediction with no dependence on either the physical parameter Λ or any choice of RP is taken to indicate that a successful PT should be based around it. This leads to ECH.

Λ -based Perturbation Theory [34]

Taking Λ (in any desired scheme, because of the Celmaster-Gonçalves relation) as the basic parameter of QCD, one should attempt to write the simplest relationship possible between Λ and the observable, $\Lambda = \Lambda(R(Q), Q)$ and expand this as a perturbative series in the observable. In the case of an observable which can be written as an effective charge, this gives Eq. (3.23).

Fastest Apparent Convergence Criterion [11]

The RP one uses when working with ECH has $a = \mathcal{R}$, so all higher-order coefficients in the perturbation series for \mathcal{R} vanish. In practice this means that when working at a given order n in perturbation theory one chooses the scheme which causes all the terms up to order n to vanish. Therefore this scheme has the “fastest apparent convergence” (FAC). Note though that this is not to say that the ECH approximants at different orders converge quickly; this may or may not be true depending on the details of the observable (if ECH is a good method, one would hope it is often true).

3.4 The Principle of Minimal Sensitivity**3.4.1 Method**

The Principle of Minimal Sensitivity (PMS) is an idea of very broad applicability. Indeed, in the paper where Stevenson first gave it this name and applied it to the problem of RP-dependence in QCD [22], he noted it had already been in use for several years in various areas of physics. Since then it has been put to a vast range of disparate uses.

The PMS simply states that if we are given an approximation which depends on some parameter arising only as part of the approximation procedure (so that

the exact result is independent of the parameter), the approximation is most believable where it is least sensitive to this “unphysical” parameter. This gives a simple way to choose an “optimal” value for the parameter (in the ideal case; in general there may be multiple “PMS points” and it may be necessary to use some other criterion for choosing between them).

To make use of the PMS in QCD, we need first to specify the approximation we want to optimise. This will consist of a perturbative approximation to a physical quantity S

$$S^{(N)}(a) = S_{\text{QPM}} + S_1 a + S_2 a^2 + \cdots + S_N a^N \quad (3.27)$$

into which we substitute the couplant evaluated at a scale μ , evolving according to the beta-function truncated to the same number of terms as S

$$\frac{da(\mu, \text{RS})}{d \ln(\mu)} = \beta^{(N)}(a) = -ba^2(1 + ca + c_2 a^2 + \cdots + c_{N-1} a^{N-1}). \quad (3.28)$$

The unphysical parameters here are $\tau = \ln(\mu/\Lambda)$ and the beta-function coefficients c_2, c_3, \dots, c_{N-1} . They are fixed by requiring the approximation be stable with respect to them, i.e.

$$\frac{\partial S^{(N)}}{\partial \tau} = 0, \quad \frac{\partial S^{(N)}}{\partial c_2} = 0, \quad \dots, \quad \frac{\partial S^{(N)}}{\partial c_{N-1}} = 0 \quad (3.29)$$

where the partial derivatives are to be taken with all other unphysical parameters fixed. The value of $S^{(N)}$ with the unphysical parameters fixed by Eq. (3.29) is the N th order PMS-approximant for S .

In general, there is no guarantee that such a stability point exists. If there is no stability point one may be able to adopt some other definition of minimal sensitivity (for example, looking for the point which minimizes the slope of $S^{(N)}$). For $N = 1$, S and all its scale derivatives are monotonically decreasing functions of μ , so there is no PMS point in any sense. Therefore, like ECH, PMS requires at least an $O(a^2)$ calculation to have been performed.

Another potential problem with PMS is that there may be multiple points satisfying Eq. (3.29). In this case, one either requires some other criterion for choosing between them, or else one can treat the variation between the values of $S^{(N)}$ at the different points as some estimate of the uncertainty on the result.

For the most phenomenologically interesting case, $N = 2$, the PMS couplant satisfies

$$\frac{2 + 3ca}{2(1 + ca)a} + c \ln \left(\frac{ca}{1 + ca} \right) = b \ln \left(\frac{Q}{\Lambda_{\mathcal{R}}} \right) \quad (3.30)$$

where $\Lambda_{\mathcal{R}}$ is the scale parameter of the effective charge defined by $S = S_{\text{QPM}} + S_1 \mathcal{R}$. Solving this equation for a , and then inserting this into the formula for $S^{(2)}$, gives the NLO PMS approximation for S .

3.4.2 Motivations

The main motivation behind the PMS was stated explicitly in Ref.[22]:

In the space of the unphysical parameters the exact result is a constant. Therefore the calculated result cannot possibly be a successful approximation where it is rapidly varying. The most reliable numerical result is likely to be where the calculation shows the correct qualitative behaviour, i.e., where the approximate result is flattest.

The PMS also draws some of its credibility from the success it finds in toy models, several of which are discussed in Stevenson's original paper [22].

One can also motivate the PMS in a different, more physical, way, in the case when the unphysical parameter can be seen as dividing some aspect of the theory into two pieces whose effects are approximated differently. For example, suppose the unphysical parameter defines an energy scale such that lower energies are considered "soft" and higher energies are considered "hard". Furthermore, suppose that the effects of these soft and hard modes are handled by different

approximations, which become increasingly accurate for the very soft and very hard modes respectively. In such a situation, the value of the unphysical splitting scale needs to be set such that both soft and hard approximations are reasonably accurate. But how can this be determined without access to exact solutions for comparison? One possibility is to compare the soft and hard approximations against *each other*. If they are sufficiently different approximations, for instance based on different physical principles, agreement between the two should be a good indicator of accuracy. But note that if both approximations agree on the effects of modes in the vicinity of the splitting scale, varying the scale will have no effect on the *overall* approximation – in other words, this value of the splitting scale is exactly the one that would be found using the PMS. A toy model illustrating this situation is the example of determining the integral of a function known only through its Taylor expansion about two different points, given in Ref.[22]. One can also consider the case of renormalization scale dependence in QCD to crudely fit this pattern. This is because one can think of μ as a UV factorization scale, with the effect of modes with $p^2 > \mu^2$ felt through the running of the coupling. The approximate $a(\mu)$ does indeed become increasingly exact as $\mu \rightarrow \infty$, although the remaining part of the approximation, the truncated expansion relating a to the observable, doesn't become exact as $\mu \rightarrow 0$. It does, however, prefer smaller values of μ , so a compromise is required, which can reasonably be determined by the PMS.

Chapter 4

NLL ECH and Event Shape Distributions

In this chapter, the Method of Effective Charges described in Section 3.3 is applied to the distributions of 1-thrust and heavy-jet mass in e^+e^- annihilation. A next-to-leading log resummation of the ECH beta-function ρ is performed, and the effect on power correction fits is investigated.

4.1 Background

As described in Chapter 1, this work is motivated by the observation of the DELPHI collaboration [13] that if one uses the Method of Effective charges to describe the means of e^+e^- event shapes, there is a very substantial reduction in the need for non-perturbative power corrections. In this chapter, we investigate whether this conclusion also extends to e^+e^- event shape distributions.

In fact, event shape distributions have previously been studied within the ECH framework [35, 36]. Ref.[35] in particular studied how the fit of the ECH results to data varied in quality for different regions of phase space. To do this an effective charge was constructed separately for each bin of the data, and NLO

QCD calculations were used to extract $\Lambda_{\overline{\text{MS}}}$ at centre of mass energy $Q = M_Z$. The consistency of these $\Lambda_{\overline{\text{MS}}}$ values between different data bins could then be examined. Non-perturbative effects were taken into account by using Monte Carlo simulations to correct the data back to “parton-level” distributions. This generally improved the consistency of the $\Lambda_{\overline{\text{MS}}}$ measurement, but with this approach it is hard to see whether the ECH distributions prefer smaller hadronization corrections than the $\overline{\text{MSPS}}$ ones. Moreover, even after these corrections were applied there were still two kinematical regions where the effective charge ceased to be a good description of the data, leading to instability in the measured $\Lambda_{\overline{\text{MS}}}$ values: the 2-jet limit where large logs enhance the higher-order perturbative coefficients (as explained in Subsection 2.3.3), and the region (which exists for many observables) where the LO result vanishes, causing $r_1 \rightarrow \infty$. The latter problem is hard to address within the effective charge approach, but the former problem seems to call for a resummation of the effective charge beta-function. The next section gives details of a recipe for carrying out this resummation.

4.2 Resummation of Logarithms in the ECH Beta-Function

It is commonly stated that the method of effective charges is inapplicable to exclusive quantities such as event shape distributions. The idea is that the dependence of the physical quantity on multiple scales invalidates the derivation of the ECH beta-function as presented here in Section 3.3. However, as pointed out in [33], this is not really the case. Given an observable $\mathcal{R} = \mathcal{R}(Q_1, Q_2, \dots, Q_n)$ depending on n scales, one can simply re-express it as $\mathcal{R} = \mathcal{R}(Q_1, Q_2/Q_1, \dots, Q_n/Q_1) \equiv \mathcal{R}_{x_2, \dots, x_n}(Q_1)$. Here the $x_i \equiv Q_i/Q_1$ are *dimensionless* quantities that can be thought of as labelling the effective charge which is now a function of one single dimensionful scale Q_1 . We can then write an effective charge beta-function for

this \mathcal{R} describing the energy evolution of our observable for fixed values of the ratios x_i . Still, this formal manipulation cannot tell us whether the ρ function we arrive at in this way will be well approximated by its NLO terms, which is what we require for most fixed-order phenomenological applications, given the current state of the art in perturbative QCD calculations. One reason in particular why this might not be the case is if some of the x_i become large - typically this leads to powers of large logs $L_i = \log(x_i)$ enhancing the coefficients r_n in the perturbation series for \mathcal{R} , and hence also the ρ_n in the corresponding $\rho(\mathcal{R})$ function. A common situation is that more logs appear as the order of perturbation theory is increased, so that for a sufficiently large L the terms all become of similar magnitude. This invalidates both the NLO (universal) approximation for $\rho(\mathcal{R})$ and NLO $\overline{\text{MS}}\text{PS}$. However, in the latter case, there is a well-known way out. If the leading powers of the logs can be identified as having some simple dynamical origin, we may be able to calculate them *to all-orders* and then effect a resummation, extending the validity of our perturbative results into the large L region. This suggests that essentially the same trick might work for the ρ function. In this section we describe how to accomplish this, expanding on ideas in Ref.[37]; an example of the phenomenological application of these ideas to event shapes is presented in the next section.

Our approach will be to start with some resummed result for the observable of interest calculated by conventional means. As an example, consider an observable of the form

$$O(L) = LA_{LL}(aL) + A_{NLL}(aL) + aA_{NNLL}(aL) + \dots, \quad (4.1)$$

where a is as usual the couplant and L is the large logarithm which this expression resums. The subscripts “LL”, “NLL” and “NNLL” stand for leading log, next-to-leading log and next-to-next-to-leading log respectively. We can relate this

observable to an effective charge

$$O(L) = r_0(L)\mathcal{R}(L) = r_0(L)(a + r_1(L)a^2 + r_2(L)a^3 + \dots). \quad (4.2)$$

Here r_0 is the leading order coefficient, whose large L behaviour is $r_0 \sim L^2$. The r_n can now be expanded in powers of the large $\log L$. In this case their leading behaviour is $r_n \sim L^n$ and we can write

$$r_n = r_n^{\text{LL}}L^n + r_n^{\text{NLL}}L^{n-1} + \dots, \quad (4.3)$$

so the structure of the ρ_n as illustrated in Eq.(3.11) implies that

$$\rho_n = \rho_n^{\text{LL}}L^n + \rho_n^{\text{NLL}}L^{n-1} + \dots. \quad (4.4)$$

Because L is a logarithm of a physical quantity, this expansion of the ρ_n is RP-independent. We can thus define resummed, RP-independent approximations to $\rho(\mathcal{R})$ such as

$$\rho_{\text{LL}}(\mathcal{R}) = -b\mathcal{R}^2(1 + c\mathcal{R} + \sum_{n=2}^{\infty} \rho_n^{\text{LL}}L^n\mathcal{R}^n) \quad (4.5)$$

$$\rho_{\text{NLL}}(\mathcal{R}) = -b\mathcal{R}^2(1 + c\mathcal{R} + \sum_{n=2}^{\infty} (\rho_n^{\text{LL}}L^n + \rho_n^{\text{NLL}}L^{n-1})\mathcal{R}^n). \quad (4.6)$$

and so on. These can be calculated order-by-order using the relations between the ρ_n and r_n , the first few of which are shown in Eq.(3.11). Alternatively, we can apply a numerical procedure to extract our desired ρ function from \mathcal{R} calculated to similar logarithmic accuracy. This is particularly simple for ρ_{LL} , as can be seen by considering the $\bar{\rho}$ corresponding to \mathcal{R}_{LL} with the one-loop beta-function

$$\bar{\rho}_{\text{LL}}(x) = \beta(a)\frac{d\mathcal{R}_{\text{LL}}}{da} = -ba^2\frac{d\mathcal{R}_{\text{LL}}}{da}, \quad (4.7)$$

with a chosen such that $\mathcal{R}_{\text{LL}}(a) = x$. The perturbative coefficients of this $\bar{\rho}$ function can be obtained from the expressions for the ρ_n , of which the first two are shown in Eq.(3.11), using $c = 0$, $c_i = 0$ and $r_n = r_n^{\text{LL}}L^n$. But then it is

easy to see that the coefficients we obtain are proportional to L^n and moreover identical to the coefficients of ρ_{LL} (because adding the sub-leading terms in $\beta(a)$ and \mathcal{R} only affects the $\bar{\rho}_n$ at next-to-leading logarithmic accuracy). In other words $\bar{\rho}_{LL}$, defined as above, is *equal* to ρ_{LL} except for the $c\mathcal{R}$ term which can easily be added (in some sense this term is NLL as it is $O(L^{-1})$ in the large L , fixed $\mathcal{R}L$ limit, but we include it in ρ_{LL} as it is obviously present in the full expression, and this avoids having to modify Eq. (3.18)). Thus $\rho_{LL}(\mathcal{R})$ can be calculated to arbitrary accuracy for a given \mathcal{R} by numerically inverting $\mathcal{R}_{LL}(a)$ to obtain the corresponding a , then substituting this a into Eq.(4.7).

Going beyond leading log accuracy things become slightly more complicated, because the $\bar{\rho}$ functions pick up terms at lower logarithmic accuracy that do not appear in our resummed approximations. For example, at NLL we will have $r_1 = r_1^{LL}L + r_1^{NLL}$, so that $\bar{\rho}_2$ will contain not only L^2 and L^1 terms, but also L^0 terms. These are not included in our definition of ρ_{NLL} , and indeed they must not be, as they are affected by the addition of the remaining missing terms in \mathcal{R} and hence are RP-dependent. However, it is still the case that the NLL terms in $\bar{\rho}_{NLL}$ are unchanged by adding sub-leading terms (in $\beta(a)$ and \mathcal{R}), and are therefore identical to the corresponding terms in ρ_{NLL} (assuming that the $\bar{\rho}$ functions are defined with beta-functions having sufficiently many terms to make this true, e.g. $\beta(a) = -ba^2(1 + ca)$ for the NLL case). So, truncating $\bar{\rho}$ by numerically taking limits ($L \rightarrow \infty$ with $L\mathcal{R}$ fixed) allows us to extract the LL and NLL terms. The generalization to higher logarithmic accuracy is straightforward.

Some physical quantities might have more divergent logarithmic behaviour, eg.

$$O(L) = A_{LL}(aL^2) + L^{-1}A_{NLL}(aL^2) + L^{-2}A_{NNLL}(aL^2) + \dots \quad (4.8)$$

In this case, $r_n \sim L^{2n}$ but the preceding argument goes through essentially unchanged, except that $\rho_n \sim L^{2n}$ as well.

Having obtained a resummed ρ function, we can proceed to extract Λ from the

observable making use of Eq.(3.15) with $\mathcal{R} = O(L)/r_0(L)$. In doing this, we may have available *exact* values for r_0 and r_1 from a fixed-order calculation, which we can use in place of their approximations from the resummed results. This allows us to combine resummed and fixed-order information in an essentially unique way (once we have fixed the definition of our effective charge), avoiding the so-called “matching ambiguity” associated with doing this in $\overline{\text{MS}}\overline{\text{PS}}$. In particular the full exact NLO coefficient r_1 in a given RS is reproduced if \mathcal{R} which solves Eq. (3.15) is expanded in the coupling a for that scheme, thanks to the RS invariant $\Lambda_{\mathcal{R}}$ which appears on the lefthand side of the equation.

This provides us with a complete method for making ECH predictions including resummations of large logarithms. In the next section we test this approach by comparing the distributions of thrust and heavy-jet mass in e^+e^- annihilation to NLL ECH predictions.

4.3 ECH for Event Shapes at Next-to-leading Logarithmic Accuracy

4.3.1 Outline

In this section we study the distributions of 1-thrust ($\tau \equiv 1 - T$) and heavy-jet mass (ρ_h). We first show the effect of replacing the hadronization corrections of [35] with an analytical power correction ansatz. For simplicity, we use a shift in the distribution by an amount C_1/Q . This form can be motivated by considering simple models of hadronization or through a renormalon analysis [2] and has been found successful phenomenologically (see for example [13]). Although better fits are often obtained using the model of [4, 28], because we are using a different perturbative approximation to standard NLO QCD, the subtractions needed to remove double counting will not in general be so simple - in particular, it is not

clear what scheme should be used for performing the subtraction.

Next we consider placing the effective charge into the exponent of the integrated thrust distribution. Even using a NLO approximation for the effective charge, this has the effect of resumming a series of logs in the distribution itself (in particular the “double logs” are included).

Finally we present results showing the effect of using the resummed ρ functions described here in Section 4.2. First we investigate the extent to which higher order $\overline{\text{MSPS}}$ logs are already included in the lower order ECH predictions (“RG-predictability”). Then we actually perform fits using the resummed ECH predictions.

For comparison, at all stages we also give results of fits to the same data using $\overline{\text{MSPS}}$ (at NLO, LL and NLL accuracy). As is customary, we use the variation of μ such that $Q/2 < \mu < 2Q$ to estimate a “theoretical error”.

The general question of separating perturbative and non-perturbative effects also deserves comment. Because perturbation theory diverges, it is not straightforward to define its sum; however, without doing this the magnitude of the “non-perturbative” effects is ambiguous. Therefore, it is preferable to combine a fit for power corrections with a renormalon resummation, as in [8, 9, 10]. We have not done so in this analysis, but as we are comparing ECH to $\overline{\text{MSPS}}$ which differ only by a convergent set of higher order terms, we believe that our conclusions regarding the relative size of power corrections stand. It would of course be interesting to investigate the effects of a renormalon resummation on our ECH results (ECH renormalon resummations have already been carried out for some single-scale observables in Ref. [38]).

Our data is taken over a wide range of centre-of-mass energies $Q = 35 - 189\text{GeV}$ (Refs.[36],[39]-[49]). Lacking information on the correlation between data points we have simply combined statistical and systematic errors in quadrature and

performed a min- χ^2 fit, allowing χ^2 to vary by 4 from its minimum to estimate a 2σ error. This over-simplistic treatment means that our errors cannot be considered reliable, however the central values of $\Lambda_{\overline{MS}}$ do give an impression of the effect of including the power corrections and logarithmic resummation into the ECH framework.

4.3.2 Analytical Power Corrections in the Approach of Burby and Maxwell

Let us now consider the effects of analytical power corrections on the results of Ref. [35]. The procedure used in Ref. [35] was to write an effective charge to represent the value of the event shape distribution integrated over each bin of the data. First, the Monte Carlo program EERAD [50] was used to compute the NLO perturbative coefficients ¹ for each bin

$$\int_{bin\ i} dy \frac{1}{\sigma} \frac{d\sigma}{dy} = A_i \alpha + B_i \alpha^2 + O(\alpha^3). \quad (4.9)$$

These were then used to write an effective charge, from which a value for $\Lambda_{\overline{MS}}$ could be extracted by feeding the data into Eq. (3.23). Here, to introduce a fit for C_1 we drop this “direct extraction” approach and instead perform a minimum χ^2 fit for $\Lambda_{\overline{MS}}$ and C_1 . For this to work, we need to exclude the regions where the EC approach cannot fit the data. For comparison with Ref. [35], we choose the same ranges selected there (based on the flatness of r_1), except that the lower end of the range is made proportional to $1/Q$ when looking at data away from $Q = M_Z$. The reason for this is that sub-leading non-perturbative effects are expected to become important for $y \simeq \Lambda/Q$ [28, 52, 53]. As we are shifting the predictions before comparing to data we require the NLO coefficients evaluated for arbitrary bin edges. We have approximated these using a set of order 6 polynomial

¹For our analysis we actually used EVENT2 [51] and we have checked that both programs give consistent coefficients.

interpolations from the output of EVENT2. We have checked by halving the Monte Carlo bin size to 0.005 that this induces no sizeable error (using the doubled sampling changes the best fit values here by less than 2%).

The results for 1-thrust and heavy-jet mass are presented in Fig. 4.1 and Fig. 4.2 respectively.

In the case of thrust it appears that the ECH results prefer larger power corrections (and significantly smaller $\Lambda_{\overline{\text{MS}}}$ values). For heavy-jet mass, the situation is similar, although the differences are not quite as extreme. However, in both cases we find comparable $\Lambda_{\overline{\text{MS}}}$ values to those found in Ref. [35] using hadronization corrected data rather than an analytical power correction ansatz. ²

4.3.3 Exponentiation

A crucial property that an event shape must possess in order for a resummation of logarithms to be feasible with present techniques is so-called exponentiation. To illustrate this property, consider the typical form of an event shape distribution as a double expansion in a and $L = \log(1/y)$:

$$\frac{1}{\sigma} \frac{d\sigma}{dy} = A_{LL}(aL^2) + L^{-1} A_{NLL}(aL^2) + L^{-2} A_{NNLL}(aL^2) + \dots \quad (4.10)$$

The A functions have a perturbative expansion $A(x) = A_0x + A_1x^2 + \dots$ and for τ and ρ_h are known up to NNLL accuracy. If the event shape exponentiates, then

²However, the values of $\Lambda_{\overline{\text{MS}}}$ quoted in Ref. [35] are actually wrongly normalized for two reasons. Firstly the factor of $(2c/b)^{(c/b)} \simeq 0.85$ was omitted, so the results are really values for $\tilde{\Lambda}_{\overline{\text{MS}}}$. Secondly, the results of EERAD were normalized to the *Born* cross-section σ_0 , whereas the data are normalized to the *total* cross-section σ , and this was not taken into account. Multiplying the EERAD perturbation series by a correction factor $\sigma_0/\sigma = 1 - \alpha/\pi + \dots$ decreases r_1 by exactly 1, increasing the extracted $\Lambda_{\overline{\text{MS}}}$ values by $e^{1/b}$. So the total correction factor to apply to the results of Ref. [35] is $(2c/b)^{(c/b)} e^{1/b} \simeq 1.11$.

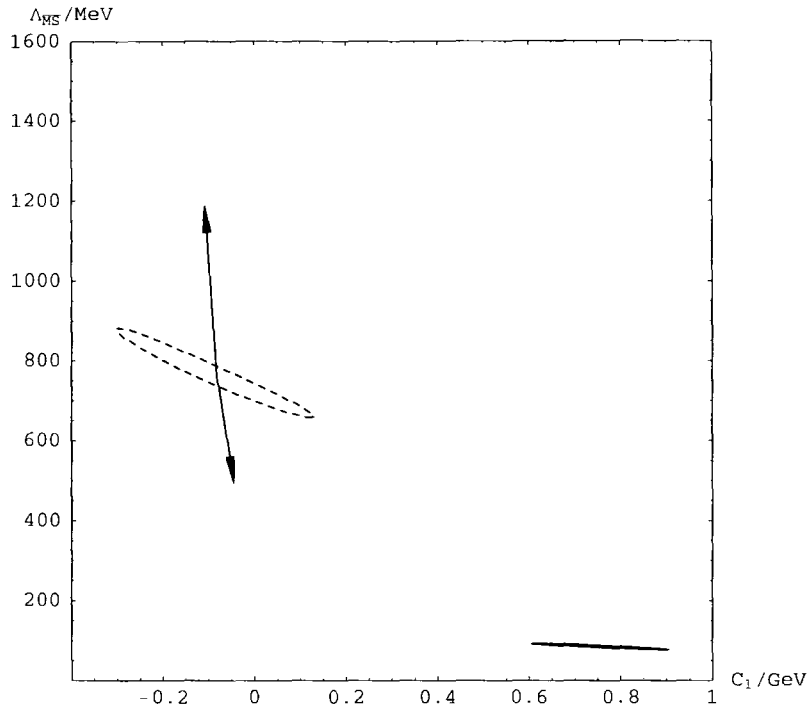


Figure 4.1: 1-thrust: Fits for $\Lambda_{\overline{\text{MS}}}$ and C_1 within the framework of Ref. [35] (solid ellipse) and standard NLO QCD perturbation theory (dashed ellipse). In the latter case the scale is chosen to be $\mu = Q$, and the effect on the central value of a change of renormalization scale by a factor of 2 is indicated by the arrows. 2σ error contours are shown (from allowing χ^2 to vary within 4 of its minimum). The fit range is $1 - T = 0.055M_Z/Q - 0.23$.

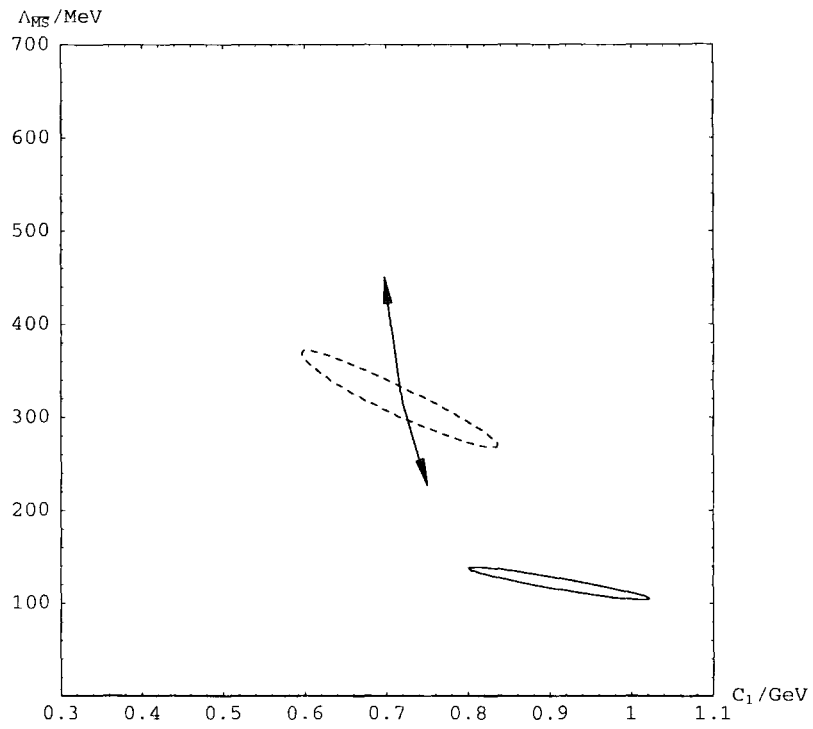


Figure 4.2: As Fig. 4.1 but for heavy-jet mass. The fit range is $\rho_h = 0.035M_Z/Q - 0.2$.

we can also write

$$R_y(y') \equiv \int_0^{y'} dy \frac{1}{\sigma} \frac{d\sigma}{dy} = C(a\pi) \exp(Lg_1(a\pi L) + g_2(a\pi L) + ag_3(a\pi L) + ag_3(a\pi L) + \dots) + D(a\pi, y) . \quad (4.11)$$

For τ and ρ_h , g_1 and g_2 are known [54]. When working with this form of the distribution it is conventional to refer to g_1 as containing the *leading logarithms* and g_2 as containing the *next-to-leading logarithms*. $C = 1 + O(a)$ is independent of y , and D contains terms that vanish as $y \rightarrow 0$. These can be calculated to NLO by comparison with fixed-order results. However, there is no unique way of including this fixed-order information into $R_y(y')$ (this is the so-called matching ambiguity). For example, it is also legitimate to include the C, D terms into the exponent (termed “log R matching”), as the difference is of order a^3 .

In Eq. (4.10), there are terms at $O(a^n)$ with up to $2n$ factors of L multiplying them. In contrast, in the exponent of Eq. (4.11) at $O(a^n)$ we find no more than $n + 1$ factors of L . The $L^m a^n$ terms with $n + 1 < m \leq 2n$ are generated by the exponentiation. For example, including just the leading order, leading log term $\sim L^2 a$ in the exponent of Eq. (4.11) leads, after the exponent is expanded out, to the entire set of double-logs $\sim L^{2n} a^n$ in Eq. (4.10). Ideally we would like to use this exponentiation property in our ECH approximation. So, let us consider the effect of defining

$$R_y(y') = \exp(r_0(y')\mathcal{R}(y')) . \quad (4.12)$$

Here all the physics is encoded into a single effective charge, which is exponentiated in its entirety. This is similar to log R matching in that if we re-expand $r_0\mathcal{R}$ in terms of a and L the C and D functions will clearly appear in the exponent. However, in this approach there is no matching ambiguity because once we have picked the effective charge the inclusion of C and D is automatically determined. The function r_0 for thrust can be found by integrating the analytically known

leading order 1-thrust distribution [17]

$$\frac{1}{\sigma} \frac{d\sigma}{d\tau} \Big|_{LO} = \frac{C_F a (3 - 9\tau - 3\tau^2 + 9\tau^3 + (-4 + 6\tau - 6\tau^2) \log(\frac{1}{\tau} - 2))}{2\tau(\tau - 1)} \quad (4.13)$$

with the boundary condition that R_τ vanishes to LO for $\tau \geq 1/3$. The result is

$$\begin{aligned} r_0(\tau) = C_F & \left(-\frac{5}{4} + \frac{\pi^2}{6} + 3\tau + \frac{9\tau^2}{4} + \left(\frac{3}{2} - 3\tau \right) (\log(1 - 2\tau) - \log(\tau)) \right. \\ & \left. - (\log(1 - \tau) - \log(\tau))^2 - 2 \text{Li}_2 \left(\frac{\tau}{1 - \tau} \right) \right). \end{aligned} \quad (4.14)$$

1-Thrust and heavy-jet mass agree at LO, so the same result holds for heavy-jet mass. A given prediction for $\mathcal{R}(y)$ now allows us to calculate a corresponding $R(y)$. Then, by taking the difference in $R(y)$ across the bins in each experimental data set, a comparison to data can be carried out, including a $1/Q$ power correction by using $R_{PC}(y) = R_{PT}(y - C_1/Q)$. In the remainder of this chapter we will consider predictions for the distributions of 1-thrust and heavy-jet mass arising from substituting various ECH approximations into Eq. (4.12).

The simplest possibility is to use a standard NLO ECH $\mathcal{R}(y)$. This only requires knowledge of r_1 , which can be easily obtained from the results of Monte Carlo calculations of the distributions to NLO. This NLO ECH, re-expanded in $a(Q)$ and L in the $\overline{\text{MS}}$ scheme, includes terms $\sim L^m a^n$ for all n and all $m \leq n + 1$. Some of these terms can be compared with their exactly known LL and NLL counterparts allowing us to determine to what extent the LL and NLL terms are ‘‘RG-predictable’’. In this context, RG-predictability refers to the extent to which the higher order coefficients in the perturbation series for \mathcal{R} are already present in some lower order ECH result. Overall, the logs are not very well predicted by the NLO ECH results except for rather small n (see Figs. 4.3 and 4.4 for NLL examples). However, the exponentiation of the effective charge will produce further towers of logs in the distributions themselves. We might therefore expect these NLO ECH results to have better behaviour in the 2-jet region than the results of Ref.[35]. This is indeed the case, as can be seen in Fig. 4.5. It is interesting to note

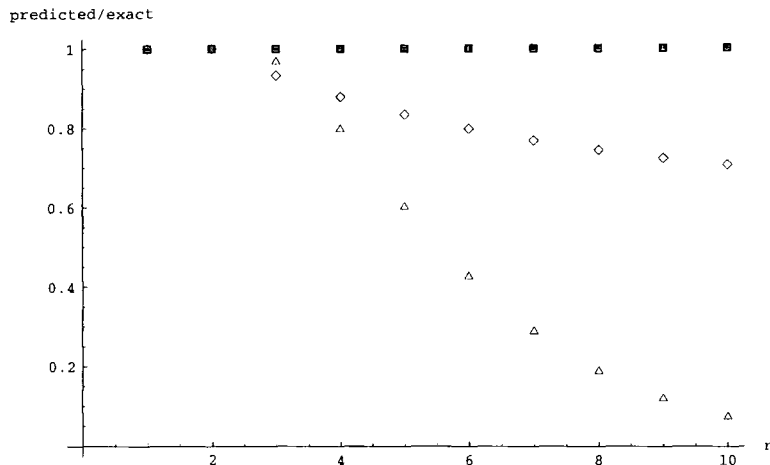


Figure 4.3: Prediction of NL $\overline{\text{MSPS}}$ logs in the exponent for 1-thrust based on re-expanding lower order ECH results in $a_{\overline{\text{MS}}}$. The ratio of the predicted NL coefficient at $O(a^n)$ with the corresponding exact coefficient is shown. Triangles are for NLO ECH, diamonds for LL ECH. As a consistency check, squares show the results for NLL ECH where the NL log must appear exactly.

that exponentiation of a NLO $\overline{\text{MSPS}}$ series in place of \mathcal{R} produces a distribution (the dashed curve in Fig. 4.5) with a badly misplaced peak (this remains the case for any reasonable value of $\Lambda_{\overline{\text{MS}}}$). Therefore, the good qualitative description of the peak is only obtained at NLO with the use of both exponentiation and ECH (until we introduce non-perturbative effects).³

³At NLO, ECH is equivalent to a scale choice $\mu = Qe^{-r_1/b}$. In the case of both thrust and heavy-jet mass $r_1 = bL/2 + \text{const} + \dots$, so using a NLO ECH is equivalent to choosing $\mu = Q\sqrt{y}f(y)$ where $f(y)$ goes to a constant as $y \rightarrow 0$. This is interesting as a “physical scale” argument where one takes, for example, the heavy-jet mass $m_h = \sqrt{\rho_h}Q$ as the scale would give $\mu = Q\sqrt{\rho_h}$. So these two scale-setting methods have the same leading ρ_h dependence, and only differ by the factor f . This factor is important, however, as its overall normalization is RS-dependent and this ensures that μ is chosen in such a way that we obtain the same ECH answer whatever RS we choose.

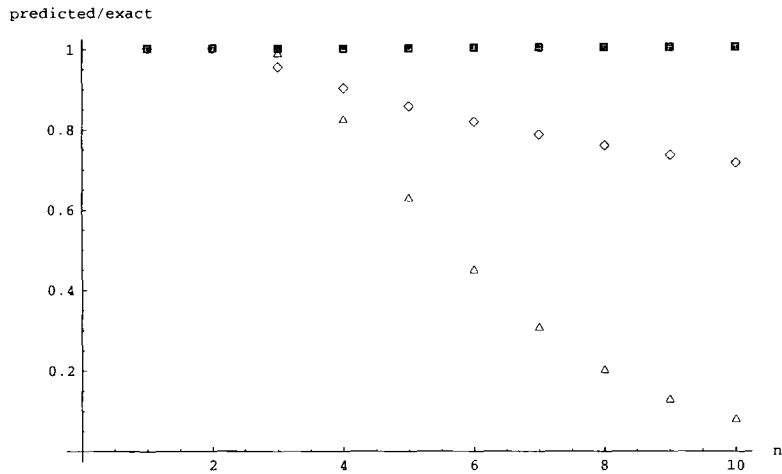


Figure 4.4: As Fig. 4.3 but for heavy-jet mass.

4.3.4 Resummation of ρ

We can now consider performing a resummation of logs in the ρ function as described in Section 4.2. First, constructing these order-by-order in \mathcal{R} allows us to again address the question of the “RG-predictability” of the $\overline{\text{MS}}$ logs. For example, one can ask how much of the NL log at $\mathcal{O}(a^n)$ in $\overline{\text{MS}}$ is included when we use the LL ECH result (of course, if we use the NLL ECH the full NL $\overline{\text{MS}}$ log is included by construction). To find out, we can re-expand the ECH results in terms of $\alpha_{\overline{\text{MS}}}(Q)$ as we did for the NLO ECH. The resulting coefficients are shown in Fig. 4.3 (for 1-thrust) and Fig. 4.4 (for heavy-jet mass) as fractions of the exact coefficients. The LO and NLO ($n = 1, 2$) coefficients agree exactly as r_0 and r_1 have been used to NLL accuracy in all the predictions. There is a clear improvement in the prediction of the NL logs as we move from NLO ECH to LL ECH as one might expect. The extent to which the NL logs really are included in LL ECH is encouraging, as it suggests that NLL ECH might do a good job of including some higher order corrections that are omitted in the $\overline{\text{MS}}$ approach.

The method described in Section 4.2 can now be used to produce numerical

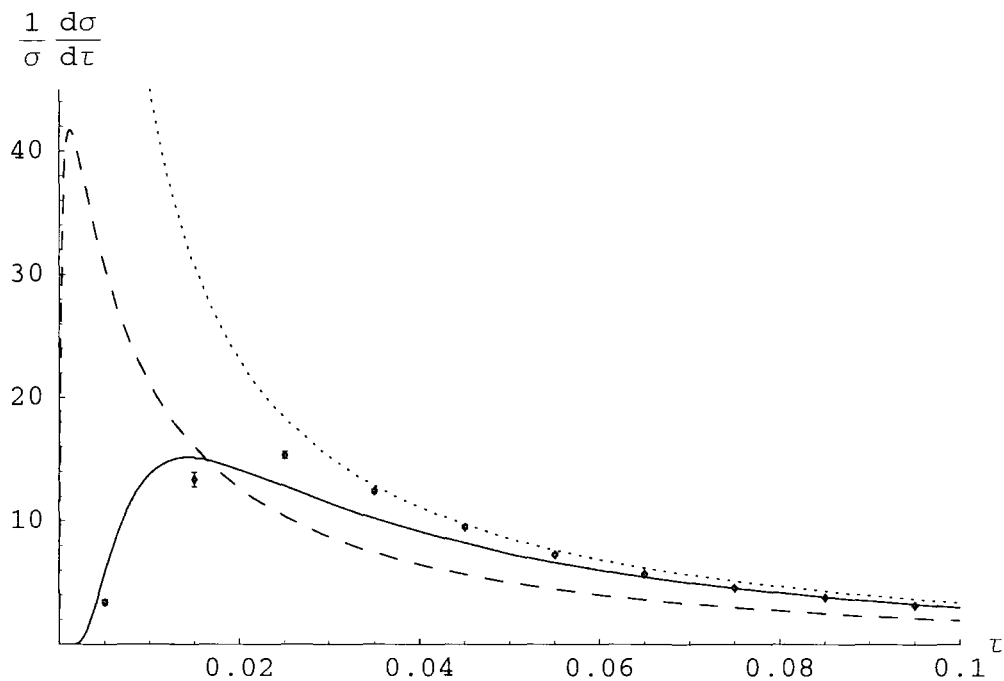


Figure 4.5: Comparison of the 1-thrust distributions calculated using various NLO approximations in the 2-jet region. The solid curve arises from the exponentiated ECH of Eq. (4.12). The dashed curve is obtained by expanding this effective charge in the $\overline{\text{MS}}$ scheme with $\mu = Q$. The dotted curve is a prediction in the approach of Ref.[35]. Throughout we have taken $Q = M_Z$ and $\tilde{\Lambda}_{\overline{\text{MS}}} = 250\text{MeV}$. For comparison, DELPHI data at $Q = M_Z$ are shown.

approximations to ρ_{LL} and ρ_{NLL} (these are not truncated at any order in \mathcal{R}). All of our calculations were carried out using the computer algebra system *Mathematica* [55], allowing the use of arbitrary precision arithmetic in taking the $L \rightarrow \infty$ limit. These ρ_{LL} and ρ_{NLL} functions can be used to make predictions for \mathcal{R} , by inserting them in Eq. (3.15) and numerically solving the transcendental equation. To ensure exact cancellation between the singularities in Eq.(3.18), for $\mathcal{R} < 0.005$ we use the exact series expansions of $\rho(\mathcal{R})$ up to to order \mathcal{R}^4 (the difference is totally negligible for all values of L we consider) This defines what we call our “LL ECH” and “NLL ECH” predictions.

4.3.5 Fits

To perform fits with these exponentiated effective charges we again need to select a fit range. After exponentiation, the problem as $r_0 \rightarrow 0$ remains, and in fact for thrust worsens; unfortunately this means we need to restrict the fits to $1 - T < 0.18$, $\rho_h < 0.24$ to obtain good fits in the ECH approach. Irrespective of the inclusion of logs, the onset of non-perturbative effects more complicated than a simple $1/Q$ shift means that we still need to impose a lower cut. These higher-order non-perturbative effects are expected to be of order $\Lambda/(Qy)$ [53] so our cut should be placed at $y \sim \Lambda/Q$ with Λ some infrared scale. One might expect the inclusion of the extra logs into ρ to improve the fit of the ECH prediction to data in the 2-jet region. Unfortunately, it turns out that including these logs actually *worsens* the behaviour of the ECH results. In this region the growth of r_1 causes \mathcal{R} to become larger (because $\Lambda_{\mathcal{R}}$ approaches Q), and this is accelerated by the addition of logs into ρ . In fact, \mathcal{R} eventually grows large enough that we encounter a branch cut in ρ which appears due to the branch cut in g_1 [54]. Clearly this behaviour is unphysical, and must be avoided in our fits to data. Presumably some other higher order corrections intervene to produce an ECH prediction which is

well-behaved in the 2-jet limit. In any case, in light of the RG-predictability of the sub-leading $\overline{\text{MS}}$ SPS logs, it is still possible that the ρ resummations improve the quality of the ECH predictions in the intermediate region, so it is worth trying to fit the data with a lower cut in place (and studying the sensitivity of the best fit parameters to the choice of this cut). Good fits are obtained over the whole energy range using $\rho_h, 1 - T > 0.05M_Z/Q$.

Any data bins not lying within the range $0.05M_Z/Q < \rho_h < 0.24, 0.05M_Z/Q < 1 - T < 0.18$ have been left out of the fit; a summary of the data we actually used is given in Tables 4.3 and 4.4. We have also removed the JADE data at 35 and 44 GeV from the heavy-jet mass fits, since its inclusion dramatically worsens the fit quality for both the $\overline{\text{MS}}$ SPS and ECH predictions. The results of fitting for $\Lambda_{\overline{\text{MS}}}$ and C_1 are shown in Figs. 4.6 and 4.7 for all three approximations. For comparison, $\overline{\text{MS}}$ SPS results are also shown. The fit range for these could in principle be extended as they do not suffer from the $r_0 \rightarrow 0$ problem that afflicts the ECH, however, in order to facilitate a direct comparison between the two approaches we have used the same fit range for both. The most notable feature of the results is the stability of the $\Lambda_{\overline{\text{MS}}}$ values found within the ECH framework as we move from NLO to LL and then to NLL accuracy, while the fit quality hardly changes. This improved stability with respect to the order of the approximation might be a consequence of the RG-predictability of the $\overline{\text{MS}}$ SPS logs discussed above, because, for example, a lot of the logs that only turn up at NLL order in the $\overline{\text{MS}}$ SPS predictions are included already at LL order in ECH. It must be noted however that despite their stability, these $\Lambda_{\overline{\text{MS}}}$ values are still smaller than the world average. Some examples of the actual NLL ECH distributions are shown in Fig. 4.8.

To investigate the sensitivity of these results to our choice of fit range we have redone the fits for a “low” range and a “high” range. The low range was determined by decreasing the upper cut until half the bins were excluded, and the

high range was determined by increasing the lower cut similarly. The effects of these changes on the central values of $\Lambda_{\overline{MS}}$ and C_1 are shown in Table 4.1 (for 1-thrust) and Table 4.2 (for heavy-jet mass). The ECH fit values for heavy-jet mass appear more stable than the \overline{MS} ones; and the stability increases as the accuracy of the predictions are increased. This is also true for the thrust, but to a lesser extent. A particular exception is that the application of NLL ECH to the “high” fit range gives a significantly different power correction compared to the “low” fit range. This is probably responsible for the relatively large χ^2 for the “normal” fit. The reason for the change in C_1 may be the $r_0 \rightarrow 0$ problem being exacerbated by the increase in size of the effective charge as more logs are added into its beta-function. Because the $r_0 \rightarrow 0$ problem represents a breakdown of our approximations, the “low” fit range results are probably more trustworthy (and in any case, agree very well with the “normal” fit range results).

Lastly, we have also considered the so-called “modification of the logs” that is often invoked in studies of event shape variables. This consists of modifying $L = \log(1/y) \rightarrow \log((2y_{max} - y)/y)$ to ensure that the resummed parts of the expression vanish at the upper kinematic limit y_{max} (which is 0.5 for both T and ρ_h). The change in central values is shown in Tables 4.1 and 4.2. One finds that the fitted values change very little. This is to be expected since the restricted fit range automatically ensures that the logarithm is essentially unchanged in that region.

4.3.6 Resummation without Exponentiation

An alternative to the approach followed here would be to apply our resummations to an effective charge associated to the distribution itself similar to the one considered in Ref.[35] but taking the bin width to 0 (the NLO approximation for this effective charge is shown as the dotted curve on Fig. 4.4). This is certainly

Prediction	Λ/MeV	C_1/GeV	$\chi^2/\text{dof.}$
NLO ECH	98,116,118	1.02,0.85,0.89	24/46,59/88,27/44
NLO $\overline{\text{MS}}$ SPS	446,463,517	1.47,1.42,1.28	26/46,57/88,23/44
LL ECH	101,119,108	0.80,0.63,0.88	23/46,63/88,30/44
LL $\overline{\text{MS}}$ SPS	371,417,478	1.12,1.02,0.83	24/46,49/88,22/44
NLL ECH	103,107,93	0.50,0.52,0.93	23/46,84/88,34/44
NLL ECH (mod)	104,110,95	0.50,0.47,0.90	23/46, 81/88, 34/44
NLL $\overline{\text{MS}}$ SPS	200,233,268	0.94,0.79,0.60	23/46, 49/88, 23/44

Table 4.1: Sensitivity of our fit values for $\Lambda_{\overline{\text{MS}}}$ and C_1 to the choice of fit range for thrust. The fit ranges are $0.05M_Z/Q - 0.1$ (low), $0.05M_Z/Q - 0.18$ (normal), $0.11M_Z/Q - 0.18$ (high).

Prediction	Λ/MeV	C_1/GeV	$\chi^2/\text{dof.}$
NLO ECH	120,114,142	1.19,1.22,0.94	19/42,50/84,29/41
NLO $\overline{\text{MS}}$ SPS	236,115,221	1.65,1.84,1.27	19/42,68/84,37/41
LL ECH	124,123,128	1.06,1.07,1.01	21/42,51/84,29/41
LL $\overline{\text{MS}}$ SPS	185,132,146	1.39,1.57,1.33	19/42,63/84,36/41
NLL ECH	125,127,122	0.99,0.97,1.04	21/42,51/84,29/41
NLL ECH (mod)	126,128,122	0.98,0.97,1.05	21/42, 51/84, 29/41
NLL $\overline{\text{MS}}$ SPS	114,82,67	1.29,1.49,1.62	19/42,64/84,37/41

Table 4.2: Sensitivity of our fit values for $\Lambda_{\overline{\text{MS}}}$ and C_1 to the choice of fit range for heavy-jet mass. The fit ranges are $0.05M_Z/Q - 0.12$ (low), $0.05M_Z/Q - 0.24$ (normal), $0.125M_Z/Q - 0.24$ (high).

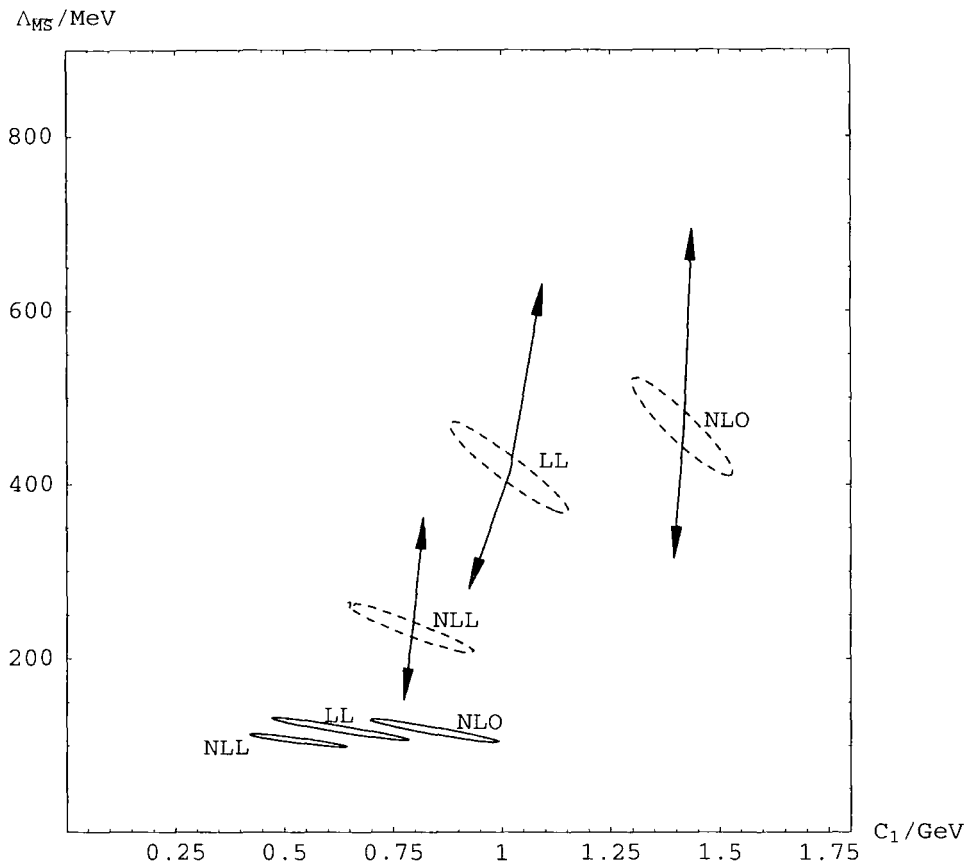


Figure 4.6: Fits to the thrust distribution for $\Lambda_{\overline{\text{MS}}}$ and C_1 . Solid ellipses use ECH, dashed ellipses $\overline{\text{MS}}\text{PS}$ (with the arrows showing the effect on the central value of varying $Q/2 < \mu < 2Q$). The ellipses indicate 2σ errors generated by allowing χ^2 to vary within 4 of its minimum. For a summary of the data used see Table 4.3.

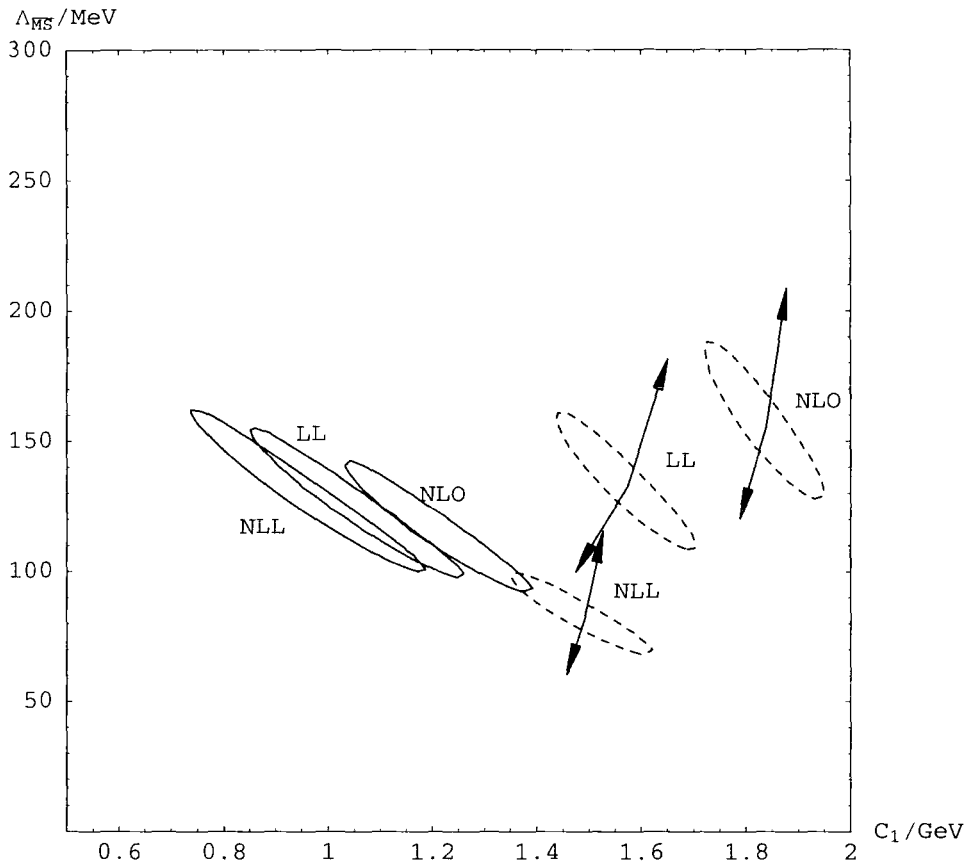


Figure 4.7: As Fig. 4.6 but for heavy-jet mass. For a summary of the data see Table 4.4.

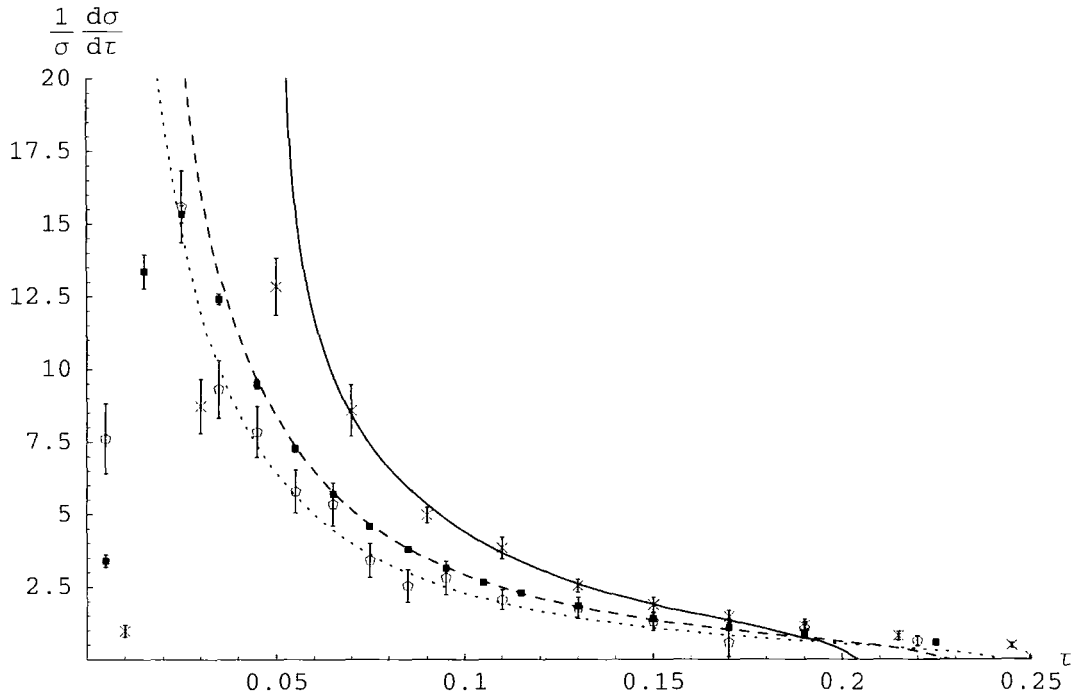


Figure 4.8: Examples of our best fit NLL ECH 1-thrust distributions. The solid curve is for $Q = 44\text{GeV}$, dashed is $Q = 91.2\text{GeV}$ and dotted is $Q = 183\text{GeV}$. These predictions are compared to data from the JADE and DELPHI collaborations at these energies; crosses are JADE data at 44GeV , boxes are DELPHI data at 91.2GeV and open circles are DELPHI data at 183GeV .

Experiment	Q	Range	Data Points	Source
ALEPH	91.2	0.05-0.18	7	[39]
	133	0.04-0.15	4	[40]
DELPHI	91.2	0.05-0.18	10	[36]
	133	0.04-0.18	5	[41]
	161	0.04-0.18	5	[41]
	172	0.04-0.18	5	[41]
	183	0.03-0.18	11	[41]
JADE	35	0.14-0.18	2	[42]
	44	0.12-0.18	3	[42]
L3	91.2	0.065-0.175	4	[43]
	189	0.025-0.175	6	[44]
OPAL	161	0.03-0.15	6	[46]
	172	0.03-0.15	6	[47]
	183	0.03-0.15	6	[47]
	189	0.03-0.15	6	[47]
SLD	91.2	0.06-0.16	3	[48]
TASSO	44	0.12-0.16	1	[49]

Table 4.3: Summary of the data used in our fits for thrust.

Experiment	Q	Range	Data Points	Source
DELPHI	91.2	0.05-0.2	8	[36]
	161	0.04-0.2	4	[41]
	133	0.04-0.2	4	[41]
	172	0.04-0.2	4	[41]
	183	0.03-0.24	10	[41]
SLD	91.2	0.08-0.24	3	[48]
ALEPH	91.2	0.05-0.2	8	[39]
L3	91.2	0.051-0.216	7	[43]
	189	0.03-0.24	14	[44]
OPAL	91.2	0.0625-0.2025	4	[45]
	161	0.0289-0.2025	5	[46]
	172	0.0289-0.2025	5	[47]
	183	0.0289-0.2025	5	[47]
	189	0.0289-0.2025	5	[47]

Table 4.4: Summary of the data used in our fits for heavy-jet mass.

possible and leads to a ρ function where the LL, NLL and NNLL terms are known. However this creates problems with the resummation which prevent this approach from yielding useful predictions. To see this, consider ρ_{LL} . As explained in Section 4.2, this is related to the leading $\log \bar{\rho}$ via

$$\rho_{LL}(\mathcal{R}) = \bar{\rho}_{LL}(\mathcal{R}) + bc\mathcal{R}^3. \quad (4.15)$$

In this (unexponentiated) case $\bar{\rho}_{LL}$ is found using the one-loop beta-function and the double logarithmic distribution

$$\frac{1}{\sigma} \frac{d\sigma}{dy} = \frac{d}{dy} \exp(-kL^2 a) = (2ke^{-L}L)a \exp(-kL^2 a) \equiv (2ke^{-L}L)\bar{\mathcal{R}}, \quad (4.16)$$

where k is a constant ($4/3$ for thrust and heavy-jet mass). This distribution has a peak as a function of a at $a_{max} = 1/kL^2$, and so its inverse only exists for $\bar{\mathcal{R}} < \bar{\mathcal{R}}(a_{max}) = e^{-1}/kL^2$. As a consequence $\bar{\rho}_{LL}(\mathcal{R})$ vanishes at this point (where a branch cut starts). Adding the $bc\mathcal{R}^3$ term to give ρ_{LL} , and later adding the NLL terms, does not remove this branch cut. As \mathcal{R} is evolved from $Q = \infty$ it increases until it reaches this maximum value, and then its evolution becomes undefined. This value turns out to be too small to allow fits to the data. One could possibly “switch branches” of ρ at this point and allow \mathcal{R} to decrease again, although this would of course still not provide a good fit to the data. Note also that this zero of $\bar{\rho}$ does *not* correspond to an “infrared freezing” type behaviour because $\bar{\rho}$ approaches the zero as $(\mathcal{R} - \mathcal{R}_{max})^\gamma$ with $\gamma < 1$ - thus the singularity in Eq. (3.15) is integrable and the zero is reached after a finite amount of evolution in Q .

4.4 Discussion and Conclusions

In Section 4.2 we showed how it was possible to build a resummation of large infrared logarithms into ECH. In principle, this allows the use of ECH for multi-scale

observables, even when the ratio between the scales grows large. The approach taken was to apply a resummation at the level of the effective charge beta-function ρ . A method was described allowing such a resummed ρ to be extracted numerically to any desired accuracy from the resummed expression for an observable in $\overline{\text{MSPS}}$.

In Section 4.3 we used the results of Section 4.2 to extend the direct extraction of $\Lambda_{\overline{MS}}$ from e^+e^- event shape observables of Ref.[35] to include a resummation of large infra-red logarithms (in this case $L = \log(1/y)$ where y is the shape variable). One could relate the observable $R_y(y')$ to an effective charge \mathcal{R} by exponentiation, $R_y(y') = \exp(r_0\mathcal{R})$. Using the NLO approximation for \mathcal{R} lead to a good fit to data. One could then numerically construct $\rho_{LL}(\mathcal{R})$ and $\rho_{NLL}(\mathcal{R})$ functions by resumming to all-orders the corresponding pieces of the ρ_n in Eq. (3.15). The LL and NLL predictions for $R_y(y')$ for a given value of $\Lambda_{\overline{MS}}$ then follow on inserting these $\rho(\mathcal{R})$ functions in Eq. (3.15) and numerically solving the transcendental equation. To model $1/Q$ power corrections we fitted to a shifted distribution $R_{PC}(y) = R_{PT}(y - C_1/Q)$. Whilst in principle straightforward a number of complications arose. In particular as $1 - T$ approaches $1/3$ the leading coefficient r_0 goes to zero, invalidating the effective charge approach. This places a rather stringent upper limit on the fit range. There are also problems in the two-jet region due to the growing \mathcal{R} running into a branch cut in ρ which appears as the image of a branch cut in g_1 in the $\overline{\text{MSPS}}$ approach. We also noted that one cannot directly relate the observables to an unexponentiated effective charge, as in Ref.[35], since in that case $\rho_{LL}(\mathcal{R})$ has a different branch cut such that the energy evolution of \mathcal{R} becomes undefined and we are unable to fit the data. Simultaneous fits for $\Lambda_{\overline{MS}}$ and C_1 were performed using data for thrust and heavy-jet mass distributions over a wide range of energies (see Tables 4.3 and 4.4). The 2σ error contours in $\Lambda_{\overline{MS}}$ and C_1 are shown in Figs. 4.6 and 4.7. NLO, LL and NLL results are shown

for both standard $\overline{\text{MSPS}}$, and for ECH. For $\overline{\text{MSPS}}$ there is a strong decrease in $\Lambda_{\overline{\text{MS}}}$ going from NLO to LL to NLL, whereas for ECH the fitted $\Lambda_{\overline{\text{MS}}}$ values are remarkably stable. The fitted value of C_1 is also somewhat smaller for ECH. We also investigated the stability of the fits to changing the fit range in Tables 4.1 and 4.2. The ECH results show more stability than $\overline{\text{MSPS}}$. This, along with the stability of the fitted values with respect to the order of approximation, leads us to believe that the fit ranges we have chosen are restrictive enough to avoid the problems that appear in the 2-jet region for LL and NLL ECH, whilst hopefully retaining the benefit of including some RG-predictable sub-leading logs into our predictions. The fits all produce $\Lambda_{\overline{\text{MS}}}$ values somewhat smaller than the world average. It is interesting to note, however, that they are of the same magnitude as those found in [35]. Converting our NLL best fit Λ values to $\alpha_{\overline{\text{MS}}}(M_Z)$ using the 2-loop beta-function gives $\alpha_{\overline{\text{MS}}}(M_Z) = 0.106$ for $\Lambda_{\overline{\text{MS}}} = 100\text{MeV}$ (thrust) and $\alpha_{\overline{\text{MS}}}(M_Z) = 0.109$ for $\Lambda_{\overline{\text{MS}}} = 125\text{MeV}$ (heavy-jet mass). Similarly small values of $\alpha_{\overline{\text{MS}}}$ have also been reported in the DGE approach (see [10]). It is possible that sizeable NNLO corrections (omitted by both the DGE and ECH resummations) might be responsible. One can attempt to allow for this by performing a three-parameter fit for $\Lambda_{\overline{\text{MS}}}, C_1$ and ρ_2^{NNLL} , but unfortunately it tends to run off to very large ρ_2^{NNLL} , in which case one would find it hard to justify ignoring other sub-leading terms. It will be interesting to see the effect of matching to fixed-order NNLO results when they become available.

It is important to note that the conclusions we have given here assume that non-perturbative effects can be well modelled by a simple shift ($y \rightarrow y - C_1/Q$) of the perturbative distribution. A possible future extension of this work could be to investigate the effect of allowing a more general form of power correction.

We would conclude that, notwithstanding the limited fit range and technical complications from which ECH suffers, there is evidence that the fitted power

corrections are reduced relative to the standard approach, although not as dramatically as in the DELPHI fits of Ref.[13] which are consistent with zero power corrections. However in that analysis corrections for bottom quark mass effects were made, which were not included in our analysis.

Chapter 5

PMS and DIS Event Shape Means

In this chapter, the Principle of Minimal Sensitivity described in Section 3.4 is applied to the means of event shapes defined in the Breit frame of ep deep-inelastic scattering (DIS). The effect of optimizing the choice of renormalization and factorization scales on the size of power corrections is investigated by comparing optimized NLO perturbation theory to data from the H1 collaboration [63].

5.1 Introduction

The Dokshitzer-Webber model described briefly in Subsection 2.5.2 can be applied not only to event shapes in e^+e^- annihilation, but also to those defined in the Breit frame of electron-proton (ep) deep-inelastic scattering (DIS) [71]. Impressively, as with the e^+e^- shapes, a good description of the data can be given for $\bar{\alpha}_0 \simeq 0.5$ (see e.g. the review Ref. [1]). As in the e^+e^- case, the power corrections for several shape variables (for example the analogue of thrust) make up a substantial part of their mean values even for $Q \sim M_Z$. It is therefore interesting to ask whether these power corrections would be reduced by optimising the choice of RP.

For DIS, however, optimisation is not so straightforward. The appearance of the proton in the initial state leads to a dependence of the event shape means on the proton parton distribution functions (PDFs) and the accompanying factorisation scale, M , as described in Section 2.4. Ideally we would like to use some optimisation criterion to choose all the unphysical parameters, but none of the above-mentioned theoretical arguments simultaneously select unique values for both μ and M . However, the Principle of Minimal Sensitivity (PMS) described in Section 3.4 does generalise very easily to the factorisation case [57, 58, 59, 60] (for recent applications to hadron-hadron interactions see Refs. [61, 62]). Moreover, the PMS tends to agree very well with the ECH as used in the DELPHI analysis when the latter can be applied. Therefore, the purpose of the present chapter is to apply the PMS to the choice of renormalization and factorisation scales in DIS event shape means, and compare NLO perturbation theory to data from the H1 collaboration [63] to see how the required power corrections are affected.

The plan of this chapter is as follows. Section 5.2 contains definitions of the observables. In Section 5.3 we review the way that dependence on μ and M arises in NLO DIS calculations, and define the PMS approximations we are going to study. Then, in Section 5.4 we describe the methods used in the calculation. Section 5.5 runs through the analysis in detail for one specific observable, the current jet thrust τ_c . Results for all the observables discussed in Ref. [63] are presented in Section 5.6. Section 5.7 contains our conclusions.

5.2 Definition of the Observables

First, let us briefly define the relevant kinematical quantities. Let P be the 4-momentum of the incoming proton and q the (space-like) 4-momentum of the virtual photon which transfers momentum from the positron to the proton. The

photon virtuality is $Q^2 = -q^2 > 0$. Bjorken x is given by

$$x_B = \frac{Q^2}{2P \cdot q}. \quad (5.1)$$

The observables considered here are all defined in the Breit frame. We indicate quantities evaluated in the Breit frame by an asterisk. With this convention the Breit frame is defined by requiring

$$2x_B P^* + q^* = (Q, \vec{0}), \quad (5.2)$$

(which fixes the frame up to a rotation) along with the conditions that \vec{P}^* point in the $+z^*$ -direction and the incoming/outgoing electron momenta lie in the (x^*, z^*) plane (which fix the rotation). In a “parton model” event where we imagine there is no radiation from the struck quark, $x_B P = \xi P$ is its momentum. Then, Eq. (5.2) implies that in the Breit frame the quark is back-scattered by the virtual photon into the $-z^*$ direction. In other words, it is scattered into the current hemisphere (CH) of the Breit frame, defined as the hemisphere for which $z^* < 0$, where it fragments to produce a current jet. The proton remnant proceeds in the $+z^*$ direction into the remnant hemisphere (RH). The Breit frame is therefore special in that it belongs to the family of frames (related by boosts along the z^* -axis) where there is a maximum angular separation between the current and remnant jets. The picture is complicated when more realistic QCD radiation is added, but still the Breit hemisphere gives a good separation without requiring detailed analysis of the hadronic part of the final state. The particular choice of the Breit frame over the other frames in this family has the consequence that at leading order the current hemisphere contains a single quark of energy $Q/2$, and so strongly resembles one hemisphere of an e^+e^- annihilation event.

The notation for event shapes in DIS is nowhere near as settled as in the e^+e^- case; in this chapter we follow the nomenclature of Ref. [63].

First, we consider five observables defined using particles in the CH only. To ensure infrared safety the total energy in the CH (evaluated in the Breit frame)

must exceed some threshold, taken to be $Q/10$, for an event to contribute to one of these variables. The z^* -axis thrust is

$$\tau_c = 1 - \frac{\sum_i |\vec{p}_i^* \cdot \vec{n}|}{\sum_i |\vec{p}_i^*|} \quad (5.3)$$

where \vec{n} is a unit vector in the z^* direction. Similarly, the z^* -axis jet broadening is

$$B_P = \frac{\sum_i |\vec{p}_i^* \times \vec{n}|}{\sum_i |\vec{p}_i^*|}. \quad (5.4)$$

The thrust-axis thrust is

$$\tau_P = 1 - \max_{\vec{n}} \frac{\sum_i |\vec{p}_i^* \cdot \vec{n}|}{\sum_i |\vec{p}_i^*|} \quad (5.5)$$

where \vec{n} is now the unit vector with respect to which the maximisation is performed (the value which leads to the maximum defines the thrust axis). The C -parameter is defined by making use of the tensor

$$\Theta_{jk}^* = \frac{\sum_i p_{i,j}^* p_{i,k}^* / |\vec{p}_i^*|}{\sum_i |\vec{p}_i^*|} \quad (5.6)$$

where $p_{i,j}^*$ is the j th component of the momentum of particle i . Θ_{jk}^* has three eigenvalues: λ_1 , λ_2 and λ_3 , in terms of which the C -parameter is

$$C_P = 3(\lambda_1 \lambda_2 + \lambda_2 \lambda_3 + \lambda_3 \lambda_1). \quad (5.7)$$

Lastly we have the jet mass

$$\rho_E = \frac{(\sum_i p_i)^2}{4 \sum_i E_i^*}. \quad (5.8)$$

Because the jet mass involves the difference between energies and 3-momenta it is especially sensitive to hadron mass effects which can lead to additional power corrections beyond the scope of the model of Ref. [4, 28]. These can be removed by defining a related observable in the so-called ‘‘E-scheme’’ [64]

$$\rho_E^{(\text{ESch})} = \frac{\left[\sum_i (E_i^*, E_i^* \frac{\vec{p}_i^*}{|\vec{p}_i^*|}) \right]^2}{4 \sum_i E_i^*}. \quad (5.9)$$

This is just ρ_E with each particle replaced by a massless particle of the same energy. Since our NLO perturbative calculations are carried out with the approximation of massless quarks, the perturbative predictions for $\rho_E^{(\text{ESch})}$ will be identical to those for ρ_E ; only the non-perturbative contributions will differ. For the purposes of this chapter, data has been obtained for $\rho_E^{(\text{ESch})}$ by applying a correction factor from PYTHIA 6.2 [65] to the ρ_E values given in Ref. [63].

The remaining two variables make use of both the CH and RH. They are defined based on two jet clustering algorithms, the factorisable Jade algorithm and the modified k_T algorithm. These clustering algorithms allow one to gather the final-state momenta into a certain number of current jets, plus the remnant jet, according to a resolution parameter y which determines how aggressively momenta are combined. This is done by examining the momenta repeatedly, and combining those that are nearest according to a distance measure specific to the clustering algorithm, until the nearest pair have a separation $y_{ij} > y$. Event shapes can be defined from these algorithms by using the value of y at which the event goes from being a 2+1 jet event (two current jets, one remnant jet) to a 1+1 jet event.

In the DIS case the distance measures need to be generalised from the e^+e^- case to include a distance between a jet and the remnant. For the factorisable Jade algorithm

$$y_{ij} = \frac{2E_i^* E_j^* (1 - \cos \theta_{ij}^*)}{Q^2} \quad (5.10)$$

$$y_{ir} = \frac{2E_i^* x_B E_p^* (1 - \cos \theta_{ip}^*)}{Q^2} \quad (5.11)$$

where i, j indicate jets, r is the remnant and p is the proton. In the same notation the k_t measures are

$$y_{ij} = \frac{2\min(E_i^{*2}, E_j^{*2})(1 - \cos \theta_{ij}^*)}{Q^2} \quad (5.12)$$

$$y_{ir} = \frac{2E_i^{*2}(1 - \cos \theta_{ip}^*)}{Q^2}. \quad (5.13)$$

The related event shapes will be denoted by y_{fJ} and y_{k_t} respectively.

For discussions of cuts and more details about the definition of each observable, see Ref. [63].

5.3 Applying The Principle of Minimal Sensitivity to DIS

The simplest application of the PMS to QCD involves the case of an observable without hadrons in the initial state (and without identified hadrons in the final state). The only unphysical parameters are then those that label the renormalization scale and scheme, as described in Section 3.4. At NLO it suffices to just consider the renormalization scale μ , as a change in scheme can be absorbed into a rescaling of μ . For an observable involving hadrons in the initial state, we also have to take into account its unphysical dependence on the parameters that label the factorisation scale (M) and scheme. In contrast with the renormalization case, the factorisation scheme dependence cannot be absorbed into the scale even at NLO. This is obvious, because to specify the FS at NLO one must give the functions $P_{a \rightarrow b}^{(1),FS}(z)$ (see Eq. (2.67)). Therefore, already at NLO, there is an infinite number of degrees of freedom in the specification of the FS. Ideally one would optimise with respect to both M and the FS; however, it is difficult to formulate a PMS condition for the FS (in x -space) [66], so here we will simply neglect the scheme dependence and work in the $\overline{\text{MS}}$ factorisation scheme at all times. With this simplification, the relevant parameters are μ and M .

The mean of some DIS observable y depending on the final state X can be expressed as

$$\langle y \rangle = \frac{\int y(X) d\sigma(ep \rightarrow X, Q)}{\int d\sigma(ep \rightarrow X, Q)} \quad (5.14)$$

where $d\sigma(ep \rightarrow X, Q)$ is the infinitesimal cross-section for the process $ep \rightarrow X$ and

Q is the virtuality of the exchanged photon. To compute such a cross-section in perturbation theory we need to factorise the process into a soft part, described by the proton PDFs $f_a(\xi, M)$, and a hard part, described by a partonic cross-section $\hat{\sigma}(e a \rightarrow X, Q, M)$

$$\frac{d\sigma(ep \rightarrow X, Q)}{dX} = \sum_a \int d\xi f_a(\xi, M) \frac{d\hat{\sigma}(e a \rightarrow X, Q, M)}{dX}. \quad (5.15)$$

As indicated, f and $\hat{\sigma}$ depend on the unphysical parameter M even before they are approximated perturbatively; this dependence cancels between them after the integral over ξ and the sum over a are performed. The dependence of $f_a(\xi, M)$ on M is given by the DGLAP evolution equations Eq. (2.66).

To arrive at a NLO approximation, we substitute into Eq. (5.15) PDFs evolving according to the NLO splitting functions, and the partonic cross-section expanded to NLO. This approximation not only prevents the exact compensation of M dependence between the PDFs and the partonic cross-section, but also introduces a dependence on the RS used for the expansion.

In summary, at NLO, our approximation for $\langle y \rangle$ will have an unphysical dependence on both M and μ and we can look for a PMS point by requiring

$$\left. \frac{\partial \langle y \rangle_{\text{NLO}}}{\partial \mu} \right|_{\mu_{\text{PMS}}} = \left. \frac{\partial \langle y \rangle_{\text{NLO}}}{\partial M} \right|_{M_{\text{PMS}}} = 0. \quad (5.16)$$

In general, the stationary point will be a saddle-point in the (μ, M) plane.

This is the most straightforward way to apply the PMS to DIS, but the multiplicity of initial states compared to the e^+e^- case allows some more involved possibilities. In particular, it is interesting to consider the possibility of using different renormalization scales in the various partonic channels. This is legitimate as the cross-section for each partonic sub-process is separately renormalization scheme invariant. However, it must be borne in mind that these cross-sections do depend on the *factorization* scheme, so only their sum is actually physically observable. Now, the usual advice is to avoid adding together observables prior

to optimisation (this makes sense as the PMS point could otherwise arise as a consequence of cancellations between the two observables, which is presumably not a good indication of reliability), but these components are not observable, so it might not be sensible to apply this rule here.

The possibility of using different scales for the $q\gamma^*$ and $g\gamma^*$ sub-processes was also raised (but not pursued) in Ref. [67], which studied the $2 + 1$ -jet rate in DIS using a number of “optimisation” methods. There the components were thought of as being in principle observable (assuming one could distinguish quark and gluon jets), because of the characteristically different final states. This would only be the case, however, if it was possible to separate the final state particles into those produced by the hard interaction and those belonging to the proton remnant. In reality, this separation depends on the FP, and so will the sub-process cross-sections.

However, for M of order the hard scale Q , the quark and gluon channels give quite different contributions to the weighted integrals in Eq. (5.14) to the extent that the NLO contributions are often of different signs. There can be large cancellations between them, and it seems plausible that we could get improved results by “optimising” them separately (because the cancellations may well be specific to NLO).

Therefore, we will consider two variants of the PMS in this chapter: PMS₁ where we optimise with respect to a single renormalization scale μ and the factorization scale M , and PMS₂ where we optimise with respect to renormalization scales μ_q and μ_g for the quarks and gluons respectively, along with M . It is also possible to assign different scales to the different flavours of quarks, but this makes no significant difference to the results because the optimisation procedure always chooses very similar scales for them. Therefore, for simplicity we confine ourselves to considering μ_q and μ_g .

For PMS₁ we can define $\langle y \rangle$ in the conventional way, by expanding the RHS of Eq. (5.14) in $\alpha_{\overline{\text{MS}}}(\mu)$ and truncating it at NLO. However, this won't work for PMS₂ because there are two different couplings, $\alpha_{\overline{\text{MS}}}(\mu_q)$ and $\alpha_{\overline{\text{MS}}}(\mu_g)$, appearing in both the numerator and the denominator. Instead we can perform a double expansion in $\alpha_{\overline{\text{MS}}}(\mu_q)$ and $\alpha_{\overline{\text{MS}}}(\mu_g)$, keeping all terms with two or fewer α 's. (We could also truncate the numerator and denominator to NLO and use the quotient as our NLO approximation; this makes no qualitative difference to the results of this chapter).

5.4 Computational Methods

NLO perturbative predictions for our observables were obtained from the matrix element integration Monte-Carlo program DISENT 0.1 [68], using the interface library NLOLIB [69]. The MRST2001E PDF set [70] was used, and throughout this chapter we fix $\alpha_{\overline{\text{MS}}}(M_Z) = 0.119$ to be consistent with these PDFs. To allow for optimisation with respect to M , many runs of DISENT were carried out at intervals $\Delta M = 1\text{GeV}$. For every value of Q and M , 10^8 events were generated to ensure the Monte-Carlo integration errors were negligible. The μ dependence was implemented by having DISENT compute the coefficients of each power of $\alpha_{\overline{\text{MS}}}$ with $\mu = Q$; the μ logs as well as the factors of $\alpha_{\overline{\text{MS}}}$ could then be added in later. This means that only one run of DISENT was required for all values of μ . However, to allow this to work it was necessary for all the events to be generated at the same value of Q , so the mean value of Q was used for each bin rather than integrating over the entire width of the bin. The effect of this was estimated by comparing the two results for $\mu = M = Q$, giving a correction factor which could be applied to the data.

The power corrections can simply be added to the perturbative prediction for

the shape means

$$\langle y \rangle = \langle y \rangle_P + \langle y \rangle_{PC}. \quad (5.17)$$

We will present fits both for a simple C_1/Q or C_2/Q^2 term, and for the more sophisticated Dokshitzer-Webber model described in Subsection 2.5.2. This was extended to DIS in Ref. [71]. According to this model

$$\begin{aligned} \langle y \rangle_{PC} = & a_y \frac{32}{3\pi^2} \frac{\mathcal{M}}{p} \left(\frac{\mu_I}{Q} \right)^p \left[\bar{\alpha}_{p-1}(\mu_I) - \alpha_{\overline{\text{MS}}}(\mu) - \frac{\beta_0}{2\pi} \right. \\ & \left. (\log(\mu/\mu_I) + K/\beta_0 + 1/p) \alpha_{\overline{\text{MS}}}^2(\mu) \right]. \end{aligned} \quad (5.18)$$

(see Subsection 2.5.2 for the notation).

The terms in $\langle y \rangle_{PC}$ involving $\alpha_{\overline{\text{MS}}}$ are to be evaluated with $N_f = 5$ and with μ the renormalization scale used in the perturbative part. Note that for our PMS optimised results this will in general differ from Q . In the case of PMS₂ the appropriate scale is μ_q as the power corrections do not receive contributions from the gluon-initiated sub-process [71].

For all our observables apart from y_{k_t} , $p = 1$ and a_F has been calculated, so we can use this formula to perform a fit for $\bar{\alpha}_0$. For y_{k_t} , $p = 2$ and a_F is unknown, which prevents a reliable extraction of $\bar{\alpha}_1$. The coefficients are:

$$\begin{aligned} a_{\tau_c} = 1 \quad a_{C_P} = \frac{3\pi}{2} \quad a_{\rho_E} = \frac{1}{2} \quad [71] \\ a_{y_{f_J}} = 1 \quad [72] \quad a_{B_P} = \frac{\pi}{4\sqrt{\frac{8}{3}\alpha_{\text{CMW}}(e^{-3/4}Q)}} + \frac{3}{8} - \frac{\beta_0}{32} - 0.3069 + \text{O}(1) \quad [73] \end{aligned} \quad (5.19)$$

In performing these fits we need to consider both experimental and theoretical sources of error. The experimental errors consist of both a statistical and a systematic component; lacking knowledge of the proper correlation between the systematic errors we have treated them as uncorrelated, and simply added them to the statistical errors in quadrature, to arrive at a composite experimental error. Where the errors are asymmetric, the maximum value was taken.

Q/GeV	7.46	8.8	14.95	17.73	23.75	36.69	57.61	80.76
μ/GeV	2.11	2.45	4.07	4.96	6.98	12.3	19.8	22.4
M/GeV	7.87	7.01	6.69	6.25	5.55	3.82	2.72	2.35

Table 5.1: PMS₁ scales for $\langle\tau_c\rangle$.

The MRST2001E PDFs allow a PDF-related error to be estimated by sampling from an ensemble of different functions. Ideally we would repeat the entire analysis with the different PDFs, but this is impractical because of needing to rerun DISENT for each value of M . Instead we have estimated the error by comparing the analyses at $M = Q$ only. However, the results are so stable with respect to changes of M that this should not be too much of a restriction (and in any case, the errors due to uncertainties on the PDFs are small).

5.5 Case Study: τ_c

In this section we show the results of our analysis, along the lines described in the preceding sections, when applied to one typical observable, $1 - T_c = \tau_c$. A summary of the results for all the observables is given in the next section.

In order to arrive at our PMS₁ predictions, we need to consider the dependence of $\langle\tau_c\rangle$ on μ and M . This is illustrated in Fig. 5.1. Note that the PMS points, defined by Eq. (5.16), are saddle points. Specifically, they are maxima in the μ -direction and minima in the M -direction. The actual PMS scales are given in Table 5.1.

The effect of choosing these scales over the standard choice of $\mu = M = Q$ is illustrated in Fig. 5.2. Evidently a substantial power correction is still required to fit the data.

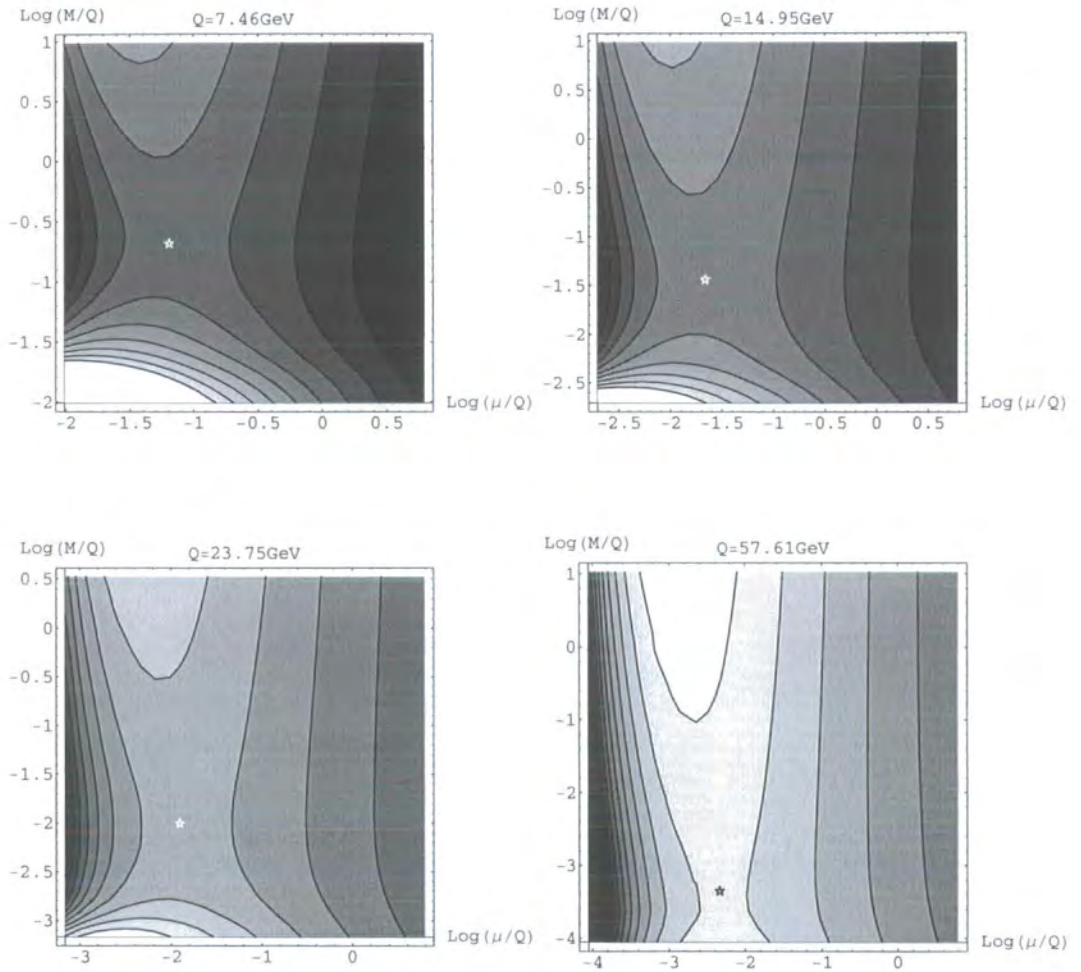


Figure 5.1: Dependence of $\langle \tau_c \rangle^{(NLO)}$ on μ and M for various values of Q . The PMS point is labelled, and the box indicates a variation of μ and M within a factor of 2 of the “physical scale” Q .



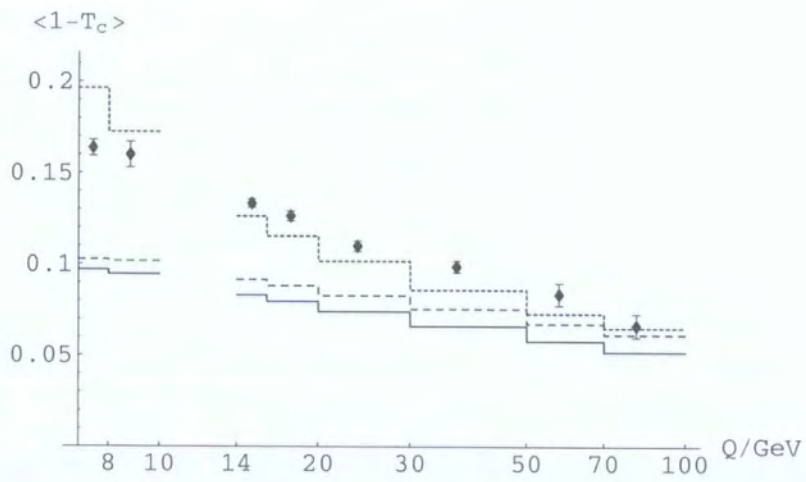


Figure 5.2: Comparison of NLO predictions to H1 data [63] for $\langle \tau_c \rangle$ (combined statistical and systematic error bars are shown). The solid curve uses $\mu = M = Q$. The dashed curve uses the PMS₁ scale choices given in Table 5.1. The dotted curve uses the PMS₂ scale choices shown in Table 5.2.

Moving on to consider the PMS₂ approximation requires us to look at the dependence of $\langle\tau_c\rangle$ on μ_q , μ_g and M . Some typical examples are illustrated in Fig. 5.3. The PMS points here are maxima in the μ_q and μ_g directions, and may be either minima or maxima in the M direction; the relevant scales are listed in Table 5.2. There is a clear difference between the values of μ_q and μ_g , the former are very small and the latter very large. The result of using these PMS₂ scales is shown as the dotted line on Fig. 5.2. Clearly, at least for large Q , the size of the required power correction is substantially reduced, but at low Q the prediction now actually *overshoots* the measurement. It is perhaps not surprising that we run into trouble here, as μ_q is extremely low (around $0.5\text{GeV} \simeq 2\Lambda_{\overline{\text{MS}}}$, so $\alpha_{\overline{\text{MS}}}(\mu_q) \simeq 0.7$).

We can see why PMS₂ makes such a large difference compared to PMS₁ by looking at the actual coefficients in the perturbative expansion for the integral

$$\int dX \tau_c(X) \frac{d\sigma(ep \rightarrow X)}{dX} = A_q \alpha_s(\mu_q) + \left(B_q + \beta_0 \log \left(\frac{\mu_q^2}{Q^2} \right) A_q \right) \alpha_s^2(\mu_q) + A_g \alpha_s(\mu_g) + \left(B_g + \beta_0 \log \left(\frac{\mu_g^2}{Q} \right) A_g \right) \alpha_s^2(\mu_g). \quad (5.20)$$

The coefficients A and B depend on both M and Q ; at $M = Q = 7.46\text{GeV}$ they are

$$A_q = 5.29, \quad A_g = 1.44, \quad B_q = 15.4, \quad B_g = -10.3. \quad (5.21)$$

On the other hand, if μ_q and μ_g are identified as in PMS₁, the coefficients in the perturbation series are simply

$$A = A_q + A_g = 6.74 \quad B = B_q + B_g = 5.10. \quad (5.22)$$

Because of the cancellation in the NLO coefficient B , PMS₁ sees a series which appears to be much more convergent than that seen by PMS₂, and this lessens the effect of the optimisation (this can be seen most easily by recalling the similarity between PMS and the Method of Effective Charges, which fixes the scale so that

Q/GeV	7.46	8.8	14.95	17.73	23.75	36.69	57.61	80.76
μ_q/GeV	0.50	0.59	0.90	1.1	1.4	2.0	3.2	4.2
μ_g/GeV	$2.3 \cdot 10^3$	$6.0 \cdot 10^3$	$6.5 \cdot 10^4$	$1.5 \cdot 10^5$	$4.1 \cdot 10^5$	$1.0 \cdot 10^6$	$1.9 \cdot 10^6$	$2.2 \cdot 10^6$
M/GeV	4.95	5.20	6.23	6.41	6.76	6.70	5.79	4.50

Table 5.2: PMS₂ scales for $\langle \tau_c \rangle$.

$B = 0$). Therefore, it may be that PMS₁ underestimates the size of higher orders in the $\mu = M = Q$ series. If this cancellation does not persist to higher orders, then one would expect PMS₂ to give a more realistic estimate of the higher order terms.

This explanation for the values of the PMS₂ scales is an over-simplification, because we aren't actually optimising the weighted integral Eq. (5.20), but rather the ratio Eq. (5.14). However, the total cross-section is convergent enough that these simple considerations do capture the essential reason behind the PMS scales shown in Tables 5.1 and 5.2. For example, the Effective Charge scales $\mu_{\text{EC}} = \exp(-B/(\beta_0 A))Q$ corresponding to these coefficients are

$$\mu = 4.0\text{GeV} \quad (5.23)$$

$$\mu_q = 0.68\text{GeV} \quad \mu_g = 2.6 \cdot 10^3\text{GeV} \quad (5.24)$$

which are all rather close to the corresponding PMS scales (although the agreement is not perfect: the EC μ_g actually falls as Q is increased).

τ_c is expected to receive $1/Q$ power corrections, which we can try to describe either by simply adding a term C_1/Q to the perturbative predictions, or by using Eq. (5.18) which relates the corrections to $\bar{\alpha}_0$. Because of the rise in the PMS₂ predictions for $Q < 10\text{GeV}$, these $1/Q$ corrections alone cannot compensate for the discrepancy between theory and data in this case. In addition, there must be

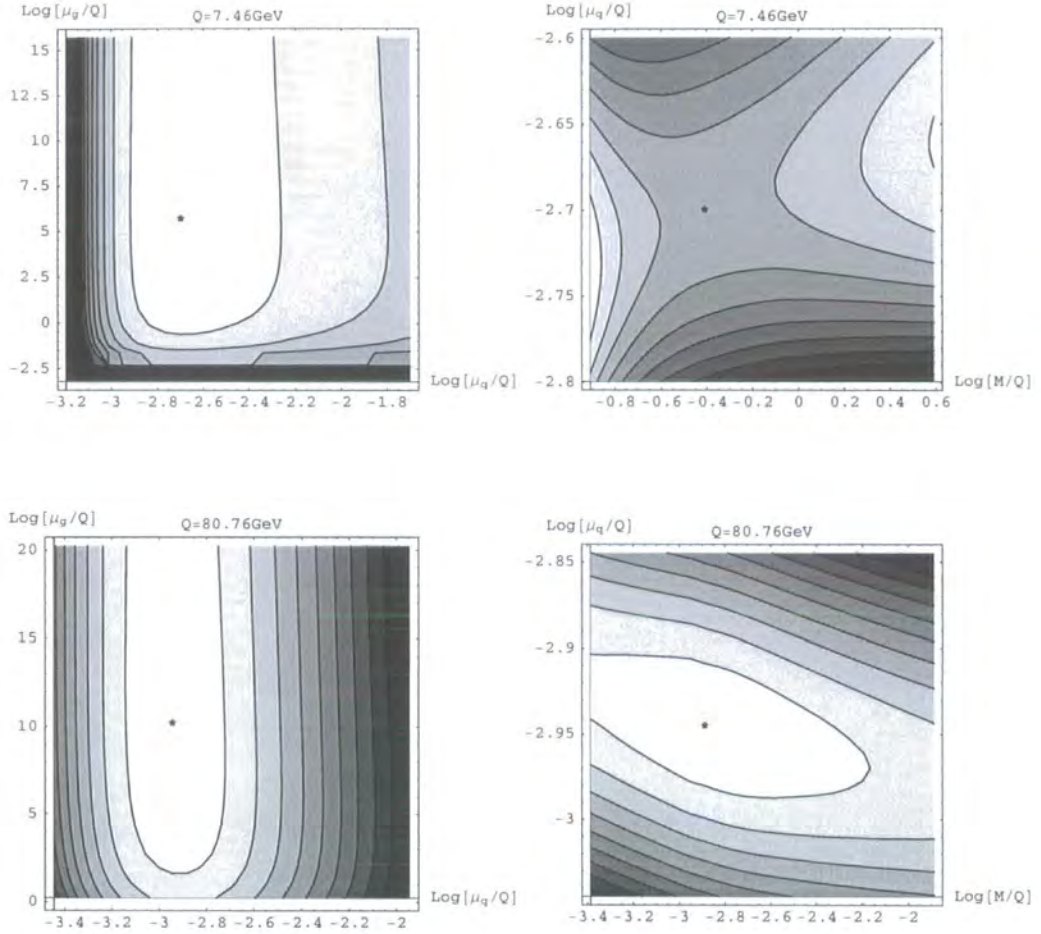


Figure 5.3: Dependence of $\langle\tau_c\rangle^{(\text{NLO})}$ on μ_q , μ_g and M for the extreme Q values. The left hand plot shows the dependence on μ_q and μ_g with M fixed to its PMS value. The right hand plot shows the dependence on M and μ_q with μ_g fixed to its PMS value. The PMS points are labelled, and the numerical values of the PMS scales are listed in Table 5.2.

large higher-order $O(\alpha_s^3)$ effects and/or sub-leading power corrections $\propto 1/Q^2$. To compare the size of the power corrections required by the different perturbative predictions, it makes sense to exclude low Q data if this gives an unacceptably bad fit. This is especially true in view of the fact that the e^+e^- data examined in Ref. [13] had $\langle Q \rangle > 45\text{GeV}$, so these additional effects might be important at low Q in the e^+e^- case also. Therefore, we performed minimum- χ^2 fits, adding in data points from the highest Q downwards until the fit probability fell below 5%. Experimental errors were estimated by allowing χ^2 to vary within 1 of its minimum value. Fitting in this way for C_1 gives

$$\mu = M = Q : C_1 = 1.23(11)\text{GeV}, \quad Q > 30\text{GeV}$$

$$\text{PMS}_1 : C_1 = 0.65(2)\text{GeV}, \quad Q > 8\text{GeV}$$

$$\text{PMS}_2 : C_1 = 0.18(3)\text{GeV}, \quad Q > 14\text{GeV}.$$

As expected, the required power correction is largest for the ‘‘physical scale’’, and smallest for PMS_2 . Of the three predictions, PMS_1 gives the best description of the data, as shown by the fact that it provides a good fit down to $Q \sim 8\text{GeV}$.

Because one expects also sub-leading power corrections to be present, it is interesting to introduce e.g. a C_2/Q^2 term into the fit, to see how this affects the conclusions:

$$\mu = M = Q : C_1 = 1.09(5)\text{GeV}, \quad C_2 = -4.3(5)\text{GeV}^2, \quad Q > 7\text{GeV}$$

$$\text{PMS}_1 : C_1 = 0.82(5)\text{GeV}, \quad C_2 = -2.5(5)\text{GeV}^2, \quad Q > 7\text{GeV}$$

$$\text{PMS}_2 : C_1 = 0.49(5)\text{GeV}, \quad C_2 = -5.3(5)\text{GeV}^2, \quad Q > 7\text{GeV}.$$

where the errors are strongly correlated. Unsurprisingly, the C_2/Q^2 term allows even the low Q data to be correctly described. The basic fact that the optimisation reduces the need for $1/Q$ power corrections does seem to survive.

Fitting for $\bar{\alpha}_0$ gives

$$\mu = M = Q : \bar{\alpha}_0 = 0.524(7), \quad Q > 8\text{GeV}$$

$$\text{PMS}_1 : \bar{\alpha}_0 = 0.596(6), \quad Q > 7\text{GeV}$$

$$\text{PMS}_2 : \bar{\alpha}_0 = 0.614(8), \quad Q > 14\text{GeV}$$

It may perhaps seem surprising that the $\bar{\alpha}_0$ values are larger for the PMS scale choices, even though the size of the power corrections seems to be reduced, as is reflected in the C_1 values. This is a consequence of using the PMS scales in Eq. (5.18), which increases the perturbative contribution and requires larger $\bar{\alpha}_0$ to compensate.

5.6 Results

In this section we summarise results for all the observables studied in Ref. [63]. The perturbative predictions are compared to data in Figs. 5.4 and 5.5. τ_c and C_P show similar features: the PMS₁ predictions are somewhat closer to the data than the physical scale ones, and the PMS₂ predictions are a lot closer, except they become too large at low energies. The PMS predictions for τ_P substantially reduce the excess of data over theory, with no evident breakdown at low Q . B_P and ρ_E also have reasonable low Q behaviour but with a lesser improvement of the fit. Turning to $\rho_E^{(\text{ESch})}$, though, the improvement (especially for PMS₂) is much more substantial. The jet transition parameters, y_{fJ} and y_{k_t} , move *away* from the data when the scales are optimised.

Table 5.3 shows fits for a C_1/Q power correction for all observables except y_{k_t} and a fit for a C_2/Q^2 power correction for y_{k_t} (y_{k_t} is the only observable whose leading power correction is expected to be $\propto 1/Q^2$). Table 5.4 shows the results of fitting for a power correction based on Eq. (5.18) for all observables bar y_{k_t} .

These fits allow us to see to what extent the discrepancy between the perturba-

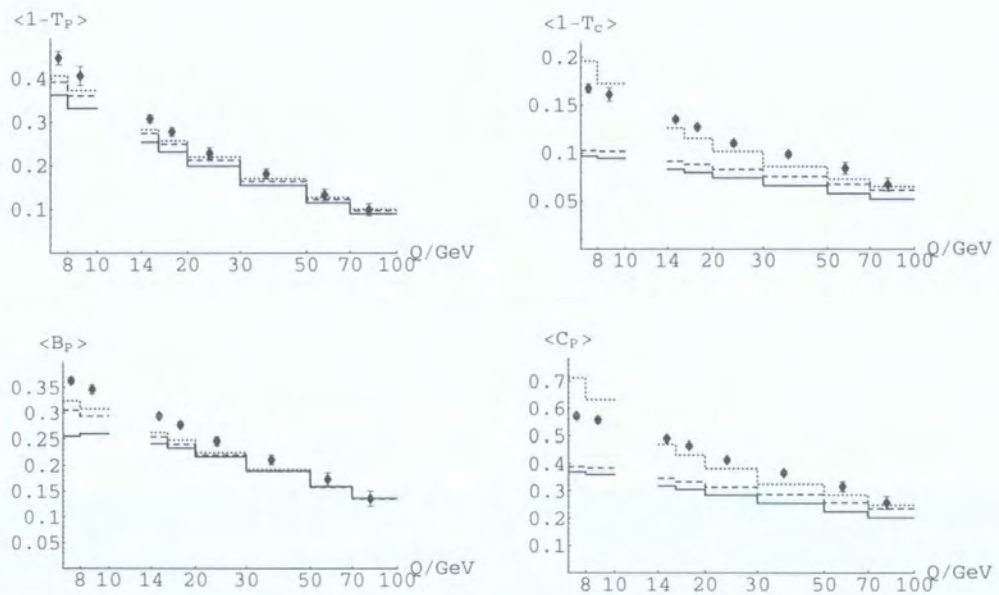


Figure 5.4: Predictions of our three perturbative predictions compared to data. The solid line uses the scale choice $\mu = M = Q$, the dashed curve uses PMS₁ and the dotted curve PMS₂. Data are shown from Ref. [63].

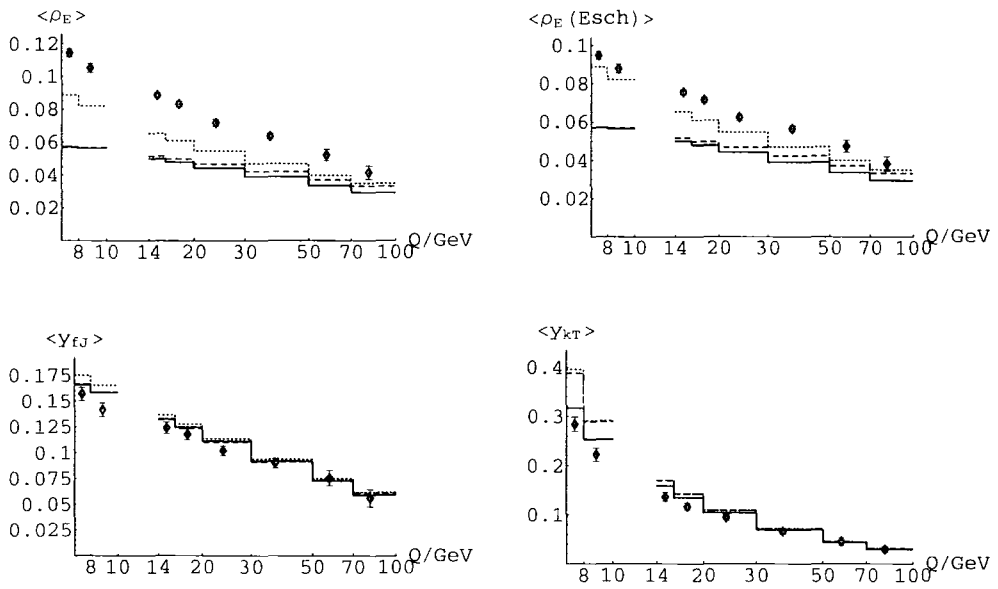


Figure 5.5: Predictions of our three perturbative predictions compared to data. The solid line uses the scale choice $\mu = M = Q$, the dashed curve uses PMS₁ and the dotted curve PMS₂. Data are shown from Ref. [63].

C_1/GeV						
Obs	$\mu = M = Q$		PMS ₁		PMS ₂	
τ_P	0.73(7)	> 7	0.45(7)	> 7	0.33(7)	> 7
τ_c	1.23(11)	> 30	0.65(2)	> 8	0.18(3)	> 14
B_P	0.79(3)	> 7	0.50(3)	> 7	0.37(3)	> 7
C_P	4.17(29)	> 30	2.26(7)	> 14	0.76(49)	> 16
ρ_E	0.92(6)	> 30	0.67(4)	> 20	0.49(4)	> 20
y_{fJ}	-0.11(3)	> 7	-0.11(3)	> 7	-0.18(3)	> 7
$\rho_E^{(\text{ESch})}$	0.65(5)	> 30	0.38(2)	> 14	0.21(2)	> 16
C_2/GeV^2						
y_{kt}	-2.70(60)	> 7	-6.03(60)	> 7	-6.30(60)	> 7

Table 5.3: Fits for C_1 and C_2 . The first number gives the best fit value and numbers in brackets indicate errors in the last digits (due to experimental and PDF uncertainties). The second number indicates the range of Q that could be fitted before the χ^2 indicated a fit probability of $< 5\%$.

tive predictions and the data visible on Figs. 5.4 and 5.5 can actually be described as a power correction. As was noted for τ_c in Section 5.5, the problems at low Q for C_P mean the fit quality is dreadful for PMS₂ unless we exclude the lowest two bins. The same is true for ρ_E (and $\rho_E^{(\text{ESch})}$). Although not obvious from Figs. 5.4 and 5.5, the “physical scale” predictions don’t describe the low energy data for these observables very well either. In fact, the best overall fits seem to be those that use PMS₁. The other observable with a large discrepancy at low Q , y_{kt} , can be described quite well by any of the scale choices provided we add the expected $1/Q^2$ power correction.

$\bar{\alpha}_0$						
Obs	$\mu = M = Q$		PMS ₁		PMS ₂	
τ_P	0.519(22)	> 7	0.533(22)	> 7	0.559(22)	> 7
τ_c	0.524(7)	> 8	0.596(6)	> 7	0.614(8)	> 14
B_P	0.568(17)	> 8	0.447(13)	> 7	0.443(13)	> 7
C_P	0.465(7)	> 16	0.527(3)	> 7	0.557(7)	> 16
ρ_E	0.808(38)	> 30	0.715(10)	> 14	0.736(7)	> 7
y_{fJ}	0.264(18)	> 7	0.261(10)	> 7	0.278(12)	> 8
$\rho_E^{(\text{ESch})}$	0.642(34)	> 30	0.572(7)	> 8	0.611(7)	> 8

Table 5.4: Fits for $\bar{\alpha}_0$. See Table 5.3 for an explanation.

5.7 Conclusions

In this chapter we have studied how power correction fits to event shape means in DIS are affected by choosing the factorization and renormalization scales using the Principle of Minimal Sensitivity. In doing this, two different prescriptions were adopted: PMS₁, where the unphysical parameters were taken to be μ and M and PMS₂, where different values of μ were used for the quark- and gluon-initiated subprocesses. The motivation behind PMS₂ was to avoid underestimating the effect of higher order corrections because of the cancellations between the $q\gamma^*$ and $g\gamma^*$ sub-processes at NLO (illustrated in Eq. (5.21)).

PMS₁ gives results that are pretty close to those found using the conventional choice $\mu = M = Q$. However, it does improve the quality of the power correction fits (see Tables 5.3 and 5.4). PMS₂ gives perturbative results that are substantially closer to the data at high values of Q , but which deviate from it at low Q (see Figs. 5.4 and 5.5). If we exclude this low Q region from the fits (as in Tables 5.3

and 5.4), PMS₂ requires much smaller power corrections to fit the data than does either PMS₁ or the choice $\mu = M = Q$.

It is possible that problems could arise from using optimisation with PDFs that were obtained without optimisation. If, say, switching to the PMS scale has a consistent effect on a number of observables, refitting for the PDFs using the PMS would cause them to change so as to counteract the effect of the optimisation. Unfortunately, optimising enough observables to be able to fit for the PDFs would be a very large undertaking, and is beyond the scope of this thesis. One might hope that this is not actually an issue, because event shapes have particularly large NLO corrections and hence are probably more sensitive to optimisation than most other observables.

The motivation for this study was to determine whether “optimised” scales could significantly reduce the need for power corrections to DIS event shape means as they appeared to do for their e^+e^- counterparts [13]. PMS₁ certainly cannot do this; PMS₂ can to some extent, but not at low energies - however, the energies where PMS₂ breaks down are much lower than those at which any e^+e^- event shape data is available. So if PMS₂ provides a better estimate of higher order terms in the perturbation series than PMS₁, it could be that the conclusions of Ref. [13] do extend to DIS event shape means. In this case, NNLO corrections would become important in both processes at $Q \simeq 20\text{GeV}$.

In summary, whether this work counts for or against the idea that power corrections can be reduced and/or eliminated by using optimised schemes depends on which of the two prescriptions, PMS₁ or PMS₂, one considers most plausible. However, as long as we only have NLO calculations to work with it will be difficult to be sure which, if any, optimisations are best (although the overall consistency of the Method of Effective Charges analysis in Ref. [13] is highly suggestive). Once NNLO computations become available for these event shape means it will be

possible to measure the convergence of the optimised approximants and compare them to each other and to the convergence in the \overline{MS} -scheme. This should provide better guidance in choosing the scheme for these observables, and allow us to more thoroughly test if the apparent power corrections really can be mimicked by an optimisation of the scheme.

Chapter 6

Summary and Outlook

In this thesis, the Method of Effective Charges and the Principle of Minimal Sensitivity have been applied respectively to event shape distributions in e^+e^- annihilation and event shape means in ep DIS. The goal was to see whether the need for power corrections would be lessened, as had been found for e^+e^- event shape means in Ref.[13].

To study the distributions, an effective charge was constructed in the exponent of the integrated distribution. Using the NLO approximation for this charge gave a surprisingly good qualitative description of the peak region for the thrust distribution. We then proceeded to perform a resummation of large logs in the effective charge beta-function ρ , to LL and NLL accuracy. Promisingly, most of the next-to-leading $\overline{\text{MS}}$ -scheme logs already seemed to be included when using the LL ρ function. However, when the beta function was actually integrated to find the distribution, it was found to diverge in the 2-jet region, spoiling the nice behaviour that was seen at NLO. This is strange as one would have expected that in this region the leading logs would dominate the ρ function, so the resummed results would be accurate. The divergence appears to be associated with the unphysical behaviour in the $\overline{\text{MS}}$ -scheme near the branch point in g_1 . Excluding the 2-jet

region, along with the area where the LO coefficient vanishes, invalidating the ECH description, power correction fits were performed. Some reduction of power corrections was seen, although the $\Lambda_{\overline{\text{MS}}}$ values were still too small.

For the DIS event shape means, we applied the Principle of Minimal Sensitivity. Optimising with respect to μ and M produced only a small change in the perturbative predictions. However, introducing a separate renormalization scale for the quark- and gluon-initiated sub-processes gave a substantial reduction in the required power corrections. This was due to large cancellations between the NLO coefficients for these sub-processes, which made the series seem more convergent when they were added together, lessening the scale dependence and so reducing the effect of the optimisation.

Neither of these studies showed effects as dramatic as those of Ref.[13]. Part of this may be due to the heavy-quark mass effects that were not corrected for in this thesis, and which therefore account for part of the measured power correction. However, there are undoubtedly other confounding factors for these observables. For the e^+e^- distributions there are the large logs which unfortunately do not appear to be controlled by resumming the ECH beta function. For the DIS event shape means there is the fact that the bulk of the data has rather low Q compared to the e^+e^- data, along with the fact that one is unable to apply the PMS to the full FS-dependence.

Nonetheless, there are signs that using these optimised approaches, the need for power corrections can be reduced. If one believes the optimised results to be more reliable than those obtained using $\overline{\text{MSPS}}$, this is a sign that a large piece of what appears to be a power-suppressed correction is just the combined effect of the first few orders of $\overline{\text{MSPS}}$ perturbation theory (obtained by re-expanding the optimised results). These do not sum to a true $1/Q$ term; it is simply that given finitely many data points, a correction falling off like powers of $\ln Q$ can

look very similar to a $1/Q$ correction. This is therefore not an example of the ambiguity in separating perturbative and non-perturbative physics mentioned in Subsection 3.1.1, which occurs because the different prescriptions for regulating the divergence of the perturbation series differ by power-suppressed terms.

Unfortunately, the need to add an essentially unknown power correction makes it harder to judge whether optimised perturbation theory actually outperforms $\overline{\text{MS}}\text{PS}$, in the sense of giving a better description of the data at NLO. The real test will come when full NNLO matrix element integration programs become available, and the predictions for the $\overline{\text{MS}}$ -scheme NNLO coefficient r_2 can be compared with the exact values. For example, for $\langle\tau\rangle$ in e^+e^- annihilation, the $\overline{\text{MS}}\text{PS}$ perturbation series is

$$\langle\tau\rangle = 1.05(a_{\overline{\text{MS}}}(Q) + 9.57a_{\overline{\text{MS}}}^2(Q) + \dots) \quad (6.1)$$

so $r_1 = 9.57$. From Eq. (3.11) we have $r_2 = \rho_2 - c_2 - r_1c + r_1^2$, where $c_2 = 33.7$ in the $\overline{\text{MS}}$ -scheme for $N_f = 5$. NLO ECH (i.e. approximating $\rho_2 = 0$) gives a prediction $r_2 = -c_2 + r_1c + r_1^2 = 69.9$. The NNLO $\overline{\text{MS}}\text{PS}$ contribution would then be about 30% as large as the NLO term. Knowledge of the exact coefficient should indicate whether ECH is on track. Also, with NLO and NNLO calculations available, the convergence of the PMS and ECH approximations can be examined, which will give another way of testing their validity.

If these NNLO calculations back up the results of applying the optimisations to event shapes at NLO (as happened for the R -ratio [74]), this will motivate using the NNLO optimisations to further increase the accuracy of perturbative QCD for little extra computational cost. However, this would deepen the mystery of why power corrections to these event shapes seem to be so small when one uses ECH/PMS. A resolution of this would hopefully give new insight into the low-energy behaviour of QCD.

Bibliography

- [1] M. Dasgupta and G. P. Salam, *J. Phys. G* **30** (2004) R143 [arXiv:hep-ph/0312283].
- [2] B. R. Webber, Lectures at the Summer School on Hadronic Aspects of Collider Physics, Zuoz, Switzerland, August 1994 [arXiv:hep-ph/9411384].
- [3] P. Nason and M. H. Seymour, *Nucl. Phys. B* **454** (1995) 291 [arXiv:hep-ph/9506317].
- [4] Yu. L. Dokshitzer and B. R. Webber, *Phys. Lett. B* **352** (1995) 451 [arXiv:hep-ph/9504219].
- [5] J. Fischer, *Int. J. Mod. Phys. A* **12** (1997) 3625 [arXiv:hep-ph/9704351].
- [6] S. Bethke, *Nucl. Phys. Proc. Suppl.* **135** (2004) 345 [arXiv:hep-ex/0407021].
- [7] G. 't Hooft, *Nucl. Phys.* **B61** (1973) 455.
- [8] E. Gardi and G. Grunberg, *JHEP* **9911** (1999) 016 [arXiv:hep-ph/9908458].
- [9] E. Gardi and J. Rathsman, *Nucl. Phys. B* **609** (2001) 123 [arXiv:hep-ph/0103217].
- [10] E. Gardi and J. Rathsman, *Nucl. Phys. B* **638** (2002) 243 [arXiv:hep-ph/0201019].
- [11] G. Grunberg, *Phys. Rev. D* **29** (1984) 2315.

- [12] J. M. Campbell, E. W. N. Glover and C. J. Maxwell, *Phys. Rev. Lett.* **81** (1998) 1568 [arXiv:hep-ph/9803254].
- [13] DELPHI Collaboration (J. Abdallah et al) *Eur. Phys. J.* **C29** (2003) 285.
- [14] Michael E. Peskin, Daniel V. Schroeder, “An Introduction to Quantum Field Theory”, (Perseus Books Publishing, 1995)
- [15] Francis Halzen and Alan D. Martin, “Quarks and Leptons: An Introductory Course in Modern Particle Physics”, (Wiley, New York, 1984)
- [16] A. Zee, “Quantum Field Theory in a Nutshell”, (Princeton University Press, 2003)
- [17] R. K. Ellis, W. J. Stirling and B. R. Webber, “QCD and Collider Physics” (Cambridge University Press, 1996), p73.
- [18] Howard Georgi, “Lie Algebras in Particle Physics” 2nd Ed., (Perseus Books Publishing, 1999)
- [19] M. Pospelov and A. Ritz, *Phys. Rev. Lett.* **83** (1999) 2526 [arXiv:hep-ph/9904483]
- [20] G. 't Hooft and M. Veltman, *Nucl. Phys. B* **44** (1972) 189.
- [21] G. 't Hooft, *Nucl. Phys.* **B33** (1971) 173.
- [22] P. M. Stevenson, *Phys. Rev. D* **23** (1981) 2916.
- [23] F. Wilczek, *Proc. Nat. Acad. Sci.* **102** (2005) 8403 [arXiv:hep-ph/0502113].
- [24] D. Gross and F. Wilczek, *Phys. Rev.* **D8** (1973) 3633
- [25] H. D. Politzer, *Phys. Rev. Lett.* **30** (1973) 1346
- [26] S. Catani, G. Marchesini and B. R. Webber, *Nucl. Phys. B* **349** (1991) 635.

- [27] Yu. L. Dokshitzer, A. Lucenti, G. Marchesini and G. P. Salam, Nucl. Phys. **B 511** (1998) 396 [hep-ph/9707532]; JHEP. **05** (1998) 003 [hep-ph/9802381]
- [28] Yu. L. Dokshitzer and B. R. Webber, Phys. Lett. B **404** (1997) 321 [arXiv:hep-ph/9704298].
- [29] A. J. Buras, E. G. Floratos, D. A. Ross and C. T. Sachrajda, Nucl. Phys. B **131** (1977) 308.
- [30] W. Celmaster and R. J. Gonsalves, Phys. Rev. D **20** (1979) 1420.
- [31] J. Chyla, Phys. Rev. D **40**, 676 (1989).
- [32] C. J. Maxwell and A. Mirjalili, Nucl. Phys. B **577** (2000) 209.
- [33] A. Dhar, Phys. Lett. **B128** (1983) 407; A. Dhar and V. Gupta, Phys. Rev. **D29** (1984) 2822.
- [34] M. J. Dinsdale and C. J. Maxwell, arXiv:hep-ph/0408114.
- [35] S. J. Burby and C. J. Maxwell, Nucl. Phys. **B609** (2001) 193.
- [36] P. Abreu *et al.* [DELPHI Collaboration], Eur. Phys. J. C **14**, 557 (2000) [arXiv:hep-ex/0002026].
- [37] D. T. Barclay, C. J. Maxwell and M. T. Reader, Phys. Rev. **D49** (1994) 3480.
- [38] C. J. Maxwell and D. G. Tonge, Nucl. Phys. B **481**, 681 (1996) [arXiv:hep-ph/9606392].
- [39] D. Buskulic *et al.* [ALEPH Collaboration], Z. Phys. C **55**, 209 (1992).
- [40] D. Buskulic *et al.* [ALEPH Collaboration], Z. Phys. C **73**, 409 (1997).
- [41] P. Abreu *et al.* [DELPHI Collaboration], Phys. Lett. B **456**, 322 (1999).

- [42] P. A. Movilla Fernandez, O. Biebel, S. Bethke, S. Kluth and P. Pfeifenschneider [JADE Collaboration], *Eur. Phys. J. C* **1**, 461 (1998) [arXiv:hep-ex/9708034].
- [43] B. Adeva *et al.* [L3 Collaboration], *Z. Phys. C* **55**, 39 (1992).
- [44] M. Acciarri *et al.* [L3 Collaboration], *Phys. Lett. B* **489**, 65 (2000) [arXiv:hep-ex/0005045].
- [45] P. D. Acton *et al.* [OPAL Collaboration], *Z. Phys. C* **55**, 1 (1992).
- [46] K. Ackerstaff *et al.* [OPAL Collaboration], *Z. Phys. C* **75**, 193 (1997).
- [47] G. Abbiendi *et al.* [OPAL Collaboration], *Eur. Phys. J. C* **16**, 185 (2000) [arXiv:hep-ex/0002012].
- [48] K. Abe *et al.* [SLD Collaboration], *Phys. Rev. D* **51**, 962 (1995) [arXiv:hep-ex/9501003].
- [49] W. Braunschweig *et al.* [TASSO Collaboration], *Z. Phys. C* **47**, 187 (1990).
- [50] W. T. Giele and E. W. N. Glover, *Phys. Rev. D* **46** (1992) 1980.
- [51] S. Catani and M. H. Seymour, *Phys. Lett. B* **378** (1996) 287 [arXiv:hep-ph/9602277].
- [52] G. P. Korchemsky and G. Sterman, arXiv:hep-ph/9505391.
- [53] G. P. Korchemsky and G. Sterman, *Nucl. Phys. B* **555** (1999) 335 [arXiv:hep-ph/9902341].
- [54] S. Catani, G. Turnock, B. R. Webber and L. Trentadue, *Phys. Lett. B* **263** (1991) 491.
- [55] Stephen Wolfram, *The Mathematica Book*, 4th ed. (Wolfram Media/Cambridge University Press, 1999).

- [56] C. J. Maxwell, Nucl. Phys. Proc. Suppl. **86** (2000) 74.
- [57] H. D. Politzer, Nucl. Phys. B **194** (1982) 493.
- [58] P. M. Stevenson and H. D. Politzer, Nucl. Phys. B **277** (1986) 758.
- [59] P. Aurenche, R. Baier, A. Douiri, M. Fontannaz and D. Schiff, Nucl. Phys. B **286** (1987) 553.
- [60] P. Aurenche, R. Baier, M. Fontannaz and D. Schiff, Nucl. Phys. B **297** (1988) 661.
- [61] J. Chyla, JHEP **0303** (2003) 042 [arXiv:hep-ph/0303179].
- [62] J. Srbek and J. Chyla, arXiv:hep-ph/0504089.
- [63] C. Adloff *et al.* [H1 Collaboration], Eur. Phys. J. C **14** (2000) 255 [Erratum-
ibid. C **18** (2000) 417] [arXiv:hep-ex/9912052].
- [64] G. P. Salam and D. Wicke, JHEP **0105** (2001) 061 [arXiv:hep-ph/0102343].
- [65] T. Sjöstrand, P. Edén, C. Friberg, L. Lönnblad, G. Miu, S. Mrenna and E. Norrbin, Computer Physics Commun. **135** (2001) 238.
- [66] J. Chyla, Z. Phys. C **43** (1989) 431.
- [67] G. Ingelman and J. Rathsman, Z. Phys. C **63** (1994) 589 [arXiv:hep-ph/9405367].
- [68] S. Catani and M. H. Seymour, Nucl. Phys. B **485** (1997) 291-419, Erratum
Ibid. B **510** (1997) 503-504.
- [69] T. Hadig and G. McCance, arXiv:hep-ph/9909491.
- [70] A. D. Martin, R. G. Roberts, W. J. Stirling and R. S. Thorne, Eur. Phys. J. C **28** (2003) 455 [arXiv:hep-ph/0211080].

- [71] M. Dasgupta and B. R. Webber, *Eur. Phys. J. C* **1** (1998) 539
- [72] B. R. Webber, in *Proceedings of the Workshop on Deep Inelastic Scattering and QCD*, Paris, France, 1995
- [73] Yu. L. Dokshitzer, G. Marchesini, G. P. Salam, *Eur. Phys. J. directC* **1** (1999) 3 [arXiv:hep-ph/9812487]
- [74] A. C. Mattingly and P. M. Stevenson, *Phys. Rev. D* **49** (1994) 437 [arXiv:hep-ph/9307266].

